

# **Design and Stability Analysis of a robust wide-area measurement based damping controller for Multiple HVDC Systems**

By

**RAJESH VAID**

A Thesis submitted to the Faculty of Graduate Studies of  
The University of Manitoba  
in partial fulfillment of the requirements of the degree of

Doctor of Philosophy

Department of Electrical and Computer Engineering  
University of Manitoba  
Winnipeg, Manitoba

Copyright © 2017 by Rajesh Vaid

April 3, 2018

## **Dedicated to Almighty,**

I would like to express my deep gratitude and sincere thanks to my advisor Prof. A. M. Gole for providing guidance during my research. I also thank him for the opportunity to work with him and the encouragement provided to explore new ideas. Prof. Gole's vast expertise and insightful suggestions provided invaluable motivation to me throughout the research for this thesis. His patience and encouragement helped me to continually improve this thesis.

My thanks are extended to the advisory committee members, Prof. Peter Graham, Dennis A. Woodford, Dr. Vajira Pathirana and Dr. V. K. Sood for their reviews, suggestions, and discussions regarding my research work over the years. I would also like to thank Prof. Cyrus Shafai for guiding me in consolidating my work. I would also like to record my thanks and appreciation for the support and help provided by the office staff, especially, Traci Gledhill, and Amy Dario of the Department of Electrical and Computer Engineering at University of Manitoba.

I wish to also thank my colleagues at The University of Manitoba and special thanks to Dr. Mukesh K Das, Prashant Agnihotri and Ajinkya Sinkar who helped me in handling a lot of issues related to my work.

Last but not the least, my parents, my wife Geeta, and my sons Raul and Rijul who have been my pillars of strength during this entire tenure. It was their patience and sacrifice due to which I was able to concentrate on the research work. Their love and care have been the major driving forces of this work.

Rajesh Vaid.

## Abstract

The presence of low-frequency oscillations in the power system network is a cause of concern. If such oscillations are not suitably damped then they can lead to catastrophic events in the power system. The issue of providing adequate damping for such oscillations has been approached in ways ranging from the use of local signals e.g rotor angle, machine speed to tune power system stabiliser, to development of power oscillation damping controllers that utilise line current, line voltage signals from special equipment (e.g. Flexible AC Transmission). The power network has embedded High Voltage DC (HVDC) transmission system and some power oscillation damping controllers make use of this resource to address the issue. The advent of Wide-Area Measurement Systems (WAMS) has enabled the use of remote system-wide information to enhance controllability of critical parameters and improve the stability of the overall system. This thesis investigates the use of such system-wide information to synthesise a feedback signal to impart damping to critical swing-modes. This research demonstrates that the use of selected system-wide information along with local signals result in a robust controller, whose performance does not deteriorate when the communication channel fails. The proposed controller utilises the concept of increasing the separation between the closed-loop poles and open-loop zeros, which leads to an increased range of controller gains to improve damping. This controller can be an add-on control module in the existing control system of the High Voltage DC transmission (HVDC) links. The research also demonstrates that varying damping controller gains beyond a given value adversely impacts system stability, which is due to an adverse interaction between the damping controller and the Voltage Source Converter (VSC) HVDC system. This instability can be accurately captured through electro-magnetic transient simulation, rather than the linearised model of the system largely due to the simplification of HVDC system in transient stability simulation. The justification for the proposed controller design is provided using eigenvalue sensitivity analysis. The frequency scanning based Nyquist analysis corroborates the occurrence of damping controller gain related system instability.

# Contents

<b>List of Symbols</b>	<b>xiii</b>
<b>List of Abbreviations</b>	<b>xiv</b>
<b>1 Introduction</b>	<b>1</b>
1.1 Background . . . . .	1
1.2 Classification of Oscillations . . . . .	3
1.3 WAMS based Damping Control . . . . .	5
1.3.1 Control Structure . . . . .	5
1.3.2 Controller Design . . . . .	8
1.3.3 HVDC for improving AC system stability . . . . .	9
1.3.4 Input/Output Signal Selection . . . . .	9
1.4 Summary of Past Research in the Area . . . . .	10
1.5 Aim and Objective of Research . . . . .	12
1.6 Outline of the Thesis . . . . .	13
<b>2 HVDC Technologies and Controls</b>	<b>16</b>
2.1 Introduction . . . . .	16
2.1.1 Advantages of HVDC over HVAC . . . . .	17
2.1.2 LCC HVDC . . . . .	18
2.1.3 VSC-HVDC . . . . .	18
2.1.4 Comparison between LCC and VSC . . . . .	19
2.2 Configurations and Topologies . . . . .	19
2.2.1 Monopole . . . . .	22

2.2.2	Bipole . . . . .	22
2.3	Basic converter control scheme . . . . .	23
2.4	Control schemes for multi-terminal VSC-HVDC system . . . . .	24
2.4.1	Master-Slave or Fixed Voltage Control . . . . .	25
2.4.2	Voltage Margin Control . . . . .	26
2.4.3	Voltage Droop Control . . . . .	26
2.5	Supplementary Control . . . . .	27
2.6	Summary . . . . .	28
<b>3</b>	<b>Analytical and Simulation Tools</b>	<b>29</b>
3.1	Analytical Tools . . . . .	29
3.1.1	Linearization of Power System Model . . . . .	29
3.1.2	Modal Analysis . . . . .	31
Eigenvalues and Eigenvectors . . . . .	31	
Participation Factors . . . . .	32	
Modal Controllability and Observability . . . . .	33	
3.2	EMT Simulation . . . . .	36
3.2.1	Classification of Transients . . . . .	36
3.3	Summary . . . . .	39
<b>4</b>	<b>Robust damping controller design for AC-DC systems</b>	<b>41</b>
4.1	Introduction . . . . .	41
4.2	Design of the Damping Controller . . . . .	42
4.2.1	Existing approaches to damping controller design . . . . .	43
An existing approach to a robust damping controller . . . . .	44	
4.2.2	The proposed design approach based on special feedback signal for a robust damping controller . . . . .	48
4.2.3	Extension of proposed approach to network with multiple HVDC systems . . . . .	51
Block diagram of the proposed controller . . . . .	52	
4.3	Design philosophy . . . . .	52

4.4	Location of HVDC link in AC-DC network for improved damping based on residue analysis . . . . .	53
4.4.1	Example: Selection of location of HVDC link based on residue analysis . . . . .	57
	Case-A: An HVDC link between bus 4-7 (4.3. . . . .	57
	Case-B: An HVDC link between bus 7-9. . . . .	59
	Case-C: Two HVDC links in the system at bus 4-6 and 8-9. . . . .	61
4.4.2	Selective modal damping with wide area control . . . . .	62
4.5	Efficacy of controller based on proposed special feedback signal . . . . .	63
4.5.1	Case study: 3-Machine, 9-Bus system . . . . .	63
4.5.2	Case study: 16-Machine 68-Bus system . . . . .	66
4.6	Summary . . . . .	69
<b>5</b>	<b>Performance evaluation of the proposed controller using Electro-Magnetic Transient simulation</b>	<b>70</b>
5.1	Introduction . . . . .	70
5.2	Corroboration of the performance of the proposed controller using EMT simulation . . . . .	71
5.2.1	Corroboratation procedure . . . . .	72
5.2.2	Conclusion . . . . .	79
5.3	Performance evaluation of the proposed controller . . . . .	82
5.3.1	Selective damping . . . . .	82
5.3.2	Effect of damping controller gains on system stability . . . . .	85
5.4	Summary . . . . .	88
<b>6</b>	<b>Frequency Scan and Nyquist Stability Criterion</b>	<b>89</b>
6.1	Introduction . . . . .	90
6.2	The Frequency Scanning Technique . . . . .	91
6.3	Nyquist Analysis . . . . .	92
6.3.1	Nyquist Stability Criteria . . . . .	93
6.3.2	Generalized Nyquist Criteria . . . . .	94
6.4	Case Studies . . . . .	95

6.4.1	POD controller - HVDC system interaction . . . . .	96
	Conclusion . . . . .	96
6.4.2	Change in AC system operating point: POD controller - HVDC system interaction . . . . .	97
	Conclusion . . . . .	99
6.4.3	Change in HVDC operating point: POD controller - HVDC system interaction . . . . .	99
	Conclusion . . . . .	99
6.4.4	Communication delay: Effect on performance of controller . . . . .	101
	Conclusion . . . . .	105
6.5	Summary . . . . .	105
<b>7</b>	<b>Conclusion and Future Work</b>	<b>107</b>
7.1	Research Contributions . . . . .	108
7.2	Suggestions for Future Work . . . . .	109
	<b>Appendix</b>	<b>111</b>
	<b>A</b>	<b>111</b>
	<b>Bibliography</b>	<b>120</b>

# List of Figures

1.1	Example of a Centralised Wide Area Controller (WAC) . . . . .	6
1.2	Example of a Quasi-Decentralised Wide Area Controller (Q-WAC) . . . . .	6
1.3	Example of a Auxiliary Wide Area Controller (AWAC) . . . . .	7
2.1	Example of a Line commutated Converter (LCC) . . . . .	18
2.2	Example of Voltage Source Converter (VSC) . . . . .	19
2.3	Example of possible Topologies of Monopole HVDC System . . . . .	21
2.4	Example of Various Topologies of Bipole HVDC System . . . . .	23
2.5	Example of d-q control scheme for a VSC-HVDC converter . . . . .	24
2.6	Example of Fixed Voltage Control . . . . .	25
2.7	Example of Voltage Margin Control . . . . .	26
2.8	Example of Voltage Droop Control . . . . .	27
2.9	Example of POD as supplementary control . . . . .	27
3.1	Example of an Inductor element represented in RLC form in EMT simulation	39
4.1	Block diagram: POD controller based on the WAMS special feedback signal	49
4.2	Structure of controller . . . . .	53
4.3	3-machine 9-bus system . . . . .	57
4.4	Root-Locus plot for the controller with varying gains for link 4-7. . . . .	60
4.5	Root-Locus plot for the controller with varying gains for link 7-9. . . . .	61
4.6	Root-Locus plot for the controller with varying gains . . . . .	64
4.7	Time domain simulation for a 4-cycle 3-phase fault at bus 7, cleared by tripping line 5-7 . . . . .	65
4.8	16-Machine 68-bus NETS-NYPS test system . . . . .	66



4.9	16-machine 68-bus: Root-locus plot indicating movement of dominant inter-area modes with varying controller gain under different conditions .	67
4.10	16-machine, 68-bus: Time domain simulation for a 4-cycle 3-phase fault at bus 45, cleared by tripping line 45-39. Two DC links are at bus 40-36 and bus 52-50 respectively. . . . .	68
5.1	The 3-machine, 9-Bus test system. . . . .	73
5.2	COI Speed for generator 1: Comparison between frequency dependent (FD)Line and FD-to-Pi model Line, with eigenvalues mentioned. The eigenvalues recorded from small-signal model match with the measured value and also with those computed through Prony analysis. . . . .	75
5.3	COI Speed for generator 2: Comparison between frequency dependent (FD)Line and FD-to-Pi model Line. . . . .	75
5.4	COI Speed for generator 3: Comparison between frequency dependent (FD)Line and FD-to-Pi model Line. . . . .	76
5.5	COI Speed for generator 1: Comparison between transient stability and PSCAD with VSC-HVDC modelled as current injection at the bus. . . .	77
5.6	COI Speed for generator 2: Comparison between transient stability and PSCAD with VSC-HVDC modelled as current injection at the bus. . . .	78
5.7	COI Speed for generator 3: Comparison between transient stability and PSCAD with VSC-HVDC modelled as current injection at the bus. . . .	78
5.8	Comparison of VSC internal current magnitude:Plot for current injection in the d-q frame of VSC-HVDC link 1(Bus 8-9) representing d-axis current at the converter (inverter bus 9). . . . .	79
5.9	Comparison of VSC internal current magnitude: Plot for current injection in the d-q frame of VSC-HVDC link 1(Bus 8-9) representing q-axis current at the converter (inverter bus 9). . . . .	80
5.10	COI Speed for generator 1: Comparison between transient stability and the PSCAD with the detailed VSC-HVDC model. . . . .	80
5.11	COI Speed for generator 2: Comparison between transient stability and the PSCAD the detailed VSC-HVDC model. . . . .	81

5.12	COI Speed for generator 3: Comparison between transient stability and the PSCAD the detailed VSC-HVDC model. . . . .	81
5.13	COI Speed for generator 3: Effect of different gains on speed of machine in transient stability model. . . . .	82
5.14	COI Speed for generator 3: Effect of different gains on speed of machine in PSCAD model. . . . .	83
5.15	Modulation power injection @ HVDC link 8-9: Comparison between transient stability and PSCAD simulation models. . . . .	84
5.16	Modulation power injection @ HVDC link 4-6: Comparison between transient stability and PSCAD simulation model. . . . .	85
5.17	Transient stability plot for varying $K_{ii}$ depicting stable system . . . . .	86
5.18	Comparison between detailed (PSCAD) VSC-HVDC model and TS current injection based HVDC model. At $K_{ii} = 53$ , the PSCAD plot shows instability, whereas the TS plot indicates stable operation. . . . .	87
5.19	Comparison between the detailed VSC-HVDC model and TS current injection model for HVDC. At $K_{ii} = 53$ , the PSCAD trace for modulation power injected signal depicts instability, whereas the TS trace depicts stable operation. . . . .	87
6.1	Example of frequency scanning technique . . . . .	91
6.2	Multi-sine signal for frequency scanning technique . . . . .	92
6.3	Example of frequency scanning of a network . . . . .	93
6.4	Frequency scan plot for the real and imaginary parts of transfer function $H(j\omega)$ for the AC-DC system . . . . .	95
6.5	Stable system condition: Nyquist contour for $K_{ii} = 51$ showing no encirclements of origin. . . . .	96
6.6	Stable system condition: Nyquist contour for $K_{ii} = 53$ showing Two encirclements of origin. . . . .	97
6.7	Stable system condition: Nyquist contour for $K_{ii} = 51$ showing one clockwise and one anti-clockwise or net zero encirclements of origin. . . . .	98

6.8	Stable system condition: Nyquist contour for $K_{ii} = 53$ showing Two encirclements of origin. . . . .	98
6.9	Stable system condition: Nyquist contour for $K_{ii} = 42$ showing No encirclement of origin. . . . .	100
6.10	Stable system condition: Nyquist contour for $K_{ii} = 45$ showing Two encirclements of origin. . . . .	100
6.11	Stable system condition: Nyquist contour for $K_{ii} = 52$ and $ K_m  = 52$ , with no communication delay shows no encirclements of origin. . . . .	101
6.12	Stable system condition: Nyquist contour for $K_{ii} = 52$ and $ K_m  = 52$ , with a communication delay of $15ms$ shows no encirclements of origin. . . . .	102
6.13	Unstable system condition: Nyquist contour for $K_{ii} = 52$ and $ K_m  = 52$ , with a communication delay of $16ms$ shows two encirclements of origin. . . . .	103
6.14	Effect of communication delay: (a) An EMT simulation with a delay of $15ms$ for local ( $K_{ii} = 52$ ) and remote ( $ K_m  = 52$ ) signal gains shows stable system. (b) As for a delay of $16ms$ with the same gains the system becomes unstable. . . . .	104
6.15	Effect of communication delay on maximum gain for remote signal $K_m$ . . . . .	105

# List of Tables

2.1	<b>Comparison between LCC and VSC-HVDC systems</b>	20
3.1	Time Duration of transient phenomena in electrical systems	37
3.2	Frequency Ranges of Transients	38
3.3	Classification of Frequency Ranges	38
4.1	Dual input-output signals	43
4.2	3-Machine 9-Bus system: Residue magnitude for 8 rad/s mode	57
4.3	3-Machine 9-Bus system: Residue angle (in deg) for 8 rad/s mode	58
4.4	3-Machine 9-Bus system: Residue magnitude for 13 rad/s mode	58
4.5	3-Machine 9-Bus system: Residue angle for 13 rad/s mode	58
4.6	3-Machine 9-Bus system: One DC link @ 4-7 with finite residue magnitude for 8 rad/s; residue magnitude for 13 rad/s is Zero.	59
4.7	3-Machine 9-Bus system: One DC link @ 7-9 with finite residue magnitudes for both 8 rad/s and 13 rad/s.	59
4.8	Selective modal damping of $\sim 8$ rad/s mode	62
4.9	16-machine system: Selective modal damping of particular swing mode	68
5.1	Selective modal damping: Table compares the change in eigenvalues for with the values of $K_m$ and the ability to selectively damp a particular mode.	83
A.1	Machine data: 3 machine 9 bus system	111
A.2	Line Data: 3 machine system	111
A.3	Load flow result: 3 machine system	112

A.4 3 machine system: Load flow data for 30% change in generation at machine- 2 and 3 . . . . .	112
----------------------------------------------------------------------------------------------------	-----

# List of Symbols

$\delta$	: Generator rotor angle
$\omega$	: Generator rotor speed
$\omega_B$	: Machine base speed
$\phi$	: Bus voltage phase angle
$\zeta$	: Line current phase angle
$\phi_d$	: Voltage phase angular difference between the buses to which a two terminal DC link is connected
$H$	: Generator inertia constant
$I$	: Line current magnitude
$I_R$	: Shunt injected reactive current
$P_e$	: Power injected by generators
$P_{sh}$	: Shunt injected real power
$Q_{sh}$	: Shunt injected reactive power
$P_{ser}$	: Series injected real power
$P_{dc}$	: Two terminal DC link power flow
$V$	: Bus voltage magnitude
$V_R$	: Series injected reactive voltage (voltage in quadrature with current)

# List of Abbreviations

AC	:	Alternating current
DC	:	Direct current
MVA	:	Mega-volt ampere
PMU	:	Phasor measurement unit
WAMS	:	Wide area measurement system
IGBT	:	Insulated gate bipolar transistor
HVDC	:	High Voltage Direct Current
FACTS	:	Flexible AC Transmission Systems
PE	:	Power electronic
LCC	:	Line Commutated Converter
GNC	:	Generalised Nyquist Criteria
VSC	:	Voltage source converter
MMC	:	Multi-modular converter
POD	:	power oscillation damping
SSR	:	sub-synchronous resonance
SCR	:	Short circuit ratio
ESCR	:	Effective short circuit ratio
PWM	:	Pulse width modulation
SPWM	:	Sinusoidal pulse width modulation
PD	:	positive definite
SPD	:	symmetric positive definite
XLPE	:	Cross-Linked Polyethylene

# Chapter 1

## Introduction

This chapter provides background information on various issues involving power systems which has bearing on this research, such as development of power systems, stability concepts, classification and related terms. It also briefly discusses the research topic as well as touches upon research motivation and the objective. This also includes a synopsis of relevant research conducted on the subject.

### 1.1 Background

Power systems have evolved over time, from generation feeding local load centers to remote generation feeding distant loads through extensive AC and DC transmission network. This evolution of the power system has meant that some of the issues (e.g. inter-area disturbance, control mode interactions) which were non-existent with local generation surfaced as power system became more complex.

Power systems regularly encounter disturbances, either due to load changes or other activities such as faults, short-circuit on a transmission line, loss of large generator or load, loss of a tie-line between subsystems etc. These disturbances can be either small or severe, and trigger relative motion between the rotors of synchronous machines. Such changes result in rotors of synchronous machines (generators) to either move fast or slow down with respect to synchronous speed, resulting in relative motion between the rotors of different synchronous machines in the network. This relative motion triggers electro-mechanical oscillations in the system, which generally is oscillatory for small disturbances (swing



modes). The characteristics of these modes can be captured in frequency ( $f$ ) and phase angle ( $\phi$ ) of system variables [1],[2]. The aim of a power system operator is to maintain the power system in a steady state for optimal operating conditions, and to that effect poor or inadequate damping of the swing modes (oscillations) is a cause of concern. If these oscillations are unchecked, it can lead to catastrophic effects e.g. tripping of generators in a plant or at generating stations in a remote location. Large disturbances are also a cause of concern and are dealt with separately [3]. All this has a profound effect on the stability of the power system. While instability in a power system can be manifested in different ways depending on operating conditions or system configuration, the traditional stability concept means maintaining synchronous operation.

*Power system stability* is defined as the ability of a power system to remain in state of operating equilibrium under normal operating conditions and to regain an acceptable state of equilibrium after being subjected to a disturbance. Generally, stability issues concerning power systems can be categorized under *Rotor Angle Stability* and *Voltage Stability*.

**Voltage stability** is the ability of the power system to maintain steady acceptable voltages at all the buses in the system under normal operating conditions and after any disturbances. A state of voltage instability develops if a disturbance such as, increase in load demand, or change in operating condition causes progressive and uncontrollable drop in voltage [1]. The main factor leading to voltage instability is the inability of the system to meet reactive power demand.

The focus of this research being improvement of rotor angle stability by damping electro-mechanical (low frequency) oscillations in power systems; the same is discussed below:

**Rotor Angle Stability.** The ability of the interconnected synchronous machines of a power system to stay in synchronism. This deals with the stability of system arising out of electro-mechanical oscillations inherent in a power system. This is further classified as below:

- i Small Signal Stability. The ability of the power system to maintain synchronism when subjected to small disturbances. Such disturbances continually occur in the system due to small variations in load and generation. These disturbances are deemed small enough such that linearisation of system equations is permitted for analysis.

Since the power system is continuously experiencing disturbances, hence it never settles to a steady state at any point in time. Thus having adequate damping of all system oscillations is critical to system stability, and therefore to system security and reliability.

- ii Transient Stability. Its the ability of a power system to maintain synchronism when subjected to a severe disturbance. The resulting system response involves large movement of rotor angle and is influenced by non-linear power-angle relationship. Herein, the stability depends on the initial operating state and the severity of the disturbance.

## 1.2 Classification of Oscillations

The oscillations or swing modes between the rotors of synchronous machines mentioned in the earlier section can be classified as intra plant, local plant or plant, inter area, control and torsional modes, and are described below [4],[5]:

- Intra Plant mode. When the machines in the same generating station oscillate with respect to each other, they are known as intra-plant mode. These oscillations are characterized by frequency in the range of 2-3 Hz.
- Local Plant or Plant mode. When a machine in the generating station oscillate with respect to the rest of the machines, it is known as local plant or plant mode. These oscillations are characterized by frequency in the range of 1-2 Hz.
- Inter-area mode. These oscillations are associated with swinging of many machines in one part of a system against machines in other parts. These oscillations are generally in the range of 0.1-1 Hz.
- Control mode. Such modes are associated with poor tuning of the controls of the other devices present in the system, such as exciters, speed governors, High Voltage Direct Current(HVDC) converters and Flexible AC Transmission System(FACTS) devices. The frequency range of such oscillations is variable.

- Torsional mode. These oscillations are associated with turbine-generator shaft system and rotational components. Such oscillations can occur due to interaction between excitation controls, speed governors, HVDC controls and series compensated lines. Since these oscillations exhibit frequency in the range of 10 Hz or above, it is also referred to as Sub-Synchronous Resonance (SSR).

Of these oscillations, intra-plant mode, local mode, control mode and torsional mode are generally categorized as local problems as they involve a small part of the system. Further, inter-area mode oscillations are categorized as *global small-signal stability* problems and are caused by interactions among large groups of generators and have widespread effects.

Damping of oscillations local to a machine, is achieved through the presence of damper bars on the periphery of the rotor of a synchronous machine. Mitigation of intra plant and local plant modes is achieved through installation of power system stabilizer (PSS); by measuring a feedback signal e.g. shaft speed or power, available locally in an area and modulate the voltage reference to the automatic voltage regulator (AVR) of the synchronous machine with required phase compensation to damp out these modes. PSS designed around frequency signal ( $f$ ), besides other signals have also been used to damp inter-area modes [6]. As the observability of inter-area modes in local signals is low, lately deployment of wide area measurement systems (WAMS) has contributed to damp inter-area modes by providing system-wide information to generate a suitable signal with rich modal observability for PSS to improve damping of these modes and enhance the stability of a power system. Even with this development, [7, 8] have reported on limited capability of PSS to damp these modes.

Enhancement of angular stability of power system has also been handled by installation of FACTS and HVDC devices. FACTS devices are primarily installed in the system to extend system flexibility such as power flow (by series device) and dynamic voltage control (by shunt devices) [9]. More recently, increasing number of HVDC systems are being installed in the ac network to transmit bulk power from remote locations (e.g. offshore wind farms, large hydro and pithead thermal) to distant load centres. The HVDC and FACTS devices utilize power electronics, which have a much faster response than conventional machines in the power system, therefore these devices (FACTS / HVDC) can be utilized to damp inter-area oscillations when installed with Power Oscillation

Damping (POD) as supplementary control function. Their location, and consequently of these devices is based on studies considering large number of power flow scenarios, their contribution to the damping inter-area swing mode depends on the modal controllability and the nature of quantity controlled [9]. As a result, enhancement of system stability through POD controllers for FACTS devices, in most cases, usually comes as a bonus. In addition, the feasibility of FACTS devices for damping of inter-area oscillations has been constantly questioned due to their high costs [10]. For the purpose of comparison, it has been reported that, the use of multiple global signals in WAMS based damping controller is more cost effective than installing new control devices [11] for the enhancement of system stability.

### **1.3 WAMS based Damping Control**

WAMS has the ability to provide accurate system-wide information on critical quantities in near real time. This information when augmented with locally available information on bus voltage magnitude, angle and frequency can be usefully employed in generating a feedback signal to actuate change. The advantages of using synchronised remote signals for improved damping of inter-area oscillations, has led to an increased interest in applying WAMS based control schemes. Extensive research has been done to explore the effectiveness and capabilities of the emerging WAMS technology in improving the overall power system stability. For example, research conducted at Hydro-Quebec showed through simulations that wide-area stabilising controllers have a significant potential in improving the dynamic performance of the power system when implemented on few sites only [12].

#### **1.3.1 Control Structure**

The configuration of WAMS based control schemes can be broadly classified into following structures:

- Centralised,
- Quasi-Decentralised,

- Two-Level

The **centralised** structure involves a Wide-Area Controller (WAC) controlling the whole power system [13, 14]. Input signals to the WAC come from pre-selected PMUs and its output signals are sent to excitation systems (represented by AVRs in the Figure 1.1) of pre-selected generators in the system. The scheme assumes non-existence of PSSs in

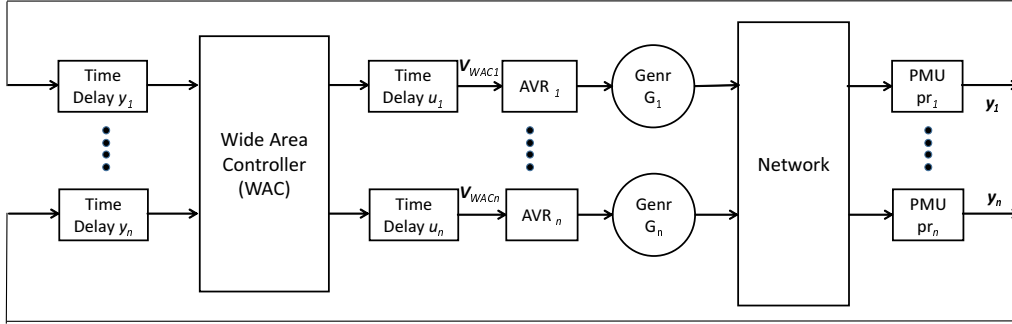


**Figure 1.1: Example of a Centralised Wide Area Controller (WAC)**

the system. This is unrealistic as PSSs do exist in real power systems and their function cannot be ignored.

The **quasi-decentralised** structure involves remote control loops added to existing decentralised control systems, i.e. PSSs, as shown in Figure 1.2 (reference and terminal voltage signals are not shown for simplicity). Some of the generators' (G) decentralised

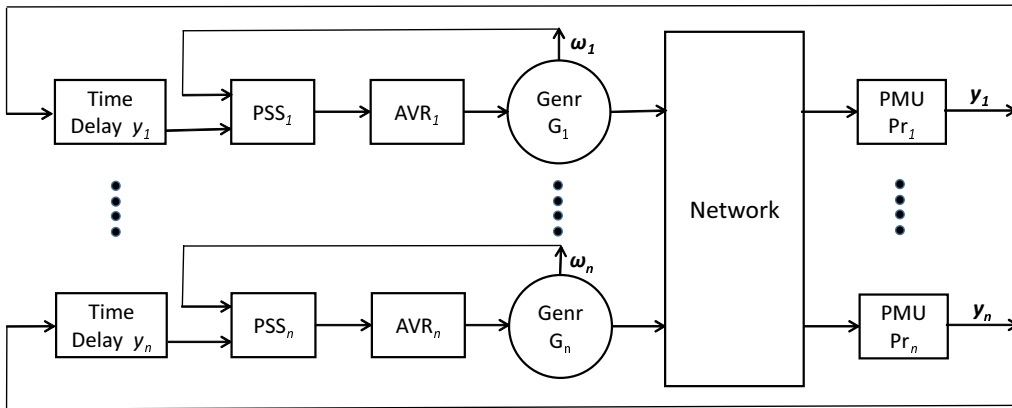


**Figure 1.2: Example of a Quasi-Decentralised Wide Area Controller (Q-WAC)**

controllers receive delayed remote signals ( $Pr_i$ ) from PMUs dispersed in the network in addition to local signals. The main principle of this structure is to strengthen the effectiveness of decentralised control systems using those remote signals. PSSs have a

conventional structure (i.e. lead/lag compensators), which in most cases and are designed based on a fixed operating condition. The structure has significant advantages in terms of reliability and operational flexibility [15, 16, 17, 18]. When the global signal is lost, then the system will be controlled by decentralised controllers using local signals.

The **Two-Level** structure of WAMS based control scheme involves adding a second layer of control systems to existing decentralised control systems resulting in a hierarchical configuration as shown in Figure1.2 [8, 11, 19, 20, 21, 22, 23].

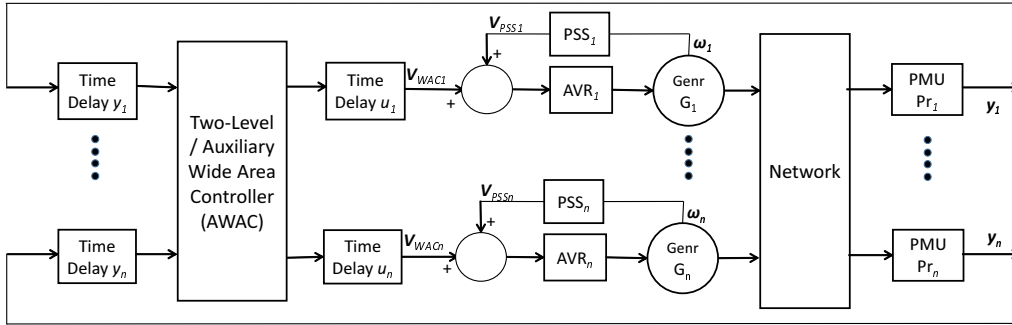


**Figure 1.3: Example of a Auxiliary Wide Area Controller (AWAC)**

Control systems in the first level are fully decentralised and consist mainly of conventional PSSs. PSSs receive local signals, i.e. rotor speed or output power, and add supplementary signals to AVRs modulated with required phase compensation (reference and terminal voltage signals are not shown for simplicity). The Auxiliary Wide-Area Controller (AWAC)(Figure1.3), in the second level receives remote signals,  $[Y_1, \dots Y_n]$ , from  $(Pr_i)$  pre-selected PMUs dispersed in the network and provides supplementary damping actions,  $[V_1, \dots V_n]$ , to  $(G_r)$  pre-selected generators added together with the local control signals from the decentralised / local controllers in the first level [20]. Local controllers, in the lower level layer ensure the minimum level of system stability and the AWAC in the higher level enhances the overall system stability. Both control systems together work to maintain system stability. If local controllers are unable to stabilise the system for certain contingencies the AWAC in the second level can provide additional support. If the AWAC is not functioning, e.g. due to communication link failures, the decentralised layer is still present under these exceptional circumstances thus serving as a fully working backup control system.

### 1.3.2 Controller Design

Several design methods have been proposed to address the problem of power system damping and control using WAMS technology. The simplest one uses a lead-lag compensator, similar to the conventional PSS [8, 12]. This wide-area controller is usually designed in a way that is similar to the conventional PSS, i.e. based on a fixed operating condition of the linearised power system model.  $H_\infty$  control has been often used to ensure the robustness of designed wide-area controller in terms of changing operating conditions and modeling errors [21, 23, 24]. Despite its clear advantages in terms of robustness, it was found that it is prone to the pole-zero cancellation between the system plant and the controller [25]. The  $H_\infty$  based control schemes typically address the worst-case scenario and are therefore intrinsically conservative when dealing with less severe disturbances and model uncertainties.

Another control design based on Linear Quadratic Gaussian (LQG) control has been introduced for WAMS based damping controllers [19]. It is considered to be a cornerstone of the modern optimal control theory and is based on the minimization of a cost function that penalises states' deviations and actuators' actions during transient periods. The essential idea of the LQG control design is to address the intrinsic compromise between an attempt to minimize the error (state deviations) and an attempt to keep control effort at the minimum. The main advantage of LQG control is its flexibility and usability when specifying the underlying trade-off between state regulation and control action. Despite the clear advantages of using LQG control for power system damping the design procedure usually is not straightforward. Specific weights on the states in the LQG cost function are derived, in most cases, according to participation factor (PF) analysis[26, 27]. The states with high participation are given higher weights. As a result of this ad-hoc procedure [24] the damping of the inter-area modes is improved [19, 28] . The cost function weights imposed on these highly participating states however do not directly address the critical inter-area modes. In addition, for power systems with multiple lightly damped inter-area modes these difficulties in the tuning process are magnified and the design becomes complex.

### 1.3.3 HVDC for improving AC system stability

An HVDC system is highly controllable due to the use of power electronics and thus offers fast response times to changes in input. It is possible to take advantage of this characteristic offered by the converter to enhance the transient stability of the AC system. After a disturbance in the power system, the HVDC link can be controlled such that the DC power can be modulated quickly to restore the power balance between generation and load on both sides of the AC system. This action by an HVDC system is usually transitory and does not affect steady state power flow. In some situations ramping up the power is necessary to assist in system stability improvement and this can be done by means of the short term overloading capabilities of the HVDC link taking into account the thermal capacity of the converters. In modern HVDC systems, the rectifiers are overrated and designed to be overloaded for a long time if necessary [1, 29].

HVDC based system stabilizers are usually designed so as to be able to modulate the power proportional to the speed difference between the rectifier and the inverter. The difference in speed means there is a difference in frequency in an interconnected AC systems [30]. In doing so, the HVDC can assist the AC system to damp the power oscillation between interconnected systems. In large scale AC-DC connected and weakly-damped systems, a coordinated technique with optimized PSS and HVDC stabilizers has been proposed to damp the oscillations. The oscillations with high sensitivity to PSS are targetted first utilizing the PSS control and later turning on the HVDC stabilizers to suppress the non-PSS targetted modes in the system with reduced modulated power [31].

### 1.3.4 Input/Output Signal Selection

The WAMS based damping controller depends primarily on the synchronised measurements transmitted from PMUs through the WAMS. Due to the costs associated with the installations of PMUs, communication infrastructure costs in particular, their number should be minimised. The same constraint applies equally to the number of used wide-area control signals sent to generators' exciters. Their number should be minimised to reduce the complexity of the overall control system and also the associated communica-



tion infrastructure costs.

Effectiveness of the WAMS based damping controller is highly dependent on the observability/controllability information carried by its input/output signals, respectively, about the modes of interest. The used sets of reduced measurement and control signals therefore should provide enough observability/controllability information, respectively, about the modes of interest to increase the effectiveness of the controller. The placement of PMUs in the context of WAMS based control schemes, aims to maximise the observability information, from a stability perspective, about the critical electromechanical (i.e. the lightly damped inter-area modes) in the system. Inputs to the WAMS based damping controller are the synchronised measurements taken from these optimally placed PMUs in the network.

The most common method of input/output signal selection for wide-area controller is based on modal controllability/observability factors, respectively. For each individual mode of interest, the measurement signal with the highest modal observability, among all candidate measurements, is selected as the input signal to the wide-area controller. Similarly, for each individual mode of interest the control signal with the highest modal controllability, among all candidate control signals, is selected as the output signal from the wide-area controller. In this widely used method, number of modes of interest decides the maximum number of input/output signals.

## 1.4 Summary of Past Research in the Area

Various architectures of WAMS based control schemes have been proposed in the literature. The centralised architecture [21, 18] ignores the existence of PSSs in the power system and therefore seems unrealistic. The quasi-decentralised and Two-Level or hierarchical structures provide significant advantages in terms of reliability and operational flexibility. They comply with real power systems; the only disadvantage being, the cost of communication infrastructure.

The quasi-decentralised architecture involves conventional PSSs augmented with additional remote signals to increase their effectiveness in maintaining the system stability [15, 32, 17, 33, 18]. The structure of conventional PSSs however is modified and there-

fore limits the application of this type of control scheme. Many utilities are reluctant to change the structure of existing PSSs, hence limiting the use of such a scheme.

The hierarchical architecture retains the advantage of keeping local controllers as they are, while only the remote feedback loops are built on top of them [8, 11, 19, 22]. The wide-area controller on the higher level focuses on stabilising the critical inter-area oscillations whereas the decentralised controllers in the lower level focuses on maintaining the adequate level of system stability. Together the control system in totality is working to ensure the stability of the system.

In a WAMS based control scheme, signals are transmitted from PMUs to the wide-area controller, through the PDC, and then back to generators involve some time delays. These transmission delays depend primarily on the type of communication link used. Time delays can deteriorate effectiveness of the WAMS [14]. Various amounts of delays in the WAMS based damping control schemes have been proposed in the literature [19, 33, 14, 34, 35]. The robustness of a controller due to time delay and loss of remote signal has also been reported [36]. The design of a controller plays an important role in focusing the control effort towards improved damping of certain modes in the system. Several control design methods have been reported in the proposed schemes ranging from conventional structure of PSSs [8, 12], i.e. lead/lag compensator, to more advanced robust control like  $H_2/H_\infty$  [21, 20] and LQG [19]. The LQG control has the advantage of flexibility and usability when specifying the underlying trade-off between state regulation and control action. However, the main difficulty in LQG control design is the handling of multiple inter-area modes simultaneously, as the tuning process of the controller becomes complex and depends primarily on analysis based on participation factors [26, 27].

WAMS based damping controller uses a reduced number of input/output signals can lead to reduced communication infrastructure costs and reduced complexity of the overall control system. The effectiveness of the WAMS based controller increases when its input/output signals have maximum observability/controllability, respectively; with the information about the critical inter-area modes of interest. The most commonly used method to select input/output signals uses the individual modal observability/controllability factors, respectively, for each mode of interest [11, 12].

HVDC transmission systems have also been added with supplementary controls to

aid in system stability improvement due to their fast response times in comparison to mechanical systems. The utility of HVDC systems to damp swings by having controls based on feedback signals from AC-DC systems was recognized in 1964-1966 [37, 38]. In some of the schemes (e.g. Eel River - Hydro Quebec, Square Butte - USA) measured frequency signal is used to damp the low frequency oscillations. Another example to offset the threat of transient instability and cascading outages is the recommendation to use fast power change [39] in an HVDC transmission system. This control scheme also relies on the frequency signal as the input to the feedback control system of the HVDC system.

## 1.5 Aim and Objective of Research

Modern power system networks operate a large number of point-to-point HVDC links to deliver bulk power. The power electronics based controls utilised in HVDC systems assure fast response times in comparison to machines, which can be effectively utilised to enhance the stability of AC system. The main aim of this research is therefore to propose a WAMS based control scheme which is simple to understand and not complex to implement. The Two-Level control structure should comply with current practices in real power systems and enable the PSSs to continue to maintain system stability as before. The added Auxiliary Wide-Area Controller (AWAC) in the higher level should enhance the system stability by focusing only on the critical inter-area oscillations. If the AWAC is controlling the whole power system then the control scheme becomes centralised. An important aim of the research is therefore to analyse the effect of the AWAC on local modes and also on local controllers including the HVDC controls.

The above aim will be achieved with the following research objectives:

- The controller design is critical in directing control effort towards enhancement of system stability and effects on other modes and controllers. The first objective of the research is to have a simple but effective control method so that the designed controller focuses only on stabilising the critical inter-area modes and leaves other modes unaffected.

- Different methods are introduced in the literature for signal selection. The most common method uses modal controllability/observability factors for an input/output pair of signals, respectively, for each individual mode of interest. The second objective is to synthesize a modified feedback signal that has good controllability/observability and leads to a simple control design in stabilising critical inter-area modes.
- Various amounts of signal transmission time delays have been reported in the literature for WAMS controllers. The third objective of the research is that a robust controller design should be applicable for a reasonable time delay. A WAMS based damping controller should be possible to withstand variations in signal transmission time delay along with communication link failures.
- The final objective of the research is to apply a Two-Level WAMS based control scheme on a relatively large simulated power system. The multi-machine power system used is the New England Test System (NETS) and New York Power System (NYPS), augmented in this thesis with multiple HVDC links, such that it has multiple inter-area modes. The special feedback control signal for the AWAC has been synthesised based on observability/controllability, of input/output signals respectively. The research objective is to demonstrate the benefits of using special feedback based WAMS damping controller in enhancing the system stability. The demonstration of the proposed control scheme is done using comprehensive small-signal and transient performance analysis over a wide range of operating conditions involving different network topologies and power transfers.

## 1.6 Outline of the Thesis

- **Chapter 1: Introduction** describes the development of power systems and the issues related to stability of power systems. It also reviews WAMS, some of the architectures of WAMS and their applications. It further describes controller design, and input/output signal selection. A summary of past research is presented along with the aim and contributions of this thesis.

**Chapter 2: HVDC Technologies and Controls** describes briefly, different HVDC technologies (LCC and VSC), various topologies therein and configurations of HVDC systems like point-to-point, multi-infeed and MTDC. It also gives an insight into major control options that can be utilised in such a scheme.

**Chapter 3: Modal Analysis of Power Systems** describes the linearization technique used for analyses of power systems. It also briefly describes various terms, namely eigenvalues, eigenvectors, participation factor and residue analysis that are used for development of control technique. It also dwells on the Electromagnetic Transients, their origin, classification and numerical method used for its simulation.

**Chapter 4: Robust Control of Multi-Infeed Systems** presents a control scheme for damping of multiple inter-area oscillations. A set of special feedback input/output signal pairs is used for the WAMS based damping controller. The multi-input, multi-output (MIMO) damping controller is designed using the modal analysis approach. The effectiveness of the controller in enhancing the system stability is demonstrated using small-signal analysis, root locus plot and transient performance analysis based on a MATLAB/Simulink model for different case studies.

**Chapter 5: Performance evaluation of the proposed controller using Electromagnetic Transient simulation** presents the needed corroboration between the linearised model and the EMT simulation. This chapter lays out the systematic approach adopted to evaluate the small-signal based proposed controller design done using transient stability program provided by the industry standard PSCAD-EMTDC tool. The chapter also demonstrates the effect of increasing controller gains on system stability, thereby showing through simulation that large a increase in controller gain results in system instability.

**Chapter 6: Frequency Scan and Nyquist Stability Analysis** provides a brief insight into the use of the frequency scanning technique to develop a transfer function model of a complex system without compromising accuracy due to simplifications. This chapter also discusses Nyquist analysis, a graphical frequency response analysis technique for single-input, single-output systems and its extension through the Generalised Nyquist Criteria (GNC) to multi-input, multi-output systems. The GNC is used to evaluate the performance of the proposed damping controller and provide qualitative information on

system stability and the critical gains. The results from the GNC analysis will be seen to corroborate the results from the EMT simulation.

**Chapter 7: Conclusions and Future work** summarizes the main conclusions of the research work presented in the thesis. Proposals for future work are also presented based on the various techniques and methodologies implemented and described in the thesis.

# Chapter 2

## HVDC Technologies and Controls

This chapter lays out the brief history of development of HVDC transmission. It also describes the advantages/disadvantages of HVDC transmission, focuses on different HVDC topologies, and the various control options that can be exercised in such schemes. It provides a brief overview on the rationale for the development of HVDC grids.

### 2.1 Introduction

The commercial supply of electric power began in the late 1880s through electrification of the Wall Street area in New York City using Direct Current (DC) technology pioneered by Thomas Alva Edison. Use of DC was the only option for electric supply until Nicola Tesla advocated for the use of Alternating Current (AC). Amidst fierce competition and lobbying for both the DC and AC options, historically known as the War of Currents [40], AC started to win primarily due to more efficient power transmission enabled by use of transformers to step up or step down voltage levels to reduce the power losses. As the need for long distance power transmission grew, the efficiency became a predominant consideration, which worked in favour of AC. AC transmission thus had unmatched popularity and growth while DC was virtually ruled out for power transmission. DC made a comeback in the context of cable transmission, when it was realized that DC could be a cost effective option even for overhead line transmission for very long (beyond 700 km) distance where AC transmission capacity is limited due to stability considerations. As the converter technology evolved over time reducing the costs, this triggered a proliferation

of long distance overhead DC links either embedded between two points within an AC system or interconnecting two separate AC systems.

From the 1970s' till the late 1990s, an HVDC converter was built with either mercury-arc or semiconductor or power electronic (PE) switches, that could be turned on in a controllable way but relied on the polarity reversal of AC system voltage for turning off (or commutation). This type of converter technology is referred to be of the Line-Commutated Converter (LCC) type. The LCC HVDC technology has since matured, and today constitutes the bulk of the installed capacity around the world. After 1997 semiconductor switches, such as Insulated Gate Bipolar Transistor (IGBT), with both controlled turn-on and turn-off capability, became commercially available at high power ratings. This enabled the use of Voltage-Sourced Converter (VSC)-based HVDC technology. The VSC technology offered significant advantages over its LCC counterpart; such as, reliable operation with weak AC systems, low cost and footprint of converter stations, use of lighter, and stronger cables which makes VSC attractive for offshore transmission. Despite this promise, the penetration of VSC technology is limited by its power ratings (under 1 GW) compared to LCC (up to 8000 MW). Rapid development in the VSC technology since has resulted in availability of relatively higher ratings.

### **2.1.1 Advantages of HVDC over HVAC**

Some of the notable advantages of HVDC over HVAC are enumerated below [41]:

- Submarine power transmission,
- Long distance overhead transmission,
- Interconnecting two asynchronous AC grids,
- Controllable power exchange between two AC grids during power trading,
- Less right of way (ROW) requirement,



### 2.1.2 LCC HVDC

The basic building block for LCC-HVDC is a PE switch - thyristor. A thyristor conducts when a gate pulse is provided and a positive voltage is applied between the anode and the cathode terminals. A thyristor cannot be turned off by removing the gate pulse, it turns off when the current through it goes below the holding current. The commutation of the current from one thyristor to another depends on the firing sequence, source inductance, and the line voltage applied across the thyristor. Thyristors are triggered in a cyclic order by providing appropriate firing pulses to the gate terminal of the thyristor to obtain a DC voltage at the output. This DC voltage can be controlled by the firing angle of the gate pulses. An example of a thyristor based converter is shown in Fig.(2.1). In the LCC converter, *the direction of the current cannot be reversed* but the voltage polarity at the converters can be reversed [1].

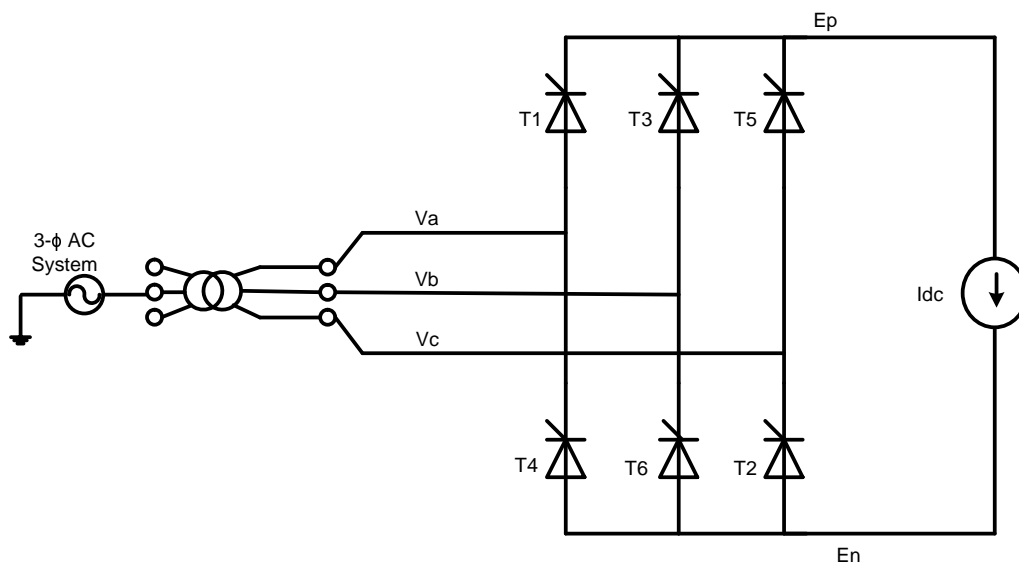
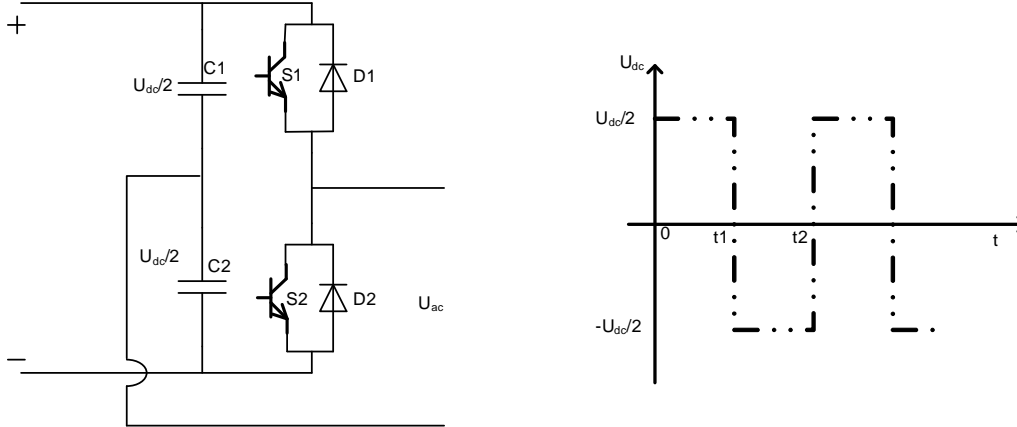


Figure 2.1: Example of a Line commutated Converter (LCC)

### 2.1.3 VSC-HVDC

In the VSC converter, the PE switch as basic building block is an IGBT with an antiparallel diode. The IGBT can be turned on by providing a gate pulse as shown in Fig.(2.2). Additionally, unlike the thyristor in the LCC, the IGBT turns off on removal of the gate pulse. The switching pulses can be produced by any of the Pulse Width

Modulation (PWM) technique such as Sinusoidal PWM, Space Vector Modulation, or Harmonic Elimination. Compared to the conventional LCC based HVDC, VSC-HVDC systems are less affected by the ac system strength [42, 43]. As the direction of power can



**Figure 2.2: Example of Voltage Source Converter (VSC)**

be changed by current reversal, hence they are suitable for use in a DC grid. Moreover, there is less or no filter requirements due to less harmonics, and provides independent control of real and reactive power.

### 2.1.4 Comparison between LCC and VSC

While LCC is a mature technology and its associated systems and electronics are well developed, VSC technology is relatively recent and evolving. Although VSC offers many advantages over LCC; the constraint of current carrying capacity of PE switch and unavailability to have a commercial DC circuit breaker have impeded the scale up of this technology. Each of the two technologies has their advantages and disadvantages; besides the differences enumerated in previous sections, a comparison between the two is provided in Table 2.1 below:

## 2.2 Configurations and Topologies

The bulk of the HVDC transmission systems across the continents deliver power from point-to-point. In addition to point-to-point operation, HVDC systems can also operate as multi-terminal HVDC (MTDC) or as multi-infeed (MI-HVDC) systems. An HVDC

	LCC HVDC	VSC-HVDC
Control	Semiconductors can withstand voltage in either polarity	Semiconductors can pass current in either direction
	Output voltage can be either positive or negative polarity to change power direction	Output voltage polarity does not change
	Current direction does not change	Current direction changes to change power direction
	Stores energy inductively	Stores energy capacitively
	Semiconductors turn on by control action	Semiconductors turn on and off by control action
	Turn-off and “commutation” rely on the external circuit	Turn-off independent of the external circuit
Power Rating	High power capability	Low power capability
Overload Capability	High	Low
AC system Strength	Requires strong AC system	Operates into a weak AC system
Power control	Active power only	Active and reactive power
Reactive Power support	Requires large amount of reactive power	Does not require reactive power
Harmonics	Generates harmonics, AC & DC filters needed, Large site area required	Insignificant lower order harmonics, no filters needed, Smaller site area required
Converter Transformer	Special transformer needed	Conventional transformer works
Cost of converter	Lower cost	Higher costs (about 10% - 15% more)
Cables	Requires MI cables; High voltage capability	Ideal for use of XLPE cables; Low voltage capability

**Table 2.1: Comparison between LCC and VSC-HVDC systems**

system with more than two points of connection between the converters and AC systems is referred to as an MTDC system. When an HVDC system, either shares a common AC bus or is connected to the buses that are electrically close, the system is referred to as a multi-infeed (MI-HVDC) system. These configurations can either be independent or

embedded within an existing AC system. An example of these systems is given below:

- **Examples of Existing LCC MTDC Systems.** As of January 2017, there are only two operational systems in the world, namely:
  - Sardinia-Corsica-Italy (SACOI) interconnection [44, 45].
  - Hydro-Quebec-New England interconnection [46].
- The existing point-to-point HVDC links either LCC or VSC form MI-HVDC, with the exception of a 5-terminal VSC-HVDC system that has been commissioned by China [47].

The HVDC systems can have any of the following topologies [29], as shown in Figs.2.3 and 2.4 below:

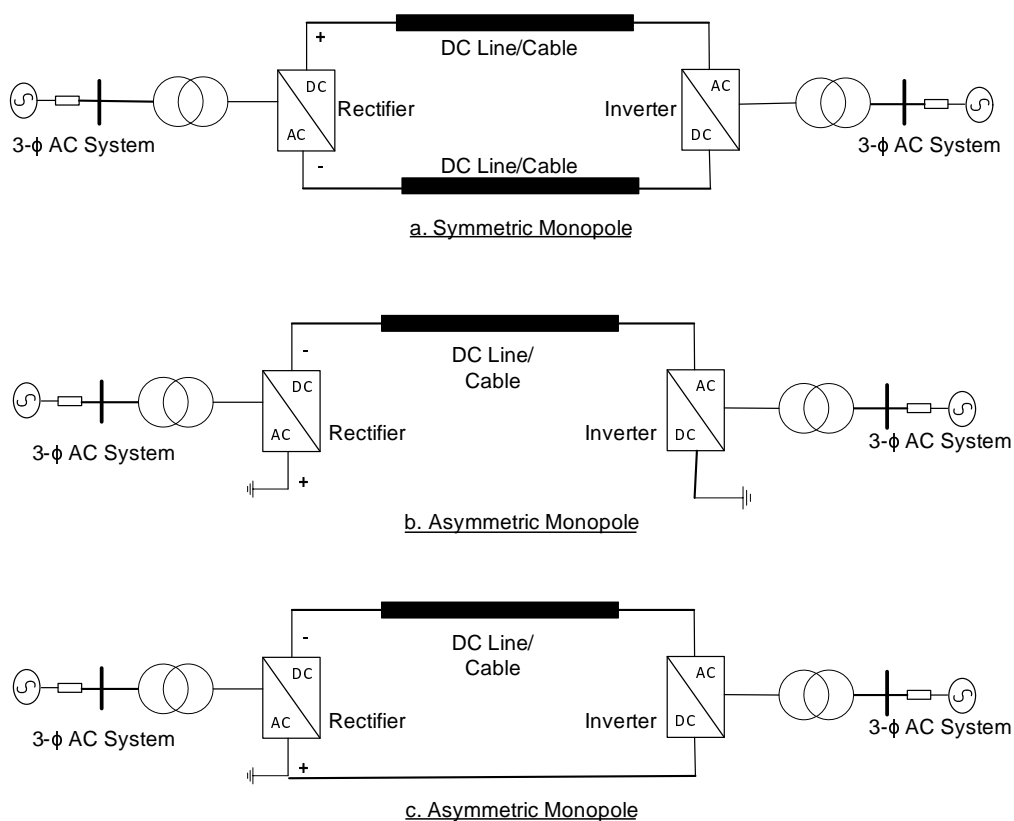


**Figure 2.3: Example of possible Topologies of Monopole HVDC System**

### 2.2.1 Monopole

- a. Symmetric Monopole. In this configuration shown in Fig.2.3(a), the center of the DC bus of each converter station is grounded and the converter stations are connected to two transmission lines at equal and opposite potentials.
- b. Asymmetric Monopole. In this configuration, each converter station is connected to a transmission line (usually negative polarity for overhead lines) while the current returns through the ground Fig.2.3(b) or a metallic return path Fig.2.3(c). For ground return configuration, each station is grounded whereas the metallic return needs only one grounding point. Metallic return is used under situations where ground return is not acceptable due to high earth resistivity, interference with underground metallic installations, or maritime regulations. The metallic return path has a very low insulation requirement. A negative polarity for the overhead transmission line is preferred over the positive polarity due to reduced corona losses and radio interference. This configuration suffers from reliability considerations in case of outage of the converter or degradation of insulation in one line is treated probabilistically as N-1. It can however be commissioned as the first phase of a bipolar installation.

### 2.2.2 Bipole

In a bipolar HVDC system, each converter station has two independent converter bridges or a group of bridges as shown in Fig. 2.4. One terminal of the DC bus of an independent group is grounded, and the other is connected to the transmission line with positive or negative polarity. Each converter pole can operate independently. Under normal conditions, the positive and the negative poles carry equal current and no current flows through the ground return path. In overhead lines, it also produces considerably less harmonic interference with nearby lines and telephonic interference compared to the asymmetric monopole link. A bipole system has one converter in each pole with a grounded midpoint (usually with a metallic return conductor) as shown in Fig.2.4. In the event of the outage of a converter pole or outage of one of the transmission lines, the other pole can be overloaded based on the reserve capacity of the converters, transmission lines, ambient condition, and duration. The converters can be operated with a reserve capacity so that

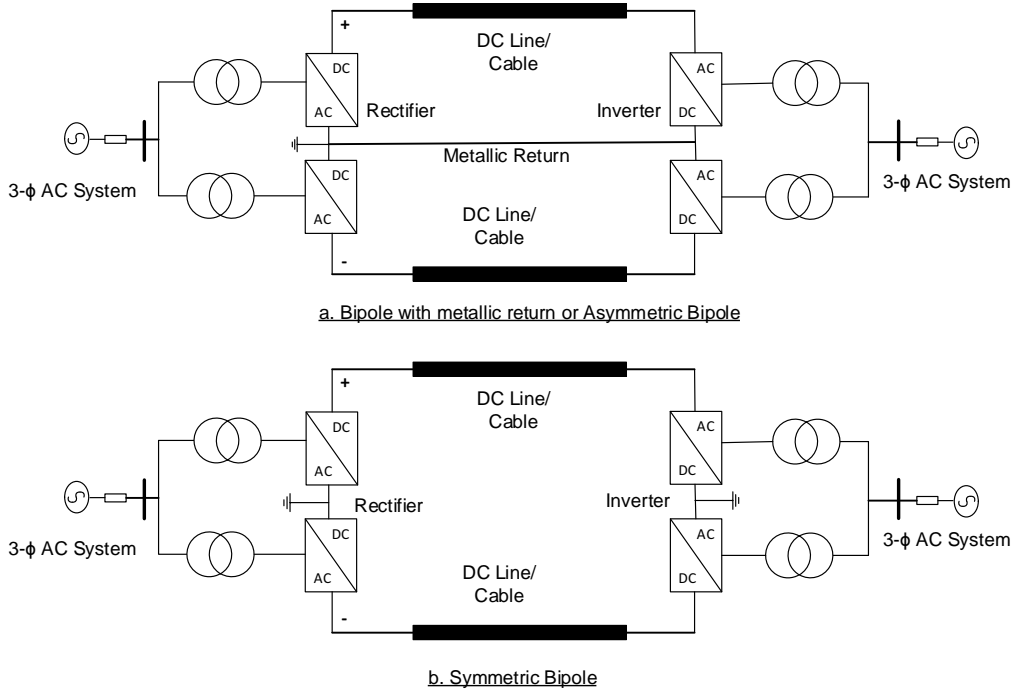


**Figure 2.4: Example of Various Topologies of Bipole HVDC System**

they can be overloaded by 200% for a short time [48]. The ground return current under such conditions will be equal to the current flowing through the healthy transmission line. When ground return is not viable, a metallic return can be used as shown in Fig.2.4(a). This configuration is called the asymmetric bipole with metallic return [48]. The insulation requirement of the metallic return pole is minimal. This line may also act as a shielding wire for overhead transmission system. From the reliability standpoint, if the outage of the converter or degradation of insulation in one line is considered as (N-1), the asymmetric bipolar link is equivalent to the double circuit line in AC systems.

## 2.3 Basic converter control scheme

In the case of LCC operating as a point-to-point HVDC link, the two converter (rectifier and inverter) stations work under different modes of operation. It is a common practice for the rectifier to control the DC line current and the inverter to control the DC voltage or commutation angle under normal operating conditions. The VSC-HVDC on the other hand offers more degrees of freedom in control options.

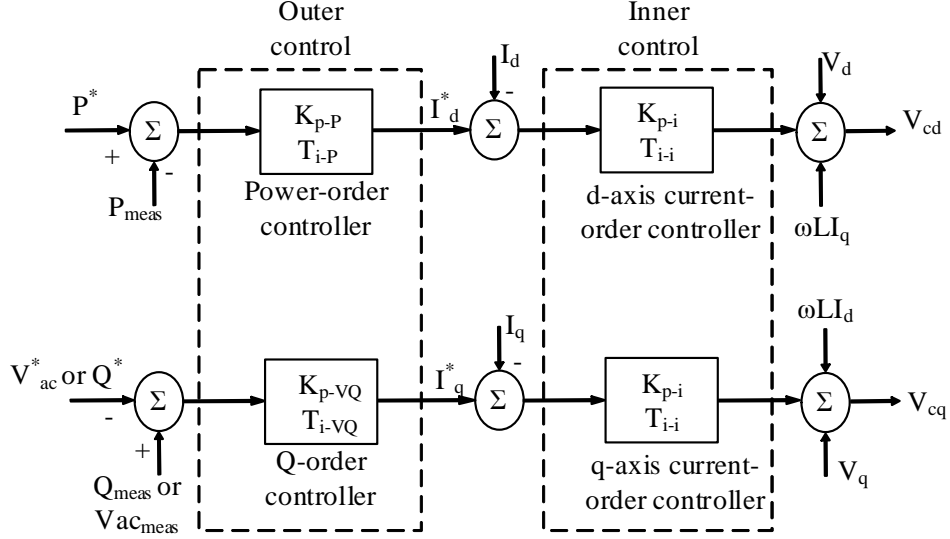


**Figure 2.5: Example of d-q control scheme for a VSC-HVDC converter**

In a VSC point-to-point HVDC link, generally the converter station acting as rectifier controls the DC voltage and point of coupling AC voltage or reactive power ( $Q$ ). The other converter, at the receiving end, which at that moment is acting as an inverter controls the real power ( $P$ ) and either the grid AC voltage or  $Q$ . A typical control scheme for one converter in a point-to-point VSC-HVDC transmission scheme is shown in Fig. 2.5. The control is established in d-q coordinates, where the d-axis current ( $i_d$ ) determines the real current component into the converter, and the q-axis current ( $i_q$ ) determines the reactive current component. Depending on the converter type, the d-axis current order could be used to control real power order ( $P$ ) and the q-axis to maintain AC voltage ( $V_{ac}$ ). As only one converter can dictate the power order, the remote converter would then be operated with  $i_d$  controlling the DC link voltage ( $V_{DC}$ ) [49].

## 2.4 Control schemes for multi-terminal VSC-HVDC system

The various degrees of freedom available with VSC-HVDC systems have led to development of different control options that are enumerated below.

- Master-Slave or Fixed Voltage Control

- Voltage Margin Control
- Voltage Droop Control

The VSC-HVDC converters when operating as a part of multi-terminal operation can operate on any of the above schemes.

### 2.4.1 Master-Slave or Fixed Voltage Control

An HVDC grid will have multiple converters interconnected depending on the topology of the network. The converters and associated equipment are called as a terminal, while the transmission medium such as overhead lines or cables are part of DC network. In this type of control setup as shown in Fig.(2.6), some converters will be responsible for feeding power to the dc network, while other converters will be drawing power. Due to various degrees of freedom available for control, converters have to be assigned controls for stable operation. In this type of control [50, 51, 52] one of the many converter stations within an MTDC grid could control the DC link voltage. This converter would also supply resistive losses in the DC link and thus act as a slack converter.

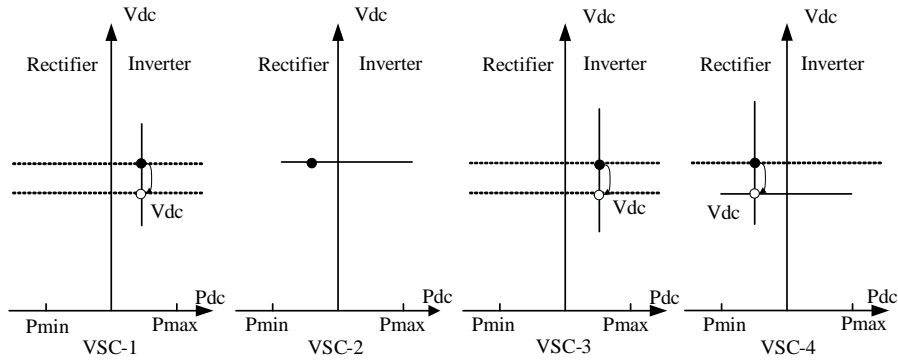


**Figure 2.6: Example of Fixed Voltage Control**

The remaining converter stations would control the active power exchange with the respective AC systems. Additionally, all the converters could control either the AC voltage or reactive power exchange at their respective AC side. In this case the rectifier at VSC-2 is tasked to control DC link voltage (at set point marked ●, in Figure2.6) and inverters are maintaining power exchange. Any change in the set point for DC voltage will not effect the power exchange, as long as VSC-2 is in service. But, such a control



setup has a serious drawback, in that, if the only converter (VSC-2) controlling the DC voltage is out of service for any reason, then the entire grid becomes unstable as no other converter is tasked for this job.

## 2.4.2 Voltage Margin Control

Realising the limiting case mentioned in the previous control mechanism, voltage margin control was proposed in [53]. In this type of control setup, one converter is assigned to control the DC voltage of the MTDC grid, but the secondary task of DC voltage control is also assigned to one or many other converters in the network. During assignment of the secondary task, a preset margin as shown in Fig.(2.7), is attributed to each of the converters at which point the designated converter takes over the task of regulating the DC voltage [51, 52, 54]. The margin is chosen judiciously, as too small a margin will result in frequent mode shift, while on the other hand a very large margin will result in under utilization of the MTDC grid. It becomes difficult to choose voltage margin when the number of converters in the system increases.

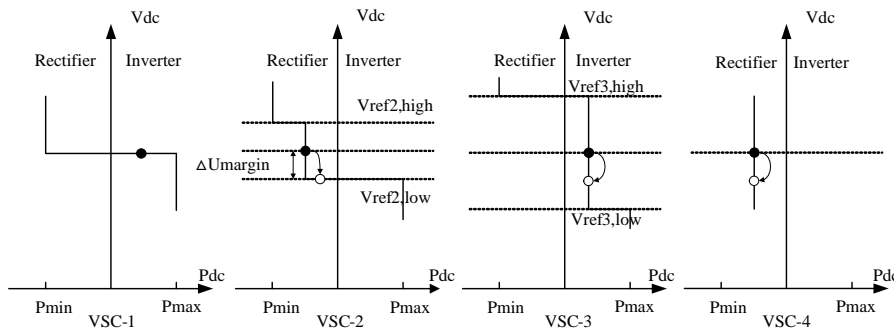


Figure 2.7: Example of Voltage Margin Control

## 2.4.3 Voltage Droop Control

In both fixed voltage and voltage margin controls, with the outage of one converter, the converter under DC voltage control picks up the entire burden of the power imbalance. This is not desirable as the AC system connected to that particular converter station will experience a large change. It is desirable that following an outage of one or more converters, all the remaining converters should share the resulting power imbalance in a

certain proportion. Fig.(2.8) shows a DC link Voltage - active power droop control [51, 52] that can be used to modify reference values of DC link voltage for stable operation.

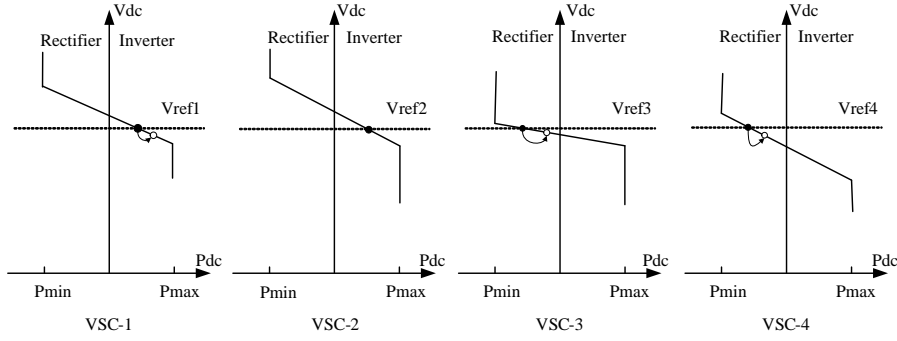


Figure 2.8: Example of Voltage Droop Control

## 2.5 Supplementary Control

- a. Power Oscillation Damping (POD). In addition to the various control schemes mentioned above, there is a growing interest in tapping into the unused potential of power oscillation damping by HVDC system. As explained in Section 2.1, fast acting PE switches in HVDC converters enable them to rapidly modulate power injection at non-generator bus (the location of HVDC converters) which aids in damping out power oscillations [55, 56, 57]. This aspect of rapid injection of power to control swings is used in POD controllers. The schematic of the controller based on compensator for this control is represented in Fig.2.9.

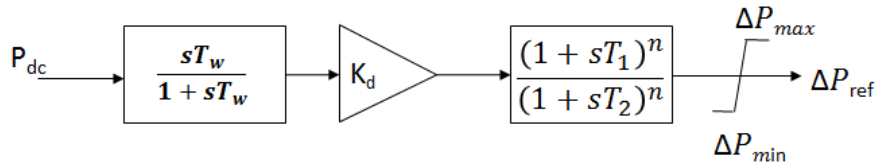


Figure 2.9: Example of POD as supplementary control

- b. Frequency control. The total power generated in a power system must match the power consumed by the loads plus the losses in the network on an instantaneous basis so as to maintain the grid frequency. The system frequency increases if the generation is

more than the demand/load, and reduces if the load exceeds the generation. Collective response of all the components (e.g., generators, loads, etc.) between supply-demand mismatch is known as *system frequency response*. The system frequency response following a large disturbance is divided into the following categories: inertial, primary frequency response, and secondary frequency response or automatic generation control (AGC) [58, 52]. Large scale integration of wind farms into power systems has led the regulators in Europe [59] and Quebec, Canada [60] to necessitate that they contribute to frequency support as part of inertial response. There are multiple approaches to achieve this, one approach is to quickly increase the torque in response to reduction in the grid frequency, which causes the turbine to slow down and release the kinetic energy stored in the blades. Another approach is to allow the turbine to accelerate initially before increasing the torque command [61]. In essence, these controls are possible due to the fast acting PE switch which have a much smaller time constant in comparison to conventional machines.

## 2.6 Summary

This chapter provides an overview of the main HVDC converter technologies, namely LCC and VSC. It briefly describes the basics and workings of both types of converters and also gives a comparison between them. The chapter also described different configurations and topologies that are possible while setting up an HVDC system. Additionally, this chapter also briefly explains various control concepts that can be utilised in the control of HVDC either as point-to-point or in the grid form. Some of these control concepts have been implemented in the simulations carried out as part of this research.

# Chapter 3

## Analytical and Simulation Tools

This chapter briefly describes the linearised power system model described through modal analysis. The characteristics of the system model are presented through defining parameters such as; eigenvalues, right and left eigenvectors, participation factor, modal controllability and observability, and residue [1, 26, 62]. A simplified State Variable Model (SVM) for an example ac system has been utilised to develop the control mechanism.

### 3.1 Analytical Tools

#### 3.1.1 Linearization of Power System Model

The SVM for the power system is based on the classical machine model, as the aim of this research is to damp out electro-mechanical oscillations by modulating dc power through HVDC. The following assumptions have been made to develop at the SVM:

- a. Generators are represented by a classical machine model and the prime mover input is held constant ( $\Delta P_m = 0$ ),
- b. Transmission lines are lossless,
- c. Active power drawn by the load is constant, reactive power is of constant susceptance type.
- d. The VSC-HVDC link is modelled as a simple current injection device. The dynamics of VSC converters are neglected as they pertain to high frequency [43] range and our

aim is to study the effect of slow electro-mechanical oscillations.

A power system can be modelled using sets of non-linear Differential-Algebraic Equations (DAEs). The set of differential equations describes the dynamic behaviour of the system and can be represented in vector-matrix format as follows:

$$\Delta \dot{\mathbf{x}} = \mathbf{A}\Delta \mathbf{x} + \mathbf{B}\Delta \mathbf{U} \quad (3.1)$$

$$\Delta \mathbf{y} = \mathbf{C}\Delta \mathbf{x} + \mathbf{D}\Delta \mathbf{U} \quad (3.2)$$

in the above (3.1) and (3.2),

$\Delta \mathbf{x}$  is the state vector of dimension  $n$ ,

$\Delta \mathbf{y}$  is the output vector of dimension  $m$ ,

$\Delta \mathbf{U}$  is the input vector of dimension  $r$ ,

$\mathbf{A}$  is the state or plant matrix of size  $n \times n$

$\mathbf{B}$  is the control or input matrix of size  $n \times r$

$\mathbf{C}$  is the output matrix of size  $m \times n$

$\mathbf{D}$  is the feed forward matrix, which defines the proportion of input which appears directly in the output, it is of size  $m \times r$ .

The equation

$$\det(\lambda I - A) = 0 \quad (3.3)$$

is referred to as the characteristic equation of matrix  $A$  and the values of  $\lambda_i$  which satisfy the characteristic equation, are the eigenvalues of matrix  $A$ . As the matrix  $A$  is an  $n$  by  $n$  matrix, it has  $n$  eigenvalues,

$$\lambda = \lambda_1, \lambda_2, \dots, \lambda_n \quad (3.4)$$

with the assumption that  $\lambda_i \neq \lambda_j, i \neq j$ .

### 3.1.2 Modal Analysis

#### Eigenvalues and Eigenvectors

The eigenvalues of the  $A$  matrix are given by the values of the scalar parameter  $\lambda$  for which there exist non-trivial solutions to the equation

$$A\phi = \lambda\phi \quad (3.5)$$

where  $\phi$  is an  $n \times 1$  vector. For any eigenvalue  $\lambda_i$ , the  $n - 1$  column vector  $\phi$  which satisfies equation (3.1) is called the *right eigenvector* of  $A$  associated with the eigenvalue  $\lambda_i$ . Therefore, we have:

$$A\phi_i = \lambda_i\phi_i \quad i = 1, 2, 3, \dots, n \quad (3.6)$$

$$\phi_i = [\phi_{1i} \ \phi_{2i} \ \dots \ \phi_{ni}]^T \quad (3.7)$$

The right eigenvector associated with a mode accounts for the mode shape. It defines the relative distribution of the mode through the system dynamic states. Each component of the right eigenvector contains information about the observability of the associated mode in the state variable corresponding to that component.

The problem of entries in an eigenvector is that they cannot be compared because they have different units and scaling, that is, entries in the eigenvector corresponding to state variables such as speed, angle, flux, voltage, etc. cannot be compared. Eigenvector has the same dimensions as the state variable and therefore is unit dependent.

Similar to equation (3.6), the  $n$ -row vector  $\psi_i$  which satisfies

$$\psi_i A = \lambda_i \psi_i \quad i = 1, 2, 3, \dots, n \quad (3.8)$$

$$\psi_i = [\psi_{i1} \ \psi_{i2} \ \dots \ \psi_{in}] \quad (3.9)$$

is called the left eigenvector associated with the eigenvalue  $\lambda_i$ . The left eigenvector associated with a mode gives the distribution of the states within a mode. It has a direct effect on the amplitude of a mode excited by a specific input. Each component of the left eigenvector contains information about the controllability of the associated mode

using the state variables corresponding to that component. The left and right eigenvectors corresponding to different eigenvalues are orthogonal. In other words, if  $\lambda_i$  is not equal to  $\lambda_j$ , then

$$\psi_j \phi_i = 0 \quad (i \neq j) \quad (3.10)$$

But in the case of eigenvectors corresponding to the same eigenvalue,

$$\psi_i \phi_i = K_i \quad (3.11)$$

where  $K_i$  is a non-zero constant. Thus it is a normal practice to *normalize* these vectors, so that

$$\psi_i \phi_i = 1 \quad (3.12)$$

Modal matrices based on individual vectors  $\Psi$ ,  $\Phi$  and  $\Lambda$  are used to clearly express the eigenproperties of  $A$ . These matrices are defined as follows:

$$\Phi = [\phi_1 \ \phi_2 \ \dots \ \phi_n] \quad (3.13)$$

$$\Psi = [\psi_1^T \ \psi_2^T \ \dots \ \psi_n^T] \quad (3.14)$$

$$\Lambda = \text{diagonal matrix of eigenvalues } \lambda_1, \lambda_2, \dots, \lambda_n. \quad (3.15)$$

### Participation Factors

The right and left eigenvectors can not be used individually to identify the relationship between the states and the modes as the elements of the eigenvectors are dependent on the units and scaling associated with state variables. The concept of a participation matrix ( $\mathbf{P}$ ) which combined the right and left eigenvectors was proposed [26, 27].

$$\mathbf{P} = [p_1 \ p_2 \ \dots \ p_n] \quad (3.16)$$

Its elements were termed participation factors (PF). The PF measures the degree of participation of a state variable in a mode. The participation factor for the  $i^{th}$  state in

the  $j^{th}$  mode is calculated as follows:

$$p_{ij} = \phi_{ij}\psi_{ji} \quad (3.17)$$

The right eigenvector element,  $\phi_{ij}$ , measures the activity of the  $i^{th}$  state in the  $j^{th}$  mode while the left eigenvector element,  $\psi_{ji}$ , weighs the contribution of this activity to the mode. Thus the participation factor  $p_{ij}$  measures the net participation of the  $i^{th}$  state in the  $j^{th}$  mode. The participation factor is a measure of the sensitivity of the  $j^{th}$  eigenvalue to a change in the  $i^{th}$  diagonal element of the matrix A . The participation factors are dimensionless and are associated exclusively with the mode. Since they deal only with state variables and do not include inputs and outputs, their use for PSS siting is considered necessary but not sufficient [63].

### Modal Controllability and Observability

Let  $\lambda_i = \sigma_i \pm j\omega_i$  be the  $i$ -th eigenvalue of the state matrix A. The real part of the eigenvalues gives the damping, and the imaginary part gives the frequency of oscillation. The frequency of oscillations in Hz is given by

$$f = \frac{\omega}{2\pi} \quad (3.18)$$

which represents the actual or damped frequency, while the damping ratio is given by

$$\xi = \frac{-\sigma}{\sqrt{\sigma^2 + \omega^2}} \quad (3.19)$$

the damping ratio  $\xi$  determines the rate of decay of the amplitude of the oscillation. The oscillatory modes that having damping ratio less than 3% are said to be critical. Using the left and right eigenvectors, the set of coupled differential equations, shown in equations (3.1) and (3.2) can be decoupled using a vector  $z$ , as follows:

$$\dot{\mathbf{z}} = \Lambda \mathbf{z} + \mathbf{B}' \Delta \mathbf{u} \quad (3.20)$$

$$\Delta \mathbf{y} = \mathbf{C}' \mathbf{z} + \mathbf{D} \Delta \mathbf{u} \quad (3.21)$$



where,

$$\dot{\mathbf{z}} = \Phi^{-1} A \Phi \mathbf{z} \quad (3.22)$$

$$\Lambda = \Phi^{-1} A \Phi \quad (3.23)$$

$$B' = \Phi^{-1} B = \Psi B \quad (3.24)$$

$$C' = C \Phi \quad (3.25)$$

To modify a mode of oscillation by feedback, the chosen input must excite that mode and it must be visible in the chosen output. The measures of these two properties are controllability and observability, respectively. If in equation (3.24) the  $i$ -th row is zero, the inputs have no effect on the  $i$ -th mode, then the  $i$ -th mode is said to be *uncontrollable*. The  $i$ -th mode is controllable by the  $j$ -th input if the product of  $\psi_i B_j$  is not zero. Similarly, the  $i$ -th mode is *observable* in the  $k$ -th output if the product of  $C_k \phi_i$  is not zero. However, if the  $i$ -th column of  $C'$  in equation (3.25) is zero, then the corresponding mode is *unobservable*. This explains why sometimes poorly damped modes are not detected by observing the transient response of a few monitored quantities.

Therefore, the  $n \times r$  matrix  $B' = \Phi^{-1} B = \Psi B$  is also called the *mode controllability* matrix, and the  $m \times n$  matrix  $C' = C \Phi$  the *mode observability* matrix [1].

If a mode is either uncontrollable or unobservable, the feedback between the output and the input will have no effect on the mode. A mode of the interest must be both controllable by the chosen input and observable in the chosen output for a feedback control to have any effect on the mode. Therefore, determination of suitable feedback variables is an important objective in any damping controller design procedure.

If the modal transformation is applied to the transfer function representation, assuming zero feed-forward matrix  $D$ , and if  $G(s) \left( \frac{y(s)}{u(s)} \right)$ , where  $y(s)$  is the output and  $u(s)$  the input; is expanded in partial fractions, then

$$G(s) = C \Phi [sI - \Lambda]^{-1} \Psi B = \sum_{i=0}^n \frac{R_i}{s - \lambda_i} \quad (3.26)$$

where,  $\Lambda$  is a diagonal matrix and  $R_i = c \phi_i \psi_i b$

Each term in  $R_i$ , of the summation is a scalar called a residue. The residue  $R_i$  of a

particular mode  $i$  gives the measure of that mode's sensitivity to a feedback between the output  $y$  and the input  $u$ . The residue is the product of the mode's observability and controllability.

The residues are related to the controllability and observability factors as follows [64].

$$R_i(k, l) = c_l \phi_i \psi_i k_l \quad (3.27)$$

where  $i$  refers to system modes,  $k$  refers to system inputs, and  $l$  refers to system outputs. A multi-input multi-output (MIMO) linear system with  $n$  eigenvalues,  $m$  inputs, and  $p$  outputs, has  $n$  matrices of residues with dimension  $m \times p$ .

## 3.2 EMT Simulation

A power system is largely non-linear and dynamic in nature due to operation of circuit breakers, clearance of faults, constant load-generation adjustments, and due to atmospheric disturbances, such as, lightning. Since the system is operating at steady state, after the disturbance it should, settle to a new acceptable steady state in a short duration. A new stable steady state can only be achieved by the redistribution of the electromagnetic and electromechanical energy in the power system, which cannot happen instantaneously, but takes some time period which results in transients. These transients may subject the system to higher stress resulting from increased current, voltage and mechanical perturbations to the rotors. The analysis of such large excursions is outside the validity of a small signal model, for example. Current, voltage, speed, torque, frequency, in the electrical systems is the main objective of Electro Magnetic Transient (EMT) analysis and simulation of transients in power systems. There are tools such as PSCAD/EMTDC, RTDS, EMTP-RV MicroTran etc. which are considered industry standard and are widely used for such analysis.

### 3.2.1 Classification of Transients

Transients can be broadly classified as follows [65, 66, 67]:

- *Atmospheric Transients* such as Lightning, Geomagnetic storms due to enhanced solar activity,
- *Switching Transients* such as those due to opening and closing of breakers, load rejection and switching of power electronic devices.

Alternately, transients can also be classified as:

- *Electromechanical Transients* resulting from interaction between the electrical energy stored in the system and the mechanical energy stored in the inertia of the rotating machines (i.e, generators and motors).
- *Electromagnetic Transients* due to the interaction between the electrical fields of capacitance and magnetic fields of inductances in power systems. The electromag-

netic phenomena may appear as travelling waves on transmission lines, cables, bus sections, and oscillations between inductance and capacitance.

Professional bodies (CIGRE, IEC and IEEE WG) have classified transients based on various criteria. Tables 3.1, 3.2 and 3.3 below provide a quick reference on classifications based on time duration, frequency range of transient, and classification of frequency ranges [65, 67].

Nature of Transient Phenomenon	Time Duration
Lightning	$0.1\mu\text{s}$ - 1.0ms
Switching	$10\mu\text{s}$ to less than 1s
Subsynchronous Resonance	0.1ms - 5s
Transient Stability	1ms - 10s
Dynamic Stability	0.5 - 1000s
Tie Line Regulation	10 - 1000s
Daily load management, operator action	up to 24h

**Table 3.1: Time Duration of transient phenomena in electrical systems**

The transient analysis of a power system requires it to be modelled in the State Variable (SV) form. A power system network is represented by its differential equations converted to passive elements (R,L and C) by making use of circuit reductions; loop and mesh equations; and Thévenin, Norton, maximum power transfer, and superposition theorems [68, 69, 41]. The synchronous machine is modelled by its state equation with current source interface to the network [70]. An example of circuit reduction is shown in Figure 3.1. Once the network is reduced and represented in the SV form; a step-by-step time-domain solution (simulation) can be carried out. Various numerical integration techniques such as the following can be utilized to simulate:

- Forward Euler
- Backward Euler
- Trapezoidal Method.
- Range-Kutta Method.

These integration methods are also categorized as follows:

<b>Origin of Transient</b>	<b>Frequency Range</b>
Restrikes on disconnectors and faults in GIS	100kHz - 50 MHz
Lightning surges	10kHz - 3MHz
Multiple restrikes in circuit breakers	10kHz - 1 MHz
Transient Recovery Voltage (TRV):	
Terminal faults	50/60Hz - 20kHz
Short line faults	50/60Hz - 1000kHz
Fault clearing	50/60Hz - 3kHz
Fault initiation	50/60Hz - 20kHz
Fault energization	50/60Hz - 3kHz
Load rejection	0.1Hz - 3kHz
Transformer energization	(dc)0.1Hz - 1kHz
Ferroresonance	(dc)0.1Hz - 1kHz

**Table 3.2: Frequency Ranges of Transients**

<b>Group</b>	<b>Frequency Range for Representation</b>	<b>Shape Designation</b>	<b>Representation mainly for</b>
I	0.1Hz-3kHz	Low-frequency Oscillations	Temporary overvoltages
II	50/60Hz-20kHz	Slow front surges	Switching overvoltages
III	10kHz-3MHz	Fast front surges	Lightning overvoltages
IV	100kHz-50MHz	Very fast front surges	Restrike overvoltages GIS

**Table 3.3: Classification of Frequency Ranges [65]**

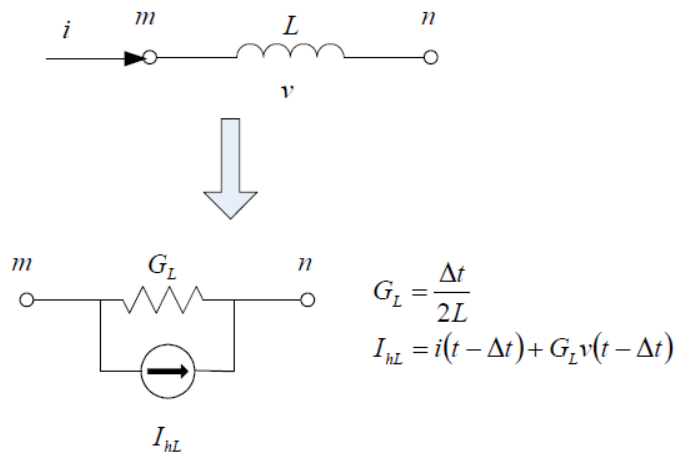


**Figure 3.1: Example of an Inductor element represented in RLC form in EMT simulation**

- Explicit Methods (which include Forward Euler and R-K Method)
- Implicit Methods (such as Backward Euler, Trapezoidal, etc).

In an *Explicit Method* the value of a dependent variable ( $x$ ) is calculated at any time step  $t$  based on the knowledge of previous value of ( $x$ ) from the previous time step. However, a significant limitation of this method is that they are not numerically A-stable [69]; hence the length of the integration time step ( $\Delta t$ ) is restricted by the small time constant of the system. While in an *Implicit Method* the value of the dependent variable ( $x$ ) is calculated as a function of its value at the previous time step and the current value (which is unknown), thus an implicit equation must be solved. The Trapezoidal Rule is most commonly used in EMT simulation since it is easy to program, and is numerically A-stable [68, 69]. In an EMT simulation model of a multi-phase system, all phases are modelled thus, unbalanced phenomena and transient behaviour of the system are well represented. Since EMT simulation uses a very small time step, typically ( $50 \mu s$ ), it can capture all the transients related to PE and switching taking place in a network.

### 3.3 Summary

In this chapter modal analysis of linearised power system model was introduced. A brief explanation of the physical interpretation of eigenvalues of the system model in the

context of power system stability was discussed. Importance of the use of right and left eigenvectors, and participation factors in small signal stability studies was addressed. Concept of modal controllability and observability, and residues which are used in power system stability studies for the selection of controller's input and output signals were laid out. A brief overview of EMT simulation, its characterization, and the various numerical integration methods that can be used in the process were mentioned. The modal analysis and EMT simulation techniques presented in this chapter have been applied to the studies carried out in this thesis.

# Chapter 4

## Robust damping controller design for AC-DC systems

### 4.1 Introduction

This chapter presents a simple but effective inter-area damping controller design based on special feedback signal, that is suitable for WAMS based application. This small-signal analysis based design approach enables damping of multiple inter-area oscillations by the modulation of real power ( $P$ ) through HVDC systems enabled with an Auxiliary Wide-Area Controller (AWAC), while leaving other modes to be controlled entirely by the local PSSs. The proposed approach is compared with an existing approach to demonstrate its design simplicity, effectiveness, applicability to large systems, and suitability to wide-area power system damping applications. The effectiveness of the AWAC design using the special feedback signal approach is verified using both small-signal and transient simulations. Its application is also demonstrated on 3-machine, 9-bus and 16-machine, 68-bus (NETS-NYPS) test systems, respectively. The special feedback signal based controller design and its validation and analysis (Chapter 5) are one of the main contributions of the research presented in this thesis document.



## 4.2 Design of the Damping Controller

The deployment of HVDC and FACTS devices combined with the use of Wide Area Measurement Systems (WAMS) has ushered in new possibilities in the design of robust and effective controls for improving angular stability [9, 71]. An HVDC transmission system allows for precise control of power flow between the buses of the interconnected ac systems, without requiring them to be synchronous [16, 72, 73, 74]. This property of being able to inject the precise amount of real power ( $P$ ) has been used to damp inter-area oscillations [56]. The location and amount of  $P$  injection to damp the oscillation depends on the bus location and type of signal used as input to the controller. An important concern while designing the damping control through HVDC/FACTS devices is the selection of feedback signals. It is well known that the feedback signal should be such that it exhibits good observability and controllability of the critical swing modes. Various signal forms have been studied and certain signals that exhibit this property have been discussed in [62, 75]. Apart from good observability and controllability of the critical swing modes, the controller based on these feedback signals should also have the following properties:

1. High observability of the swing modes of concern,
2. It should result in residues which remain in the same quadrant for all the swing modes of concern, and which do not change significantly with change in system conditions [74]. Also, the residue angles should lie in the close vicinity of each other. This results in a simplified controller design and, for small gains, the movement of all the swing modes are unidirectional [36]. If the residues are not in the same quadrant, and if the residue angles are not in the close vicinity, then any control effort may result in sub-optimal or conflicting movement of the swing modes.
3. Should not result in open loop zeroes lying close to the swing modes. When high gains are used with closed-loop control, the closed-loop poles tend to move towards the open-loop zeroes, which limits the damping.
4. The feedback signals should not result in adverse interaction with other non-swing modes. This is needed to ensure that, when affecting damping of the targeted

modes the controller should not destabilise non-targeted modes.

### 4.2.1 Existing approaches to damping controller design

The problem of inter-area oscillations has been one of the areas of concern for power engineers for a long time. Various solutions over time have been proposed and applied. Historically [76], this problem when noticed in the 1920's was solved by the use of damper windings in the generators and turbine-type prime movers with favorable torque speed characteristics. Later in the 60's the problem was handled with the use of high-response fast acting exciters fitted with additional damping signals. Damping controller design has evolved over the time, with controllers designed around the use of signals, such as rotor angle ( $\Delta\delta$ ), speed ( $\Delta\omega$ ). The controllers based on these local signals ( $\Delta\delta$ ,  $\Delta\omega$ ) acted by modulating the reference inputs of the exciters using Power System Stabilizers (PSS) [1].

The advent of WAMS has made it possible to synthesise signals that provide better systemwide information and can therefore result in more efficient control. Research has established that there exist certain dual pairs (input-output) of signals that can be used to affect the damping of inter-area modes without adversely effecting other swing modes. This is possible because, for such a dual input-output pair of signals the mode observability and mode controllability are proportional and differ only by a scalar [75]. A list of dual input-output pairs of signals [62] that can be used is summarised in Table 4.1.

<b>Input</b>	<b>Signal</b>	<b>Device</b>
$\Delta P_{sh}$	$\Delta\phi$	STATCOM with energy source
$\Delta Q_{sh}$	$\frac{\Delta V}{V_o}$	STATCOM, SVC
$\Delta I$	$\Delta V$	STATCOM
$\Delta V$	$\Delta I$	SSSC
$\Delta Q$	$\frac{\Delta I}{I_o}$	TCSC, SSSC
$\Delta P_{ser}$	$\Delta\zeta$	SSSC with energy source
$\Delta X_{ser}$	$I_o\Delta I$	TCSC

**Table 4.1: Dual input-output signals**

## An existing approach to a robust damping controller

Recently, Agnihotri [36] has proposed a new and more robust controller design that always provides improved damping even if remote signal is lost based on a dual input-output pairs of signal as given in [62, 75]. This controller adheres to the properties mentioned in Section 4.2. The controller design was developed with the following assumptions for simplification of analysis:

- The losses in the transmission lines are neglected.
- Load active and reactive power is constant,
- Generators are represented by the classical model and the prime mover input is held constant.
- The VSC-HVDC link is modelled as a current injection. As the aim of the research is to damp electro-mechanical oscillations, the high frequency modes are not modelled when the current source representation is used.

The state-space formulation leading to the eigenvalue sensitivity is as follows:

$$\begin{bmatrix} \dot{\Delta\delta} \\ \dot{\Delta\omega} \end{bmatrix} = A \begin{bmatrix} \Delta\delta \\ \Delta\omega \end{bmatrix} + BU \quad (4.1)$$

$$\mathbf{y} = C \begin{bmatrix} \Delta\delta \\ \Delta\omega \end{bmatrix} + DU \quad (4.2)$$

where vector of controllable inputs is  $\mathbf{U} = [\Delta\mathbf{P}_{sh}]$  for the VSC-HVDC,

and the vector of measured variables  $\mathbf{y} = [\Delta\phi]$  for the VSC-HVDC.

The matrices in (4.1) and (4.2) have the following structure [62]:

$$A = \begin{bmatrix} [0] & I \\ -M^{-1}A_r & [0] \end{bmatrix} \quad (4.3)$$

$$A_r = A_{11} - [A_{12}]J_rA_{21} \quad (4.4)$$

$$B = -M^{-1} \begin{bmatrix} [0] \\ B_\omega \end{bmatrix} = - \begin{bmatrix} [0] \\ M^{-1}A_{12} \end{bmatrix} J_r \quad (4.5)$$

$$C = -[C_\delta \quad [0]] = -J_r \begin{bmatrix} A_{21} & [0] \end{bmatrix} \quad (4.6)$$

$$J_r = [A_{22}]^{-1} = D \quad (4.7)$$

The matrix  $M$  is a diagonal matrix with  $\frac{2H_i}{\omega_B}$  as its  $i$ th diagonal element, where  $i$  denotes the machine number. The sub-matrix  $A_{ij}$  relates input variables  $\mathbf{U} = [\Delta \mathbf{P}_{sh}]$  to the output  $\mathbf{y} = [\Delta \phi]$ . This matrix is obtained from the linearized real and reactive power balance equations for shunt connected device [62].

For example,  $A_{22}$  denotes the Jacobian matrix  $\left[ \frac{\partial P_{sh}}{\partial \phi} \right]$  which is evaluated at the equilibrium point, and which is obtained from the real power balance equations at every node of the network. It has also been shown in [62] that:

1. For a lossless transmission system, the matrices  $A_{ij}$ ,  $A_r$  and  $D$  are symmetric, while

$$C_\delta = B_\omega^T \quad (4.8)$$

2. For an  $n$  machine system, the matrix  $A$  has  $(n - 1)$  pairs of purely imaginary eigenvalues (the swing modes).
3. Let the  $i^{th}$  eigenvalue be denoted by  $\lambda_i$ . The right eigenvectors  $\mathbf{e}_i$  and left eigenvectors  $\mathbf{f}_i$  corresponding to the eigenvalue  $\lambda_i$  are related to each other by the following equation.

$$\mathbf{f}_i = \begin{bmatrix} f_{\delta i} \\ f_{\omega i} \end{bmatrix} = h_i \begin{bmatrix} \lambda_i M e_{\delta i} \\ M e_{\omega i} \end{bmatrix} = h_i \begin{bmatrix} M e_{\omega i} \\ M \frac{e_{\omega i}}{\lambda_i} \end{bmatrix} \quad (4.9)$$

where  $e_{\delta i}$  and  $e_{\omega i}$ , and  $f_{\delta i}$  and  $f_{\omega i}$  denote the right and left eigenvector components corresponding to the rotor speeds and angles respectively. ' $h_i$ ' is an arbitrary scalar constant.

4. Due to the symmetry of  $A_r$  and diagonal nature of  $M$ ,  $e_{\delta i}$  may be chosen to be real.

The change in an eigenvalue due to a small perturbation in the  $A$  matrix,  $\Delta A$ , is given

by [4], whereas,

$$\Delta\lambda_i = \frac{\mathbf{f}_i^T \Delta \mathbf{A} \mathbf{e}_i}{\mathbf{f}_i^T \mathbf{e}_i} \quad (4.10)$$

In the analytical treatment of the feedback signal based on input-output pair of type  $(P_{sh}, \phi_{dij})$ , where “ $P_{sh}$ ” is DC power modulation,  $\phi_{dij}$  is the voltage phase angle difference between the buses of dc link  $i, j$ . It has been shown [36, 62] that, the input-output pair ‘ $u$ ’ and ‘ $y$ ’, which are a subset of the controllable inputs  $\mathbf{U}$  and measured variables  $\mathbf{y}$ , which are defined as:  $u = P_{dc}$  and  $y = \phi_d$ , results in the following expression:

$$u = -S\mathbf{U} \quad (4.11)$$

$$y = S\mathbf{Y} \quad (4.12)$$

where  $S$  indicates the relationship between the controllable shunt active power injection and DC power flow; such that  $S(i) = -1$  and  $S(j) = +1$ , if the DC link is connected to bus  $i$  and bus  $j$  and the DC power flow is from bus  $i$  to bus  $j$ , all the other terms of  $S$  being zero. Then substituting equations (4.11) and (4.12) in equation (4.1) and equation (4.2), respectively, results in

$$\dot{X} = AX - BS^T u \quad (4.13)$$

$$y = S\mathbf{Y} = SCX - SDS^T u \quad (4.14)$$

Application of *control law*,  $u = Ky$ , to equation (4.14) results in the following,

$$y = SCX - SDS^T Ky$$

$$y = \frac{SCX}{(I + KSDS^T)} \quad (4.15)$$

Through the mathematical treatment it can be shown that equation (4.1) transforms to the following expression:

$$\dot{X} = A - \frac{KBS^T SC}{(I + KSDS^T)} X$$

which results in a SVM expression:

$$\begin{bmatrix} \dot{\Delta\delta} \\ \dot{\Delta\omega} \end{bmatrix} = (A + \Delta A) \begin{bmatrix} \Delta\delta \\ \Delta\omega \end{bmatrix} \quad (4.16)$$

where

$$\Delta A = -\frac{KBS^TSC}{(I + KSDS^T)} \quad (4.17)$$

Then using (4.10) and (4.17), the change in the eigenvalue is given by

$$\Delta\lambda_i = -\frac{e_{\delta_i}^T B_\omega S K S^T B_\omega^T e_{\delta_i}}{2e_{\delta_i}^T M e_{\delta_i} (I + KSDS^T)} \quad (4.18)$$

If  $K$  is much smaller than  $I$ , then equation (4.18) assumes the form,

$$\Delta\lambda_i \approx -\frac{e_{\delta_i}^T B_\omega S K S^T B_\omega^T e_{\delta_i}}{2e_{\delta_i}^T M e_{\delta_i} (I)} \quad (4.19)$$

Therefore, the implications of the change in eigenvalue as given by equation (4.18), for any control effort are as follows:

1. If  $K$  is positive, it leads to increase in the damping of all the swing modes. *This sensitivity proof is valid only for small values of  $K$*  [36]. In this case, the denominator term with  $K$  equals the identity matrix and can be ignored as shown in the approximation in equation (4.19).
2. Also with  $SDS^T \neq 0$ , the poles and zeros are *interleaved* with finite magnitude of zeros [62]. So, as the closed-loop poles approach the open-loop zeros they begin to turn towards the  $j\omega$  axis, resulting in reduced damping. Therefore, interleaving of closed-poles and open-loop zeros restricts the range of controller gain.

It can therefore be inferred from the design that, the existing controller although effective, has a limited available range to improve damping of inter-area oscillations. An example will be shown later to compare with the proposed approach.

## 4.2.2 The proposed design approach based on special feedback signal for a robust damping controller

The damping controller design in the previous section is robust to change in operating and network conditions and also to the loss of communication. However, it offers a narrow range of operation for controller gains. The narrow range of performance for this controller is due to the fact that as the controller gain is increased, the effect of the denominator in the equation (4.18), becomes pronounced. Therefore, as the controller gain  $K$  is increased, this leads to the closed-loop poles turning towards the open-loop zeros, thus limiting the damping of the targeted swing modes.

Therefore, to have a damping controller that offers a wide range for controller gain  $K$  and improved damping of swing modes it is necessary that, the controller has the following characteristics:

- It should exhibit ability to move the open-loop zeros as far as possible and preferably far into the left hand plane. Thus by increasing the gain  $K$ , improved damping can be achieved to a better degree.
- As can be seen from the state-space equation (4.2), the feed-forward term  $D$  hinders the ability of the controller to achieve good damping, as we want controller gain  $K$  to directly affect the movement of the targeted eigenvalues in the LHP parallel to the axis. This effect of  $D$  is visible in equation (4.18). The controller design should be able to neutralise the effect of  $D$ , to allow for better movement of the eigenvalues.

The focus of the research presented herein is to develop a controller that increases the separation between the closed-loop poles and open-loop zeroes, while maintaining the other good properties mentioned in [36, 62, 77], to improve damping of swing modes.

The proposed formulation of controller design is based on a special feedback signal, that neutralises the effect of ‘D’ by considering the signal of the form  $(\phi_{dij} - \alpha P_{sh})$ , i.e. bus phase angle difference minus  $\alpha \times P_{shunt}$  (which is implemented by considering  $y_{sp} = SY + SDS^T u$ ). The diagram depicting controller and the system is shown in Fig. 4.1. The controller allows for a 10% modulation of DC power over the rated capacity.

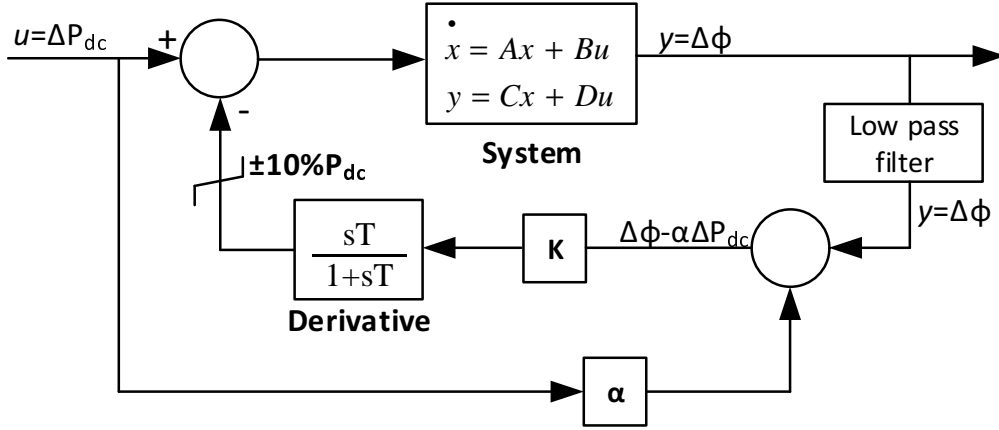


**Figure 4.1: Block diagram: POD controller based on the WAMS special feedback signal**

The mathematical treatment (proof) on the efficacy of the controller implemented based on the special feedback signal is given below. The analysis of the system makes use of the SVM in (4.1), (4.2) and is based on the control law given in equation (4.20)

$$u = K \frac{d}{dt} y_{sp} \quad (4.20)$$

The state variable equation (4.1) in conjunction with equation (4.11) can be written as:

$$\dot{X} = AX - BS^T u \quad (4.21)$$

and, equation (4.2) as:

$$Y = CX + DU \quad (4.22)$$

Also  $y_{sp} = SY + SDS^T u$ , thus substituting for  $y_{sp}$  in the control law equation (4.20), yields:

$$u = K[S\dot{Y} + SDS^T \dot{u}] \quad (4.23)$$

Substituting equation (4.23) in equation (4.21) yields

$$\dot{X} = AX - KBS^T[S\dot{Y} + SDS^T \dot{u}] \quad (4.24)$$

As  $Y = CX + DU$ , substituting for  $U (= -S^T u)$  from equation (4.11) and differentiating



results in

$$\dot{Y} = C\dot{X} - DS^T\dot{u} \quad (4.25)$$

Thus on substitution of equation (4.25) in equation (4.24) the following results:

$$\dot{X} = AX - KS^TBS[S(C\dot{X} - DS^T\dot{u}) + SDS^T\dot{u}] \quad (4.26)$$

But, we know from equation (4.6) that  $C = -[C_\delta \quad 0]$  and thus  $y = CX$  can be rearranged as follows:

$$y = -[C_\delta \quad 0] \begin{bmatrix} \Delta\delta \\ \Delta\omega \end{bmatrix} \quad (4.27)$$

which on differentiating equation (4.27) yields the following:

$$\dot{y} = -[[0] \quad C_\delta] \begin{bmatrix} \Delta\delta \\ \Delta\omega \end{bmatrix} \quad (4.28)$$

Substituting equation (4.28) in equation (4.26), and simplifying gives us:

$$\dot{X} = (A - KS^TB_\omega S[[0] \quad -C_\delta])X \quad (4.29)$$

It can be observed that, the perturbation in A matrix,  $\Delta A$  in equation (4.16) is given by the following:

$$\Delta A = -KS^TB_\omega SC_\delta \quad (4.30)$$

Therefore, comparing equation (4.30) with (4.17) it can be seen that the denominator term is not present. Thus, on substituting for  $\Delta A$  in equation (4.10) it can be shown that the change in eigenvalue ( $\Delta\lambda_i$ ) is given by the expression below:

$$\Delta\lambda_i = -\frac{e_{\delta_i}^T B_\omega S K S^T B_\omega^T e_{\delta_i}}{2e_{\delta_i}^T M e_{\delta_i}} \quad (4.31)$$

Thus comparing the change in the movement of eigenvalue ( $\Delta\lambda_i$ ) given in equation (4.31) with that in equation (4.18); the special feedback signal based controller exhibits the

following properties:

- Allows for better movement of closed-loop poles as the controller gain is increased because the open-loop zeroes move significantly away from the  $j\omega$  axis. The increase in the pole-zero separation is achieved by negating the feed-forward effect (introduced by feed-forward matrix D)[62].
- Retains the other good properties of [36], such as robustness towards the change in the operating point and network topology. Since any change in network topology and/or in operating condition will alter  $B_\omega$  and  $e_{\delta_i}$  which are always positive. Hence choosing any  $K > 0$  will always result in improved damping, because this will make  $\Delta\lambda_i < 0$  in Eq.4.31.

### 4.2.3 Extension of proposed approach to network with multiple HVDC systems

The development of the controller design presented above assumed the existence of a single DC link embedded in the AC system. However, this controller design can be extended to multiple HVDC systems, i.e. AC networks with more than one DC links. When wide-area measurements are available, the proposed controller in Fig. 4.2, can be extended to  $n$  multiple DC links, embedded in an AC network by formulating the controller gains as a matrix [K], instead of a scalar that was used for the single link.

$$K = \begin{bmatrix} K_{11} & \dots & K_{1n} \\ \vdots & \ddots & \vdots \\ K_{n1} & \dots & K_{nn} \end{bmatrix} \quad (4.32)$$

The resultant matrix treatment results in similar equation to (4.31), except that the expression would become,

$$\Delta\lambda_i = -(2e_{\delta_i}^T M e_{\delta_i})^{-1} e_{\delta_i}^T B_\omega S K S^T B_\omega^T e_{\delta_i} \quad (4.33)$$

In (4.32)  $K_{ii}$  refers to the local gain to the local special feedback signal  $\Delta\phi_{di} - \alpha\Delta P_{dci}$ , while  $K_{ij}$  refers to the gain applied to the feedback signal  $\phi_{dj} - \alpha\Delta P_{dcj}$  from the remote

$j^{th}$  link obtained using WAMs.

The  $K$ -matrix provides the following additional advantages that aid in control of multiple HVDC systems:

1. The gains can be tuned to selectively control the eigenvalue movement of a critical swing mode.
2. The matrix- $K$  retains the property of the robustness towards the change in the network topology and operating point, as discussed in [36] which is due to a “positive definite (PD)” nature of gain matrix  $K$ .
3. If the  $K$ -matrix is selected as in the previous step, then it ensures that the damping of the targeted modes is always better than when there is “No control” [36]. It also shows that the controller is robust to loss of communication. This can be observed from equation (4.32), wherein, when  $K_m = 0$  even then the eigenvalues of the  $K$ -matrix resulting from positive  $K_{ii}$  are positive definite.

### Block diagram of the proposed controller

As a part of this research, a controller design to effectively damp low frequency (electromechanical) oscillations has been developed based on a special feedback signal. The block diagram of the proposed controller, shown in the Fig. 4.2, is similar to that in [36] except for the selected feedback signal. The controller captures the phase angular difference between the DC links ( $\Delta\phi_{dij}$ ), and a tunable parameter  $\alpha$  which combines with the DC line power  $P_{dc}$  as its input, based on which, it modulates the DC line power ( $\Delta P_{dc}$ ) to affect damping of the desired swing mode. The controller gains  $K_{ii}$  relate to the gain of the local link, while the gain  $K_m$  relates to the non-local link. *So as to not exceed the converter rating significantly, the controller restricts the modulated DC power to  $\pm 10\%$  of the rated power.*

## 4.3 Design philosophy

After selecting the input-output signal which is the best pair based on the nature of equipment available, the design philosophy used for the proposed controller can be summarised

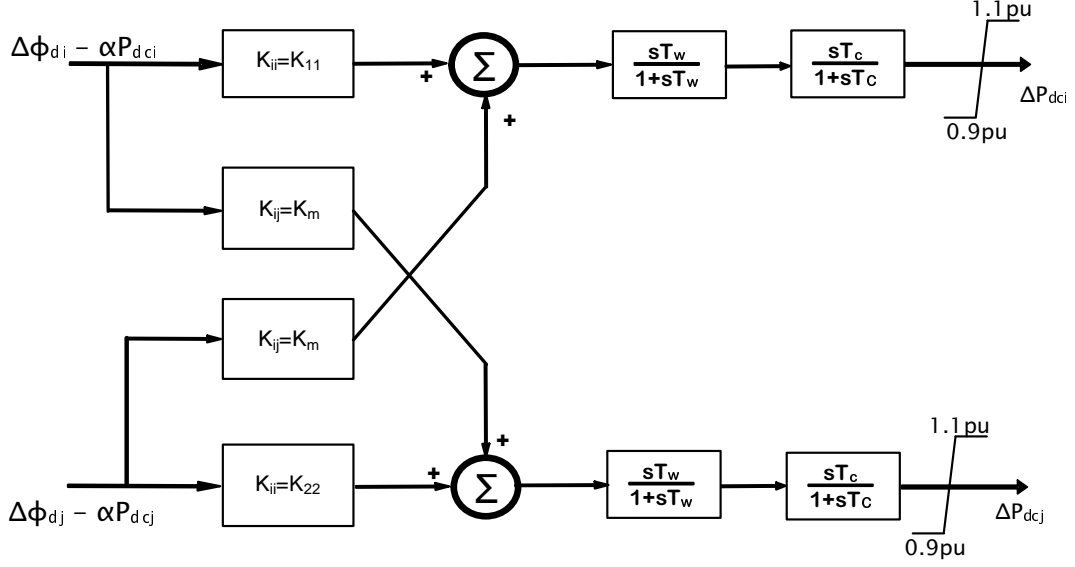


Figure 4.2: Structure of controller

in the following steps:

1. Select the optimal location for the converter based on residue analysis so as to achieve maximum damping influence.
2. Select individual gains  $K_{11}$  and  $K_{22}$  as shown in Fig. 4.2 to give the required damping performance. Note that,  $K_m$  is purposely not included so as to ensure good damping even with the loss of communication.
3. Introduce  $K_m$  to target a specific mode(s) for which the damping is to be further improved.

#### 4.4 Location of HVDC link in AC-DC network for improved damping based on residue analysis

The growth of power systems globally is fuelled by increasing demand and also due to the increasing share of renewable energy (RE) resources. These RE resources (solar PV, wind) are often located far from the load centres. This augmentation of conventional power system and the need to deliver energy directly to load centres, has lead to increase

in the number of HVDC links in the AC networks. An HVDC link is generally installed with one or more of the the following aims:

- a. The transmission of bulk power (as is the case for most point-point links),
- b. To interconnect asynchronous, or geographically different areas (as in the case of most back-to-back links),
- c. To improve the stability of an AC system; (rarely a primary consideration)

In (a), the rectifier-converters are normally located in close vicinity of large scale generation and the inverter-converters are located close to load centres. Whereas in (b), an HVDC link is used to connect two AC systems operating on different frequency or two geographically/politically independent areas. In such a case both the converters can be located in the same place (Back-to-Back link) or can be separated by a very small line. As for (c), a detailed analysis on the impact of DC power injection on factors affecting stability of an AC system be undertaken. There are two methods for this analysis, which are briefly described below.

The discussion below applies to controllers in individual links and does not include the positive definite gain matrix  $[K]$  developed in Section-4.2.3 i.e. we consider only one DC link at a time with  $K_{ii}$  in Fig. 4.2. This is step 1 of the design philosophy described in Section-4.3.

The **first approach** is based on computing the observability and controllability of the swing modes at non-generator bus. The controllability of a swing mode for a given input is given by equation (3.25). A higher controllability of a critical swing mode is the measure of effort needed for compensation, and it is location dependent. Similarly, observability of a swing mode for a given input is given by equation (3.24). Thus, observability of a critical mode in a signal helps to narrow the choice of a feedback signal to be employed [16, 74]. A “good” candidate for a feedback signal should be one that has the least adverse effect on *other* swing modes (i.e., other than the swing mode(s) being targeted for damping). With this approach, employing a selected pair of input-output signals, such as phase angle ( $\phi$ ) or bus frequency  $\left(\frac{d\phi}{dt}\right)$ , which are recognized as a dual input-output

pair, as discussed in Section-4.2.1, the modal controllability and observability vectors are parallel [62]. Therefore, the bus location with larger magnitude of controllability will have better observability for that swing mode.

The **second approach** is based on computation of the residue corresponding to the  $i^{th}$  eigenvalue as described in Section 3.1.2. A brief description about residue calculation is given below.

The transfer function of a system obtained from its state-space model  $[ABC]$  (assuming  $D = 0$ ) is given as follows:

$$G(s) = C(sI - A)^{-1}B \quad (4.34)$$

which can be further expressed as,

$$G(s) = \sum_{i=1}^n \frac{R_i}{s - \lambda_i} \quad (4.35)$$

where,  $R_i = C\phi_i\psi_iB$  is known as the modal residue and it is the product of modal observability ( $C\phi_i$ ) and modal controllability ( $\psi_iB$ ). As the residue is a complex variable, both magnitude and phase must be considered. The relationship between the output and input for a closed-loop system, can be defined as follows:

$$u = ky \quad (4.36)$$

where,  $k$  is the feedback gain. If we consider  $x = \Phi z$  where,  $\Phi$  is the eigenvector matrix for  $A$ , then, using SVM equations (4.1), (4.2) and (3.24), (3.25), we get the modal formulation with modal vector  $z$  (assuming  $D = 0$ ) shown below: (Note: we consider here the situation with distinct eigenvalues)

$$\dot{z} = \Phi^{-1}A\Phi z + \Phi^{-1}Bu \quad (4.37)$$

$$y = \Phi Cz \quad (4.38)$$

then combining (4.36) through (4.38) results in the following:

$$\dot{z} = \Phi^{-1}A\Phi z + \Delta k\Phi^{-1}B\Phi C z \quad (4.39)$$

$$\dot{z} = (\Lambda + k \times \Phi^{-1}B\Phi C)z \quad (4.40)$$

where  $\Lambda = \Phi^{-1}A\Phi$  where  $\Lambda$  is a diagonal matrix containing all the eigenvalues of  $A$ , and  $\Phi$  and  $\Phi^{-1}$  are the right and left eigenvectors, respectively. It can thus be observed from equation (4.40) that, less control effort  $k$  is needed if the magnitude of the residue ( $\Phi^{-1}B\Phi C$ ) is large and vice-versa.

The above concept has been applied to find the residue for various sets of bus pairs in the system with the selected input-output signal pair,  $(\Delta P_{sh}, \Delta\phi_{dij})$ . For an HVDC system,  $\Delta P_{sh}$  is the  $P_{dc}$  and  $\Delta\phi_{dij}$  is the voltage phase angular difference between the AC buses between which the DC link has been connected. Using this approach, the HVDC system is modelled as defined in the eigenvalue sensitivity analysis in Section-4.2.1. Thus, the residue ( $R_i$ ) for the critical swing mode ( $\lambda_i$ ) is computed for each pair of buses. This indicates that, for a given pair of buses, the residue with the largest magnitude for the critical swing mode provides the ideal location where this mode will have the highest controllability and observability. Thus, evaluating the values of residues gives an ideal position for an HVDC link to target the  $i^{th}$  swing mode through the modulation of DC power. This residue criterion has been utilized in this research to select the location of an HVDC link.

The position of HVDC links in the 3-machine 9-bus system, Fig.4.3, has been arrived at on the basis of residue analysis as discussed above. The eigenvalue analysis reported two swing modes with frequency 8.91 rad/s and 13.67 rad/s. Based on this observation, a residue analysis was carried out for various combinations of bus pairs to evaluate the position of a DC link. The values pertaining to the residue magnitude and angle for 8.91 rad/s (say 8 rad/s mode) and 13.67 rad/s (say 13 rad/s mode) are given in Tables (4.2), (4.3) and Tables (4.4),(4.5), respectively. As the DC links are not to be placed at the generator bus, the residue values corresponding to Buses 1 - 3 are not computed.

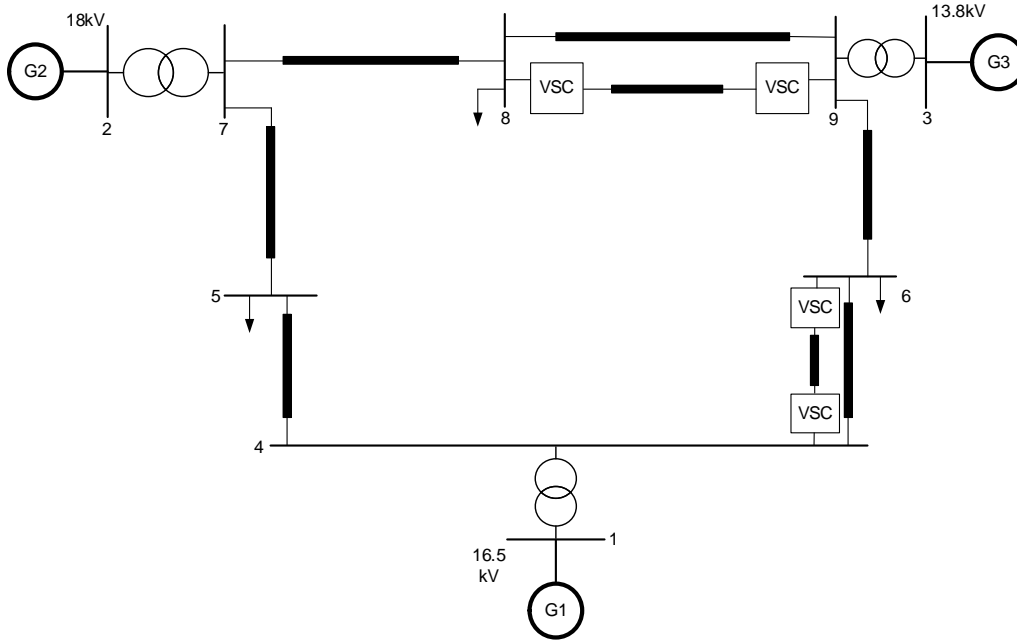


Figure 4.3: 3-machine 9-bus system

From Bus To	Bus 4	Bus 5	Bus 6	Bus 7	Bus 8	Bus 9
Bus 4	0	0.02	0.02	0.17	0.15	0.08
Bus 5	0.02	0	0.00	0.07	0.06	0.02
Bus 6	0.02	0.00	0	0.07	0.05	0.02
Bus 7	0.17	0.07	0.07	0	0.00	0.02
Bus 8	0.15	0.06	0.05	0.00	0	0.01
Bus 9	0.08	0.02	0.02	0.02	0.01	0

Table 4.2: 3-Machine 9-Bus system: Residue magnitude for 8 rad/s mode

#### 4.4.1 Example: Selection of location of HVDC link based on residue analysis

**Case-A: An HVDC link between bus 4-7 (4.3).**

It can be seen from Table. 4.2 that, the largest magnitude of the residue for the 8 rad/s mode is when the DC link is between bus 4-7, whereas the residue magnitude for the 13 rad/s mode for the same link is zero. So, based on residue analysis, at this location the DC link enabled with the proposed damping controller will only be able to affect damping for the 8 rad/s swing mode. This is because, the change in controller gain will only affect 8 rad/s mode due to the finite value of residue, whereas, the 13 rad/s mode will be negligibly affected, as the residue magnitude for this mode is zero. The movement



Bus From To	Bus 4	Bus 5	Bus 6	Bus 7	Bus 8	Bus 9
Bus 4	0	75.40	77.21	84.24	81.00	82.06
Bus 5	75.40	0	0	89.98	85.02	90.14
Bus 6	77.21	0	0	88.79	83.89	88.93
Bus 7	84.24	89.98	88.79	0	0	89.28
Bus 8	81.00	85.02	83.89	0	0	78.05
Bus 9	82.06	90.14	88.93	89.28	78.05	0

Table 4.3: 3-Machine 9-Bus system: Residue angle (in deg) for 8 rad/s mode

Bus From To	Bus 4	Bus 5	Bus 6	Bus 7	Bus 8	Bus 9
Bus 4	0	0.00	0.02	0.00	0.00	0.06
Bus 5	0.00	0	0.02	0.00	0.00	0.07
Bus 6	0.02	0.02	0	0.04	0.01	0.01
Bus 7	0.00	0.00	0.04	0	0.01	0.10
Bus 8	0.00	0.00	0.01	0.01	0	0.05
Bus 9	0.06	0.07	0.01	0.10	0.05	0

Table 4.4: 3-Machine 9-Bus system: Residue magnitude for 13 rad/s mode

Bus From To	Bus 4	Bus 5	Bus 6	Bus 7	Bus 8	Bus 9
Bus 4	0	81.51	59.86	41.34	0	73.64
Bus 5	81.51	0	60.16	29.92	0	72.99
Bus 6	59.86	60.16	0	52.94	45.53	89.95
Bus 7	41.34	29.92	52.94	0	64.06	66.76
Bus 8	0	0	45.53	64.06	0	68.21
Bus 9	73.64	72.99	89.95	66.76	68.21	0

Table 4.5: 3-Machine 9-Bus system: Residue angle for 13 rad/s mode

of eigenvalues resulting due to increase in controller gain ( $K_{ii}$ ) from 2 to 20 is shown in Table. 4.6. The root-locus plot in Fig. 4.4 shows the movement of eigenvalues with the change in damping controller gains, when the DC link is selected to be installed between bus 4-7. The Fig. 4.4 shows that the damping of the 8 rad/s swing mode improves with increase in controller gain, whereas there is negligible affect on the 13 rad/s swing mode. This accurately corroborates the inferences which have been drawn from the above discussion about the residue magnitudes.

Gain (K)	8 rad/s	13 rad/s
No Control	-0.1493 + 8.915i	-0.3331 + 13.669i
K = 2	-0.69593+ 8.125i	-0.3513 + 13.670i
K = 4	-1.218 + 7.35i	-0.3630 + 13.669i
K = 6	-1.7596 + 6.53i	-0.3710 + 13.666i
K = 8	-2.4010 + 5.546i	-0.3767 + 13.664i
K = 10	-4.0725 + 3.364i	-0.3809 + 13.663i
K = 20	-	-0.3919 + 13.657i

**Table 4.6: 3-Machine 9-Bus system: One DC link @ 4-7 with finite residue magnitude for 8 rad/s; residue magnitude for 13 rad/s is Zero.**

**Case-B: An HVDC link between bus 7-9.**

Again, from Table. 4.2 and 4.4 respectively, it can be observed that the largest magnitude of the residue for the 13 rad/s mode is when the DC link is between bus 7-9, whereas the residue magnitude for the 8 rad/s mode for the same link is finite (0.02). Based on this, the DC link enabled with the proposed damping controller at this location will be able to affect damping for both the swing modes. This is because, the change in controller gain will affect both the 8 and 13 rad/s, respectively. The movement of eigenvalues resulting

Gain (K)	~ 8 rad/s	~13 rad/s
No Control	-0.1493 + 8.915i	-0.3331 + 13.669i
K = 2	-0.1951 + 8.847i	-0.7464 + 13.522i
K = 4	-0.2387 + 8.797i	-1.039 + 13.394i
K = 6	-0.2787 + 8.760i	-1.2564 + 13.286i
K = 8	-0.3145 + 8.731i	-1.4246 + 13.196i
K = 10	-0.3466 + 8.709i	-1.5586 + 13.120i
K = 20	-0.4629 + 8.649i	-1.9613 + 12.872i

**Table 4.7: 3-Machine 9-Bus system: One DC link @ 7-9 with finite residue magnitudes for both 8 rad/s and 13 rad/s.**

due to increase in controller gain ( $K_{ii}$ ) from 2 to 20 is shown in Table. 4.7. The root-locus plot in Fig. 4.5 shows the movement of eigenvalues with the change in damping controller gains, when the DC link is selected to be installed between bus 7-9. Fig. 4.5 shows that the damping for both the 8 rad/s and 13 rad/s swing modes improves with increase in controller gain. It can also be observed that the leftward movement of 13 rad/s mode is larger compared to the 8 rad/s mode, which is also expected as the residue for the 13 rad/s swing mode is larger. Again this observation accurately corroborates the inferences

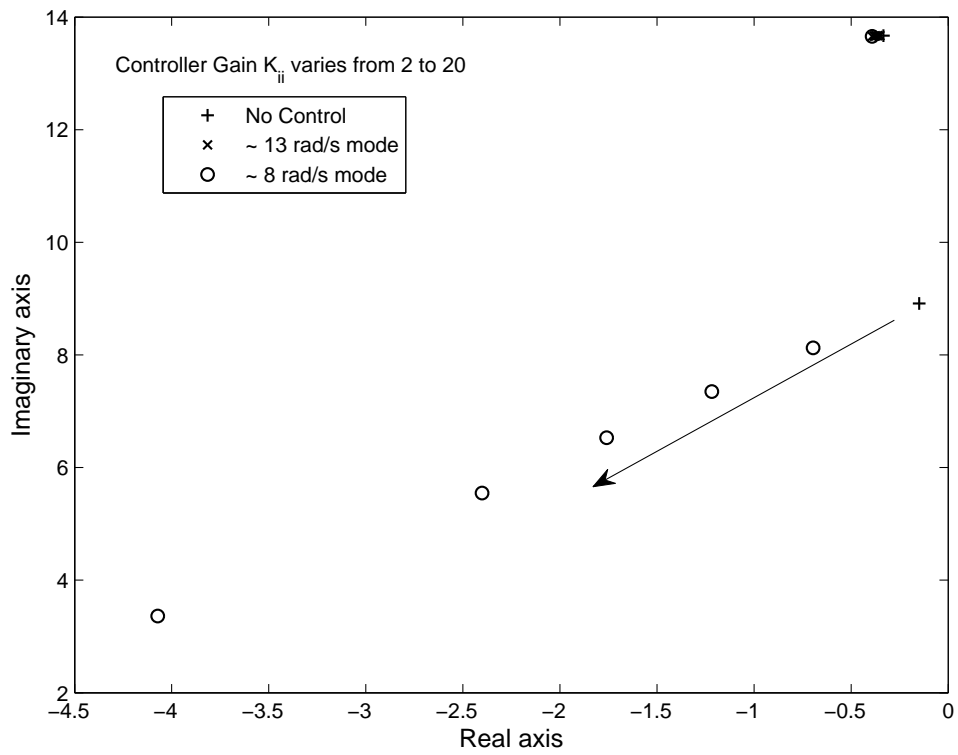


**Figure 4.4: Root-Locus plot for the controller with varying gains for link 4-7.**

that have been drawn from the discussion about the residue magnitudes.

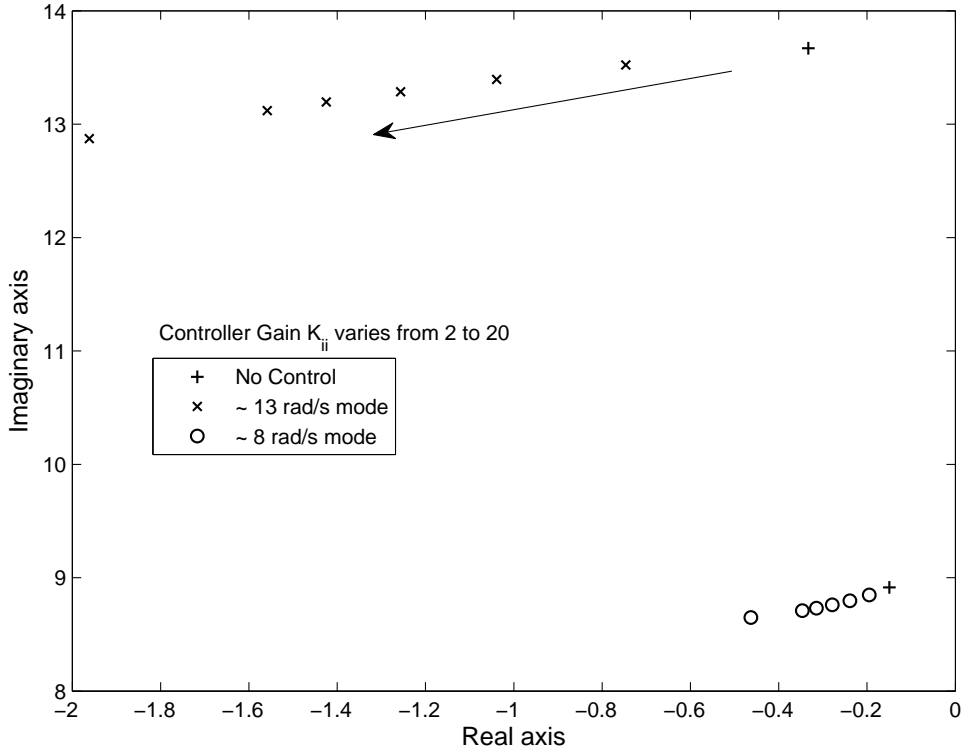


**Figure 4.5: Root-Locus plot for the controller with varying gains for link 7-9.**

**Case-C: Two HVDC links in the system at bus 4-6 and 8-9.**

The aim of this thesis is to select an optimum location for more than one point-to-point HVDC link, such that the damping controller is able to achieve improvement in the damping of both the swing modes. On perusing the residue data given in Tables. 4.2 - 4.5, we consider locating the two links between bus 4-6 and 8-9, respectively. For the link between bus 4-6, the residue magnitudes are 0.02 for 8 rad/s and 0.02 for 13 rad/s (grey cells in Tables.4.2 - 4.5), whereas for the link between bus 8-9 the residue magnitudes are 0.01 for 8 rad/s and 0.05 for 13 rad/s (grey cells in Tables.4.2 - 4.5). The following can therefore be inferred from this information:

- As the controller gain is increased, the modulation of DC power  $P_{dc}$  on both the links will help to improve damping for both the modes. This is due to the residue magnitudes being close.
- Also, for any increase in the controller gain, the movement of the eigenvalues for both the swing modes will be in close vicinity, as the angles for both the swing

modes are in close vicinity.

The root-locus plot for changing controller gains for both the swing modes is shown in Fig. 4.6. Any other location for the two HVDC links will not offer such controllability for both the swing modes.

#### 4.4.2 Selective modal damping with wide area control

As described in Section-4.2.3, using a PD matrix always gives guaranteed improved response as compared to no control. Only question is how to select the gain parameters, e.g.  $K_m$ . Any value of  $K_m$  that maintains the PD nature of the  $K$  matrix will improve damping of all targeted modes. However, some  $K_m$  values may be better for certain specific mode(s). If a given mode is to be targeted, additional frequency domain studies can be carried out with varying  $K_m$ . It should be noted that including  $K_m$  gives superior performance for all modes. However, there is a choice of values for  $K_m$  that can be selected so that certain modes of interest are damped more than others. This is demonstrated in Table (4.8), when the local gains were kept constant as  $K_{11} = K_{22} = 100$ , while different values were selected for  $K_m$  to selectively damp a particular swing mode of interest. As can be observed in Case-I, with selection of gain  $K_m = 100$ , the damping

Case	Swing Mode - I	$\zeta$ (%)	Swing Mode - II	$\zeta$ (%)
No Control	$-0.333 \pm j13.669$	2.43	$-0.149 \pm j 8.915$	1.67
Case - I	$-0.381 \pm j13.632$	2.79	$-0.500 \pm j 8.753$	5.7
Case - II	$-1.325 \pm j13.751$	9.59	$-0.171 \pm j 8.917$	1.92

Table 4.8: Selective modal damping of  $\sim 8$  rad/s mode

of Swing Mode-II improved from 1.7% to 5.7%. Similarly for Case-II, when  $K_m = -100$  was selected it resulted in improvement of Swing Mode-I from 2.4% to 9.6%. It should also be noted that in both these cases, the damping of the non-targeted swing mode is always better than than the “No Control” case.

## 4.5 Efficacy of controller based on proposed special feedback signal

The efficacy of the proposed controller in imparting improved damping is further illustrated by the use of case studies on 3-machine, 9-bus and 16-machine, 68-bus test systems.

### 4.5.1 Case study: 3-Machine, 9-Bus system

The performance of the existing controller presented in Section-4.2.1, has been compared with that of the proposed controller using the eigenvalue sensitivity analysis. The movement of the eigenvalues resulting from the change in controller gains is compared between the earlier damping approach in [36] based on  $\frac{d\phi}{dt}$  signal versus the proposed modified signal for the test system using root-locus plot. The advantage of the new signal is wider separation between open-loop poles and zeroes. Fig. 4.6 shows the root-locus plot for the swing modes when the controller gains are varied from 20 to 200, under the following conditions:

- a. When no control is exercised (\*),
- b. When the control is based on local signals ( $\times$ ),
- c. When control is based on the proposed controller (+),

It can be observed from Fig.4.6 that,

- a. when the control signal is based on existing signals ( $\times$ ), as the value of the controller gain is increased the swing modes start to move towards the open-loop zero for higher gain, which in this case turns the poles to move towards the  $j\omega$  axis, i.e. results in poorer damping with sufficiently higher gains.
- b. whereas, in the case of the controller based on special feedback signal (+), as the value of the controller gain is increased, the eigenvalues move deeper into the left half plane (LHP), thus result in increased damping.

The efficacy of the proposed controller was further validated by performing time-domain simulation using MATLAB. In this simulation, a 3-phase fault that last for 4-cycles was

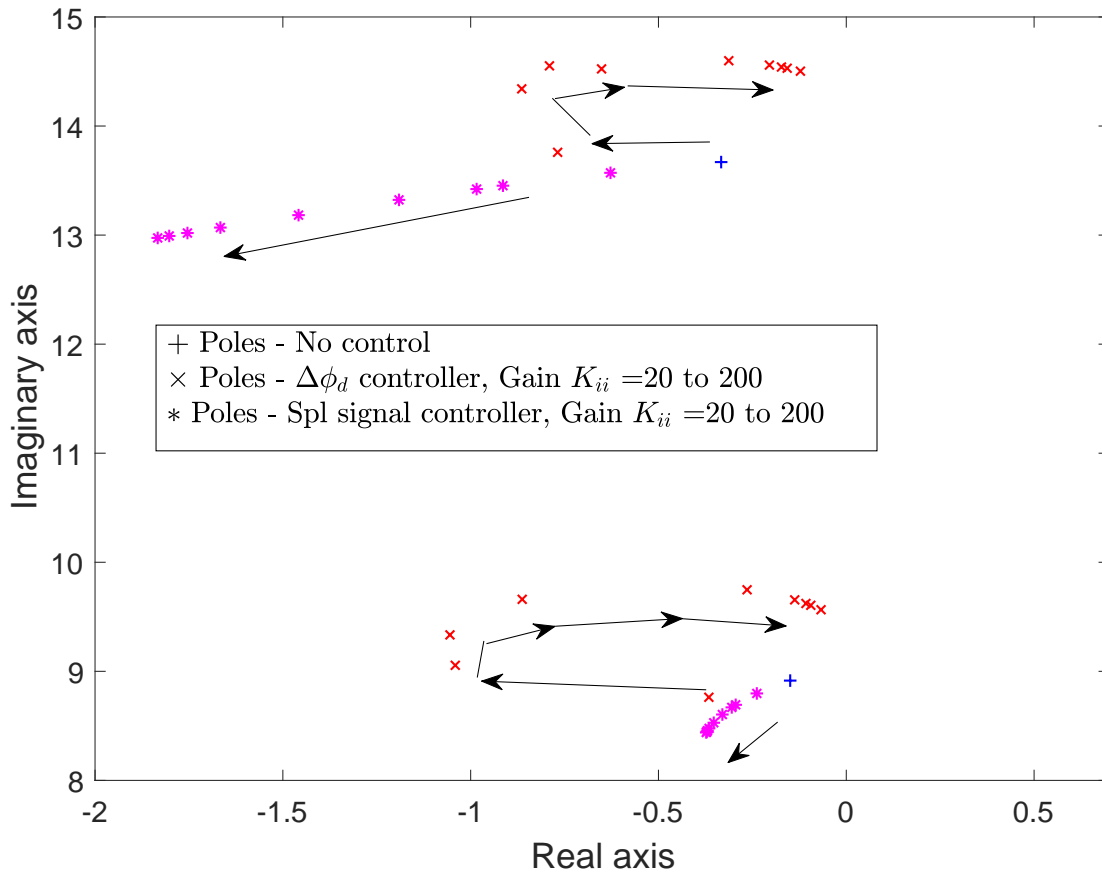


**Figure 4.6: Root-Locus plot for the controller with varying gains**

applied at bus 7, and was followed by tripping line 5-7. This action excites the 8 rad/s mode between machines 1 and 2. Fig. 4.7 shows the time response plot with and without the damping controller. It can be observed that, in comparison to the controller based on local control, the proposed controller which uses non-local signals has a better response.

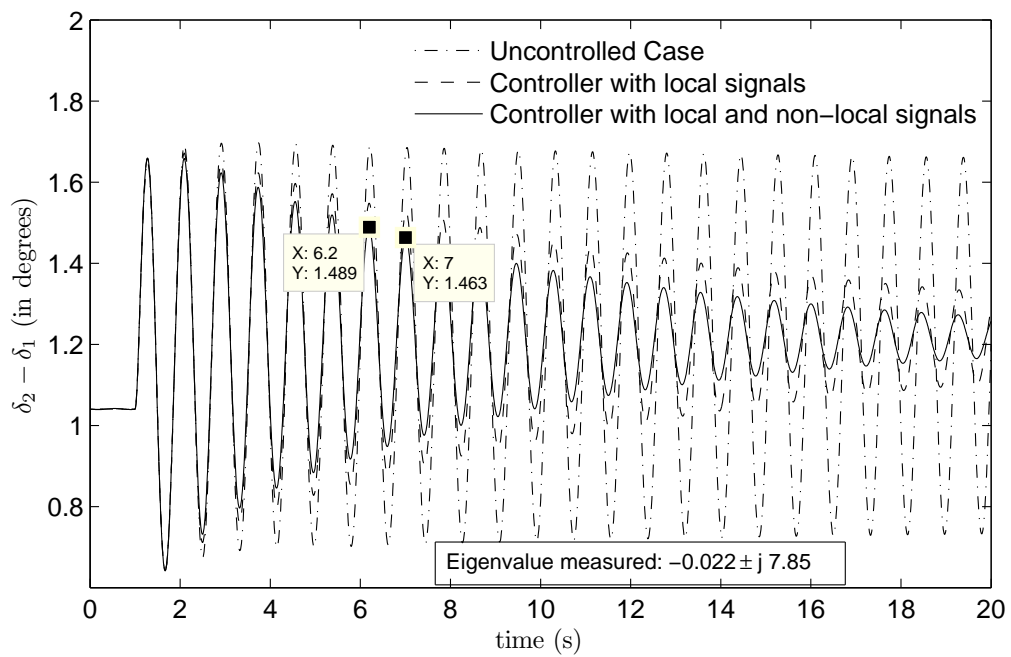
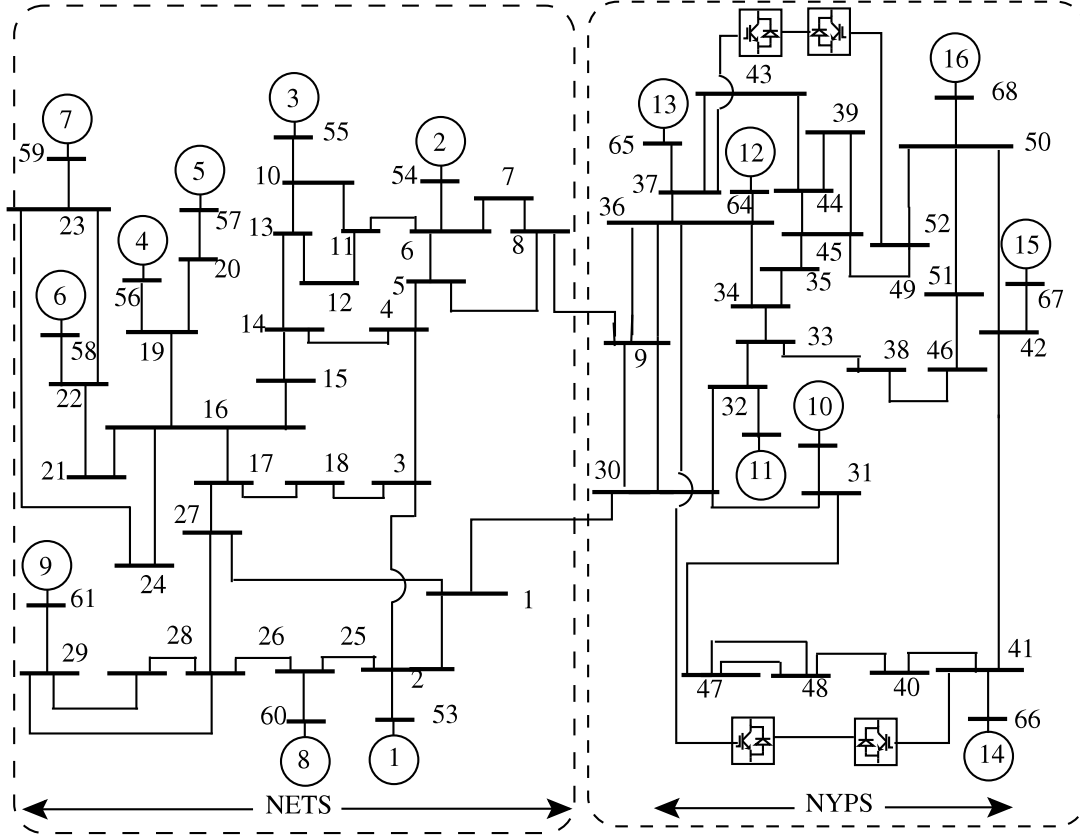


Figure 4.7: Time domain simulation for a 4-cycle 3-phase fault at bus 7, cleared by tripping line 5-7



## 4.5.2 Case study: 16-Machine 68-Bus system

The objective of this case study is to further validate the proposed controller design based on the special feedback signal over a large network,(see Fig. 4.8). The base case



**Figure 4.8: 16-Machine 68-bus NETS-NYPS test system**

powerflow, network data and dynamic data has been adopted from [4]. Using eigenvalue analysis, it was found that the system has three dominant inter-area swing modes namely  $\sim 2.6\text{rad/s}$ ,  $\sim 3.5\text{rad/s}$  and  $\sim 4.5\text{rad/s}$  respectively. Subsequent to determination of the inter-area swing modes, as for the 3-machine, 9-bus test system, residue analysis was also performed on the 16-machine power system with regard to modulation of DC power and its corresponding effect on bus voltage phase angle. It was observed that VSC-HVDC links between buses 40-36 and 52-50, respectively, are the best candidate locations because these locations exhibit good controllability of the three dominant inter-area swing modes.

Similar to the case study involving the 3-machine, 9-bus system, the following is observed from Fig. 4.9 (when the DC links are present between bus 40-36 and bus 52-50, respectively):

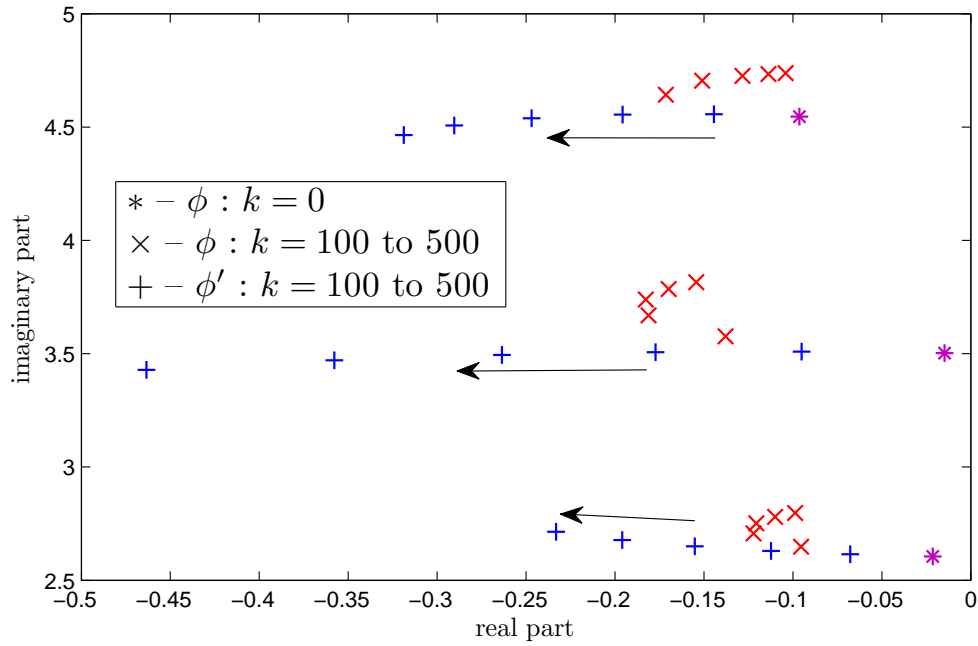


**Figure 4.9: 16-machine 68-bus: Root-locus plot indicating movement of dominant inter-area modes with varying controller gain under different conditions**

- for the controller based on local signals ( $\times$ ), an increase in the controller gain leads to the eigenvalues of the dominant inter-area swing modes moving towards the  $j\omega$  axis, thereby resulting in lower damping.
- for the controller based on the special feedback signal ( $+$ ), a similar increase in the controller gain moves the concerned eigen-values of the swing mode(s) further into the left half plane (LHP) thus resulting in better damping of the swing modes.

The damping effect introduced by the proposed controller was further validated by performing time domain simulation using MATLAB. In this simulation, a 3-phase fault that last for 4-cycles was applied at bus 45, followed by tripping of line 45-39. This action excites  $\sim 3.5$  rad/s mode between machines 14 and 16. Fig. 4.10 shows the time response with and without the damping controller. It can be observed that in comparison to the controller based on local control, the proposed controller which uses non-local signals has a better response.

Selective modal damping. Also, as in the 3-machine system, selective modal damping is achievable in this system. This is demonstrated in Table (4.9), when the local gains were selected as  $K_{11} = 50$  and  $K_{22} = 500$ , while different values were selected for  $K_m$

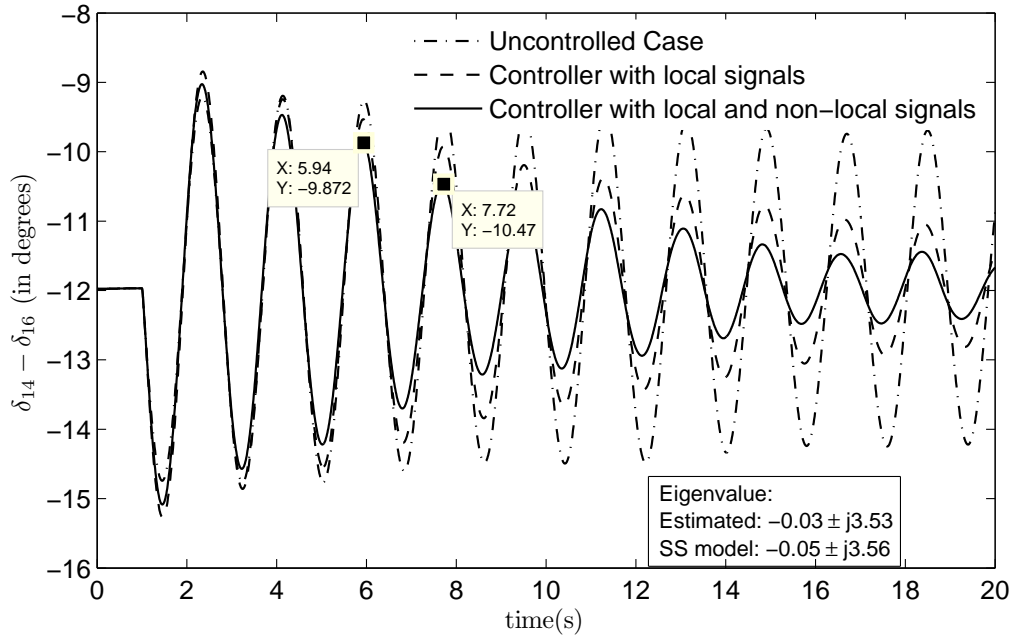


**Figure 4.10: 16-machine, 68-bus: Time domain simulation for a 4-cycle 3-phase fault at bus 45, cleared by tripping line 45-39. Two DC links are at bus 40-36 and bus 52-50 respectively.**

to selectively damp a particular swing mode of interest. Once again as demonstrated for

Case	Swing Mode - I	$\zeta$ (%)	Swing Mode - II	$\zeta$ (%)	Swing Mode - III	$\zeta$ (%)
No Control	$-0.096 \pm j4.546$	2.11	$-0.015 \pm j3.502$	0.43	$-0.021 \pm j2.605$	0.81
Case - I	$-0.115 \pm j4.509$	2.55	$-0.674 \pm j3.392$	19.5	$-0.096 \pm j2.678$	3.6
Case - II	$-0.945 \pm j4.356$	21.2	$-0.050 \pm j3.560$	1.4	$-0.391 \pm j2.821$	13.73

**Table 4.9: 16-machine system: Selective modal damping of particular swing mode**

the 3-machine system, it is observed that in Case-I, with selection of gain  $K_m = 125$ , the damping of Swing Mode-II improved from 0.4% to 19.5%. While in Case-II, when  $K_m = -125$  was selected it resulted in improvement of Swing Mode-I and Swing Mode-III from 2.11% to 21.2% and 0.81% to 13.73% respectively. It should also be noted that in both these cases, the damping of non-targeted swing mode is always better than the “No Control” case.

The design of the proposed controller has been developed based on certain assumptions, such as the classical model of machine and that the system is lossless. In the real world this is not the case, thus the proposed controller design also needs to be validated.

The validation of the proposed controller design will be dealt with in the next chapter.

## 4.6 Summary

This chapter described the existing approach to damp inter-area (low frequency) oscillations in a power system by the modulation of real power. An eigenvalue sensitivity analysis of this approach was discussed, which highlighted the limited range of control available using this approach. A novel, improved damping controller design was proposed that utilizes system-wide information to synthesise a special feedback signal. The proposed design retains the good qualities such as robustness to change in operating and network condition while providing an extended range of operation to damp inter-area oscillations using VSC-HVDC system. An eigenvalue sensitivity analysis in support of the proposed design was also presented. This is the main contribution of this research. The proposed controller was further extended to multiple HVDC systems in an AC network. The chapter also highlighted the ability of the proposed controller to selectively damp a critical swing mode of interest by judiciously selecting controller gains. Finally, this chapter also discussed residue analysis and its influence on selecting location of HVDC links in an AC system from the point of improving the stability of the interconnected AC-DC system.

# Chapter 5

## Performance evaluation of the proposed controller using Electro-Magnetic Transient simulation

### 5.1 Introduction

The previous chapter described the design procedure for the proposed controller using small signal analysis and its application to multiple HVDC systems embedded in an AC network. The performance of the proposed controller was demonstrated through eigenvalue movement for various controller gain using a root-locus plot and also by time-domain simulation using a MATLAB/Simulink based transient stability program. In this chapter, the performance of the proposed controller designed using a linearised model is analysed using the Electro-magnetic Transient (EMT) simulation program.

The transient stability simulation model of the test system (with the proposed controller) in the last chapter, did not model the switching in the power electronic (PE) equipment or the details of the controller. A comprehensive evaluation of the test system, which models all components in full detail, provides a deeper insight into the system behaviour. This component level model can be developed in an EMT simulation platform

such as PSCAD/EMTDC, which is an industry standard. The process to set up EMT simulation, wherein at each step the performance of the proposed controller was matched with transient simulation:

- Develop an EMT simulation model for the AC network with one-to-one correspondence to that with the transient stability model. Initialise the system to the same conditions as in transient stability.
- Introduce the current injection model for the power electronic equipment into the EMT simulation,
- Replace the power electronic components with the detailed model,
- Evaluate the interaction between the damping controller and AC-DC network due to change in gain of the damping controller.

The process is described in greater details in the later sections in this chapter.

## 5.2 Corroboration of the performance of the proposed controller using EMT simulation

Before undertaking the process of corroboration it is important to understand the difference between TS and EMT simulation.

**Transient Stability (TS).** TS programs are used to study the electromechanical transients in the network and are valuable in determining the stability of very large electrical networks. In these programs, the principal factors affecting the low frequency (electromechanical) oscillations are modelled in detail using differential equations with the remainder of the electrical network being represented in fundamental frequency steady-state phasor form. Typically, these programs can be used to model extremely large networks, but are restricted in their dynamic representation to low frequency phenomena (0–5 Hz) [78].

In TS programs, the transmission lines and other network impedances are represented using algebraic “phasor models” and the dynamic modelling is confined to rotating machines, exciters, governors and turbines, and a few other elements. As high-frequency

dynamics are ignored, a larger integration step (typically half a cycle) is possible and large power systems with 50000 or more buses can be modelled. Traditionally, TSA models have been used to study rotor angle deviations and determine transient stability performance following system disturbances.

**EMT.** EMT simulation tools represent a power network in very high detail. EMT programs are able to simulate phenomena such as switching transients which cover the frequency spectrum from DC to tens of kHz. Such programs have been used to study lightning, switching, and fault transients in equipment and to model power electronics based equipment such as HVDC converters and FACTS controllers [79].

To realise the full potential and the range of gain for the proposed controller model, where all details of the system are modelled, it needs to be evaluated using an EMT simulation platform (PSCAD/EMTDC). The procedure to develop the model in an EMT simulation platform is outlined in following sub-sections.

### 5.2.1 Corroboratation procedure

To corroborate the results obtained using the transient stability program, the 3-machine, 9-bus system [80] (for system data, refer to Appendix A) has been simulated using the PSCAD/EMTDC simulation software. The corroboratation was carried out on the test system augmented with two VSC-HVDC links between bus 6-4 and bus 8-9, respectively, as depicted in Fig. 5.1. For the VSC-HVDC link A-B, A denotes the rectifier and B denotes the inverter. Thus, the DC power flows from A to B. An incremental approach was adopted to develop the system in the PSCAD/EMTDC platform.

The starting point for any analysis begins with establishing an operating point which initialises the system. The system load-flow solution provides this initial (steady-state) operating condition. The load-flow solution generated through transient stability software is used in both, the PSCAD/EMTDC and transient stability simulation. The transient stability simulation begins from the steady-state condition, whereas the PSCAD/EMTDC simulation starts from rest. Thus, the PSCAD model is allowed to reach the operating point determined above. Thereafter, the system is subjected to a similar disturbance in both the platforms and the system response to this disturbance is analysed. This

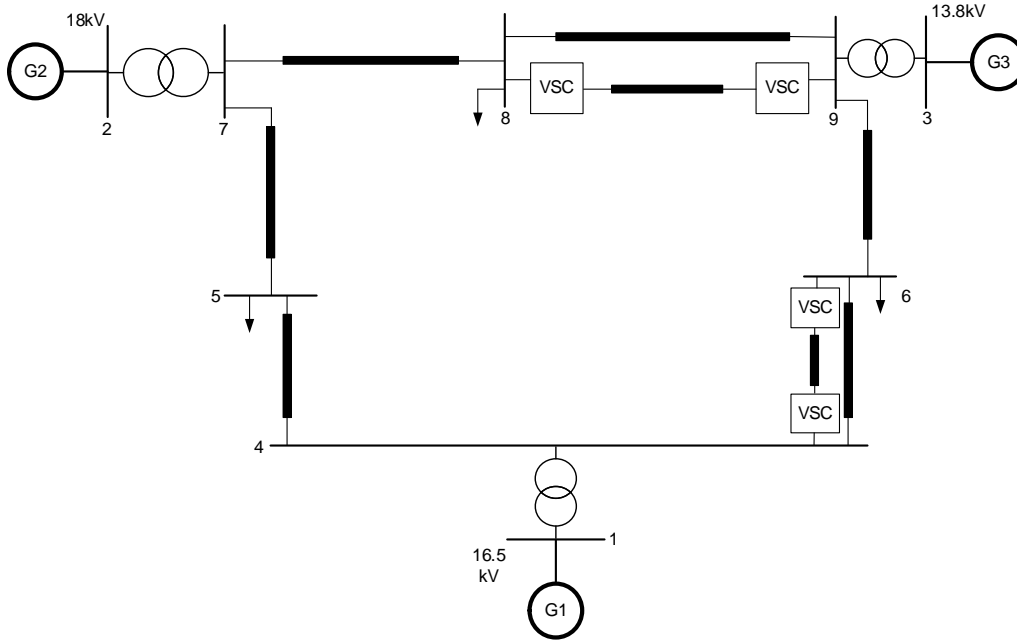


**Figure 5.1: The 3-machine, 9-Bus test system.**

disturbance, in the form of a 2-cycle, 3-phase fault (duration  $t = 0.032s$ ), is simulated at time  $t = 2s$  at Bus 5, which is followed by tripping of the transmission line 4-5 to clear the fault. An eigenvalue analysis was also carried out as per the model developed in Section-4.2.2 of Chapter 4, and the eigenvalues for the system are  $-0.4113 \pm j 6.9913$  and  $-0.9491 \pm j 14.2197$ . The Centre-Of-Inertia (COI) speeds for the synchronous machines were plotted to compare the responses obtained from the two simulation programs. The advantage of plotting the COI speeds is that, the common-mode oscillation between the machines is neutralised and it affords a stable reference for measurement. The incremental approach adopted for evaluation is mentioned in the steps below:

- a. **Step 1.** When developing the model of the test system in the PSCAD/EMTDC platform, the synchronous machines were replaced by a voltage source thereby neglecting machine dynamics, and the transmission lines were modelled using a nominal  $\pi$ -model. Also, for further simplification, the VSC-HVDC transmission links were not modelled as part of the system, as in steady-state the links are transmitting no power. Thus, the simulation test system comprised only the AC transmission network with voltage sources. This initial simulation was undertaken to ensure that the load-flow result obtained in transient stability matched with the PSCAD/EMTDC and the initial



conditions for the two simulations were identical.

b. **Step 2.** The voltage sources from step 1, were replaced with the detailed synchronous machine model, without changing any other component in the simulation system. On execution of the simulation the following challenges were encountered:

i. The machine data, as available for the test system in [80], did not provide the values for sub-transient quantities ( $x_d''$  and  $T_{q0}''$ ). The authors suggests using the same values for both the quantities for the TS simulation.

ii. As the available test system data for the synchronous machine had the same values for transient and sub-transient reactances, this violated the expected range of these values for the PSCAD/EMTDC machine model, and resulted in an error.

iii. To overcome this problem, some arbitrary value falling within the expected range of the PSCAD/EMTDC model was fed to the model. This resulted in numerical instability of the simulation. The issue was resolved by providing realistic values for these ( $x_d''$  and  $T_{q0}''$ ) quantities leading to a stable solution.

iv. The amended machine data as at (iii) above, had changed from the test system data in step 1, due to substitution of realistic inputs for sub-transient quantities ( $x_d''$  and  $T_{q0}''$ ). Therefore, the amended machine data was given to transient stability program and the load-flow solution for the test system was again matched between the two simulation platforms.

c. **Step 3.** The transmission lines are generally characterised as short (<80km), medium (80km - 160km) or long (>160km) lines and are therefore modelled accordingly. The nominal  $\pi$ -model of a transmission line is good for up to medium length lines, while the long lines are required to be modelled in greater detail using distributed parameters. The PSCAD/EMTDC software provides the option to model transmission lines based on the length, either as Bergeron ( $\pi$ ) or frequency dependent (FD) phase model. The **Bergeron model** is based on a travelling wave line model while the L and C elements of a  $\pi$  section are represented in a distributed manner, and lumped resistance (R). This model is roughly equivalent to using an infinite number of  $\pi$  sections, except that the resistance is lumped [81]. While the **Frequency Dependant (Phase) line model** is

also based on the travelling wave line model, it incorporates the frequency dependence of distributed RLC parameters [81].

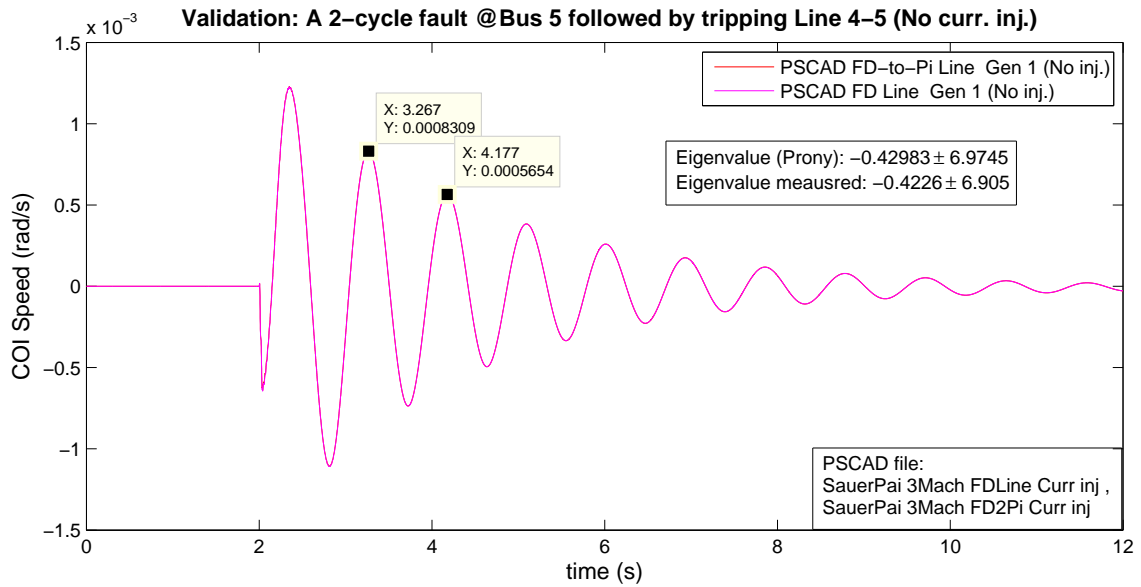


Figure 5.2: COI Speed for generator 1: Comparison between frequency dependent (FD)Line and FD-to-Pi model Line, with eigenvalues mentioned. The eigenvalues recorded from small-signal model match with the measured value and also with those computed through Prony analysis.

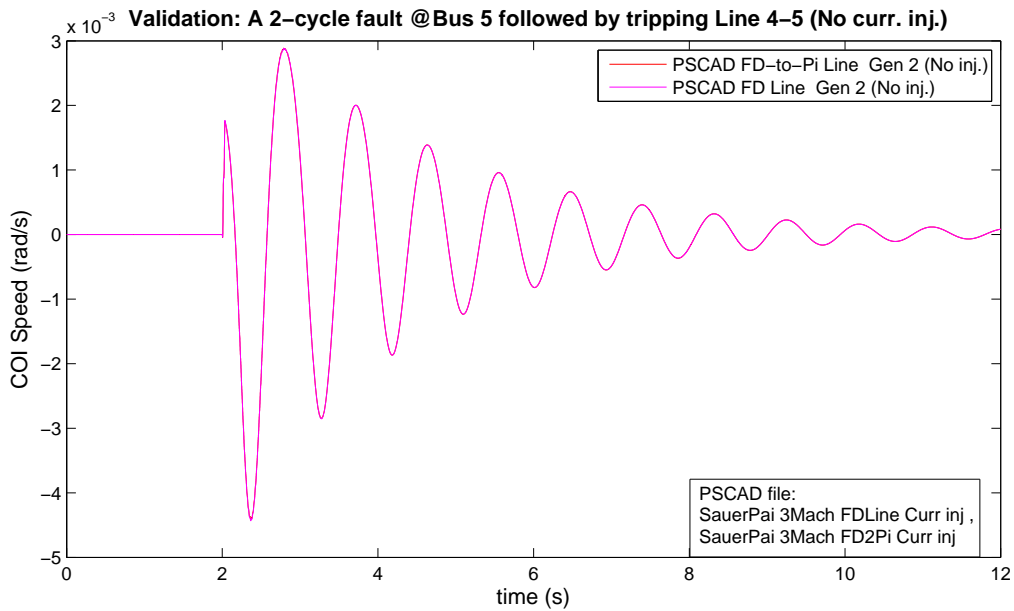
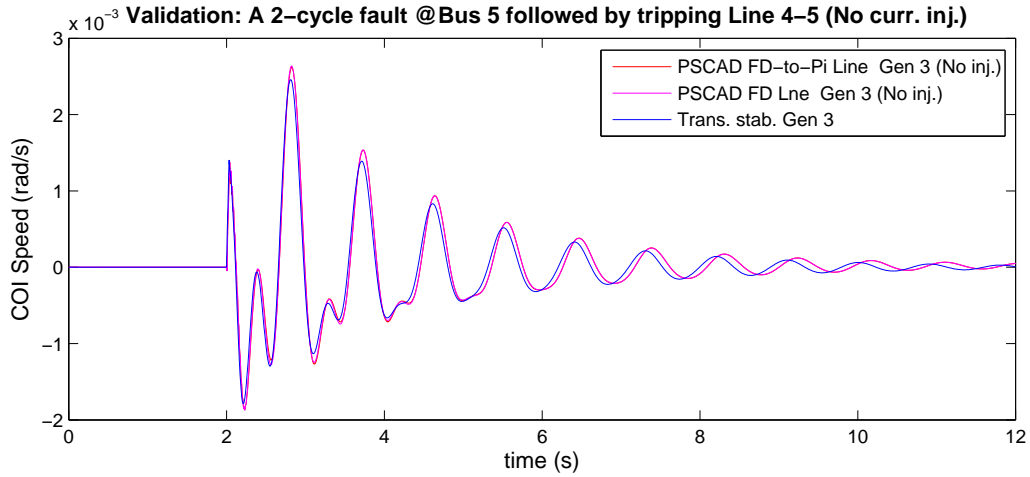


Figure 5.3: COI Speed for generator 2: Comparison between frequency dependent (FD)Line and FD-to-Pi model Line.



**Figure 5.4: COI Speed for generator 3: Comparison between frequency dependent (FD)Line and FD-to-Pi model Line.**

Therefore as a logical next step, the transmission line was simulated in both  $\pi$  and FD (phase) models separately and the results compared. As the TS software models transmission lines as  $\pi$  model, the actual value of line parameters in terms of resistance (R), inductance (L) and capacitance (C) were obtained from the FD line model and used as input to transient stability software. The COI speed of the machines was plotted for comparison and the results are shown in Figs. 5.2 - 5.4. It can be concluded from the simulation plots that the transient stability and the PSCAD/EMTDC models show a very good match.

Inference. The above traces indicate that either  $\pi$  or FD transmission line model captures the modal information required for TS analysis and, thus, both are suitable for low frequency analysis.

- d. **Step 4.** At this point, the VSC-HVDC link was introduced in to the test system and was modelled as a current injection source at the bus. The current injection by the rectifier converter of the VSC-HVDC link was assumed to be  $-P_{dc}$ , whereas the inverter converter was assumed to be  $+P_{dc}$ . The current injection modelling in the EMT simulation replicated the TS simulation model. The proposed damping controller implemented in the transient stability program was replicated in the combined AC-

DC system in the PSCAD simulation. The system was subjected to a disturbance as mentioned in Section 5.2.1 and the results from the simulation in terms of the COI speed of the three machines has been plotted in Figs. 5.5 - 5.7.

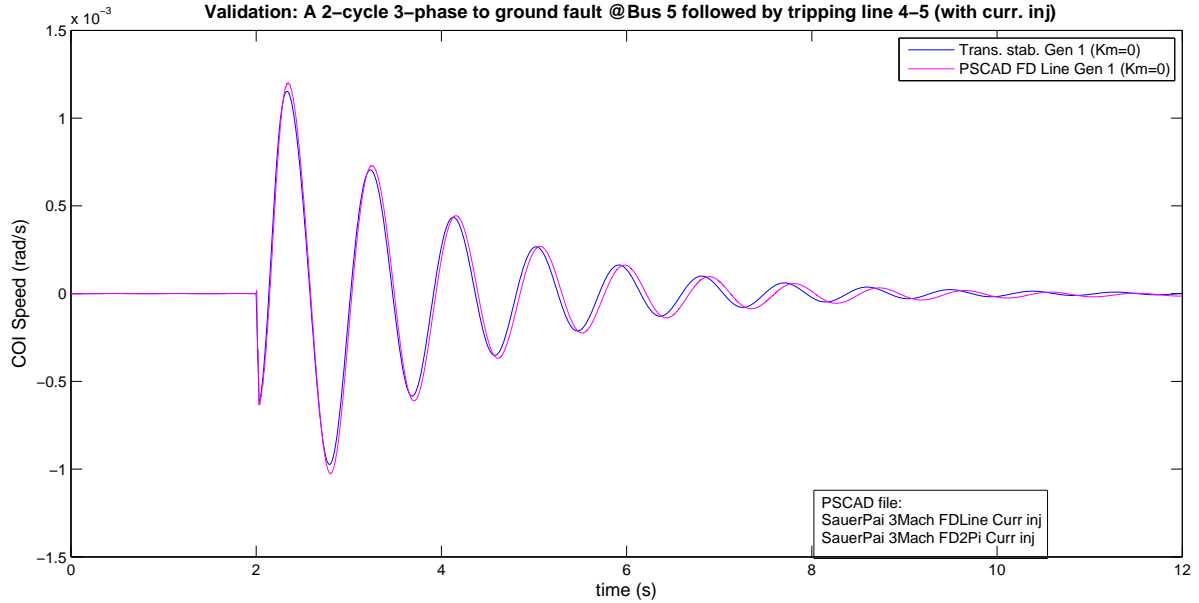


**Figure 5.5: COI Speed for generator 1: Comparison between transient stability and PSCAD with VSC-HVDC modelled as current injection at the bus.**

Inference. The plots in Figs. 5.5 - 5.7 reflect that the current injection model of the HVDC system in TS analysis agrees well with the EMT model. The TS model is therefore suitable for analysis in low frequency range.

- e. **Step 5.** In this step, the 3-machine test system augmented with two VSC-HVDC links as simulated in step 4 was modified. The DC-links were represented using a detailed model of VSC-HVDC link instead of the current injection model. The detailed PSCAD model of VSC-HVDC simulates a 2-Level based switching model of the VSC-HVDC. The VSC-HVDC offers various options for control at its terminals which are detailed in Section 2.4. Initially, in the PSCAD simulation, the controls at the VSC rectifier were modelled as DC voltage ( $V_{dc}$ )/AC voltage ( $V_{ac}$ ); while at the inverter controls were modelled as real power ( $P$ )/  $V_{ac}$ . The transient stability model on the other hand only considers real power modulation, while keeping the reactive power ( $Q$ ) constant at zero (0) for all the converters. Therefore, the VSC-HVDC system controls in PSCAD

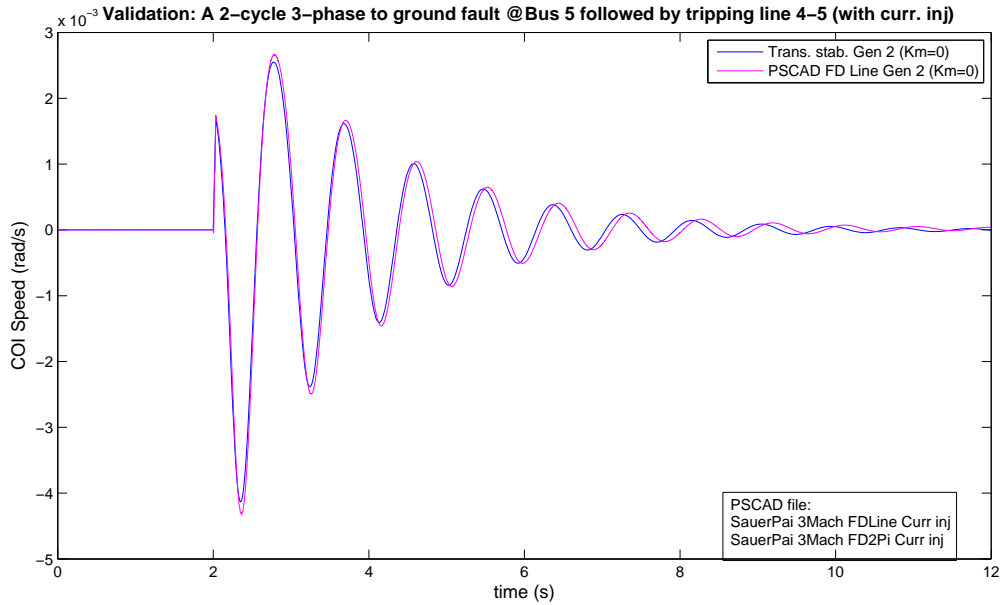


Figure 5.6: COI Speed for generator 2: Comparison between transient stability and PSCAD with VSC-HVDC modelled as current injection at the bus.

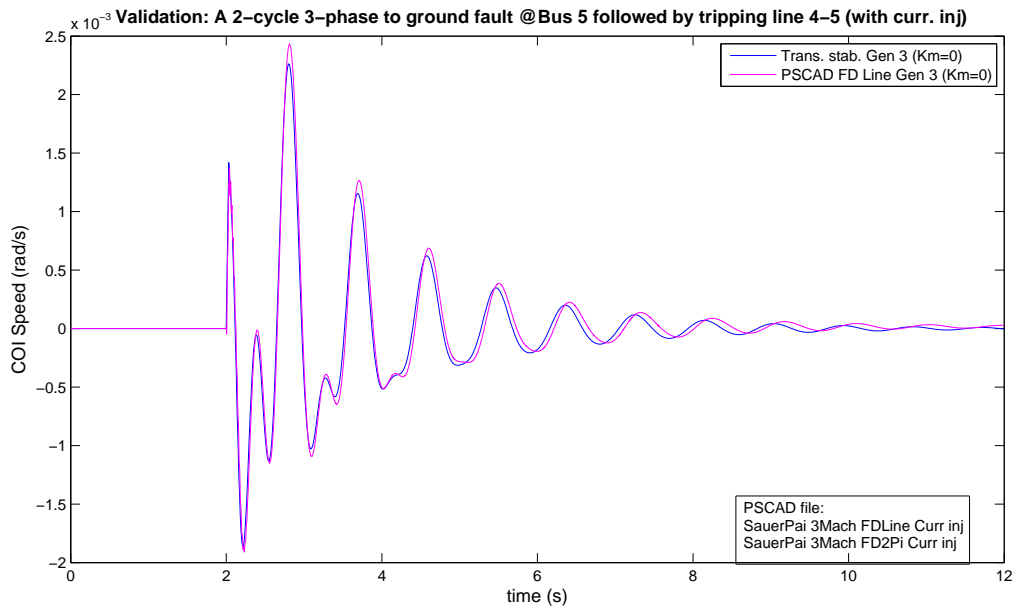
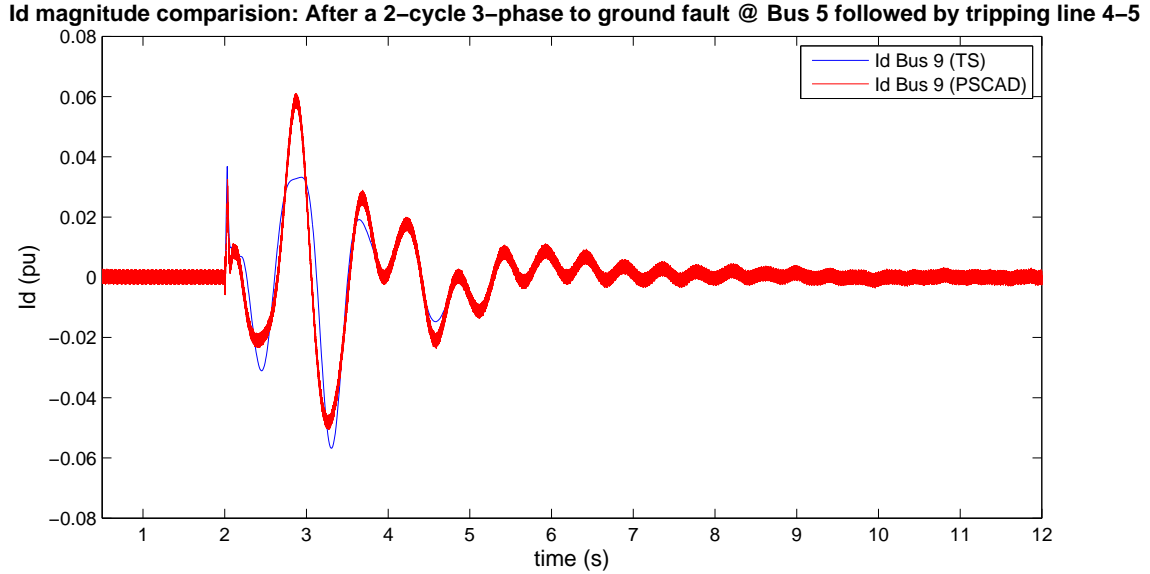


Figure 5.7: COI Speed for generator 3: Comparison between transient stability and PSCAD with VSC-HVDC modelled as current injection at the bus.

were modified, the rectifier controls -  $V_{dc}$  and  $Q$ , and the inverter controls -  $P$  and  $Q$ ; with  $Q$  kept as constant ( $Q = 0$ ) on both ends. The plots in Figs. 5.8 and 5.9, respectively, show the change in internal currents  $i_d$  and  $i_q$  that are used to control the

power of the VSC. The PSCAD plot very accurately captures the high frequency (HF) harmonics generated in the VSC due to the high frequency switching of the IGBTs.



**Figure 5.8: Comparison of VSC internal current magnitude:Plot for current injection in the d-q frame of VSC-HVDC link 1(Bus 8-9) representing d-axis current at the converter (inverter bus 9).**

The result of the simulation i.e. COI speed of the machines are shown in Figs. 5.10 - 5.12:

Inference. The Figs. 5.10 - 5.12 indicate that TS analysis does not capture the high frequency modes that are captured by EMT simulation. However, the TS model and the EMT model agrees well once the high frequency transients subside. It can therefore be inferred that, the TS model is suitable for modelling lower frequency dynamics.

## 5.2.2 Conclusion

. The following conclusions can be drawn from the various corroborative steps undertaken to compare the small-signal based model implemented in transient stability and the EMT simulation platforms results:

1. The  $\pi$ -model and the FD line model of the transmission line agree with each other. Thus the  $\pi$ -model of the transmission line in transient stability is suitable for analysing low frequency phenomenon.

**lq magnitude comparison: After a 2-cycle 3-phase to ground fault @ Bus 5 followed by tripping line 4-5**

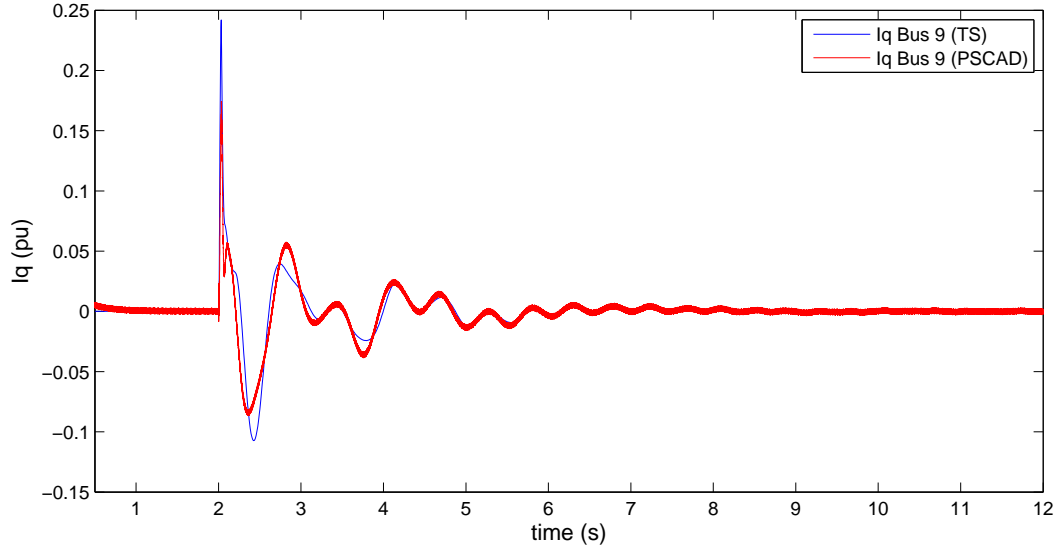


**Figure 5.9: Comparison of VSC internal current magnitude: Plot for current injection in the d-q frame of VSC-HVDC link 1(Bus 8-9) representing q-axis current at the converter (inverter bus 9).**

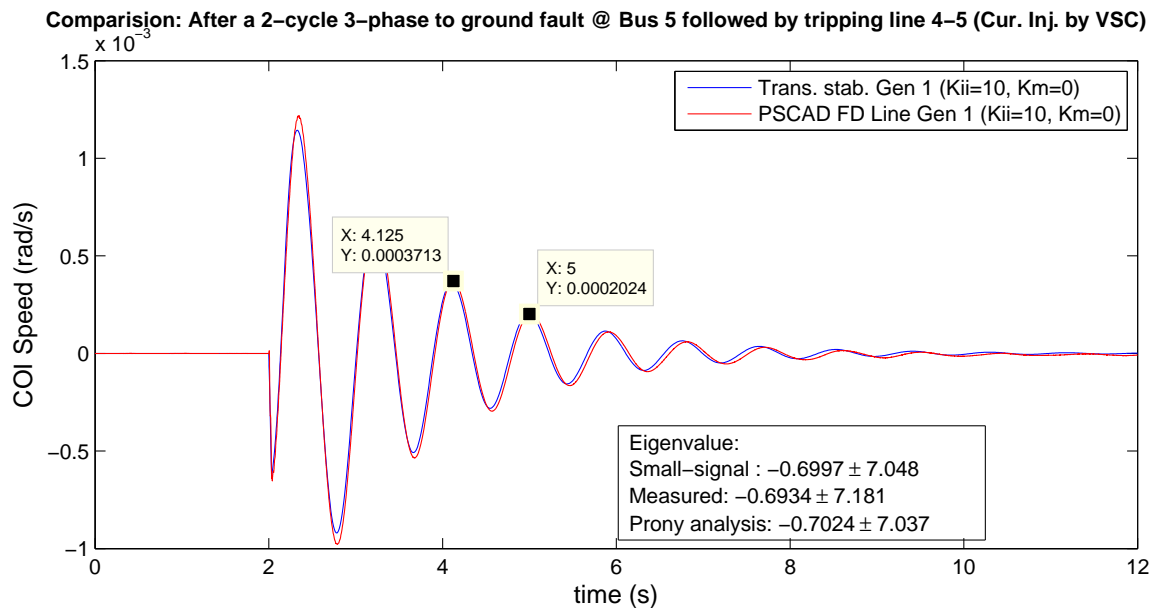


**Figure 5.10: COI Speed for generator 1: Comparison between transient stability and the PSCAD with the detailed VSC-HVDC model.**

2. The eigenvalue analysis of the system recorded through the small-signal model is accurately captured in the EMT simulation, as is apparent from Fig. 5.2. This confirms that the linearised system model is suitable for the analysis of low frequency oscillations.

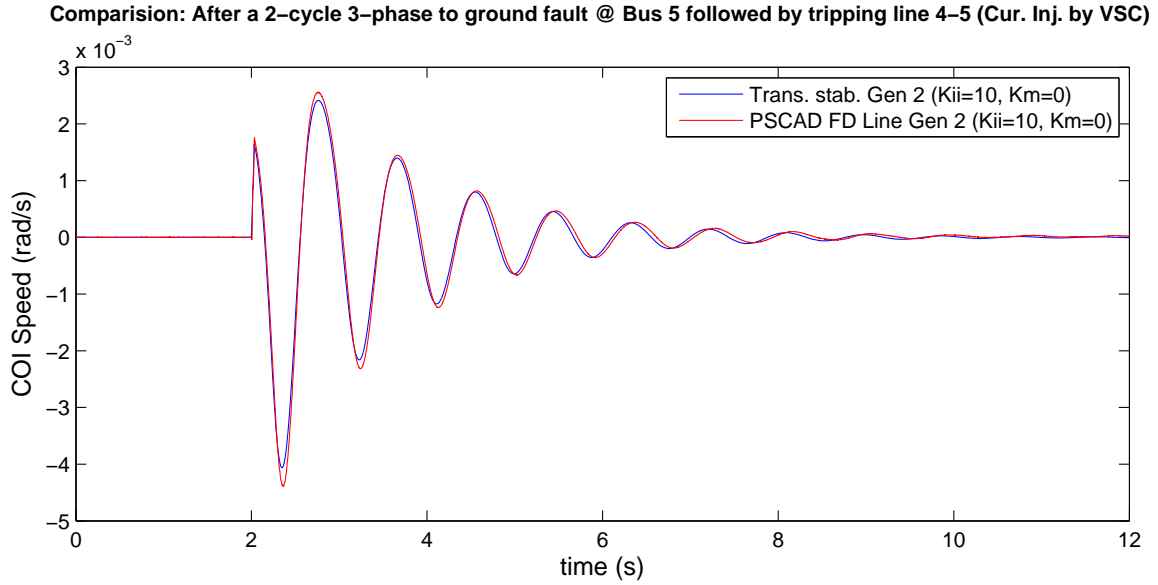


Figure 5.11: COI Speed for generator 2: Comparison between transient stability and the PSCAD the detailed VSC-HVDC model.

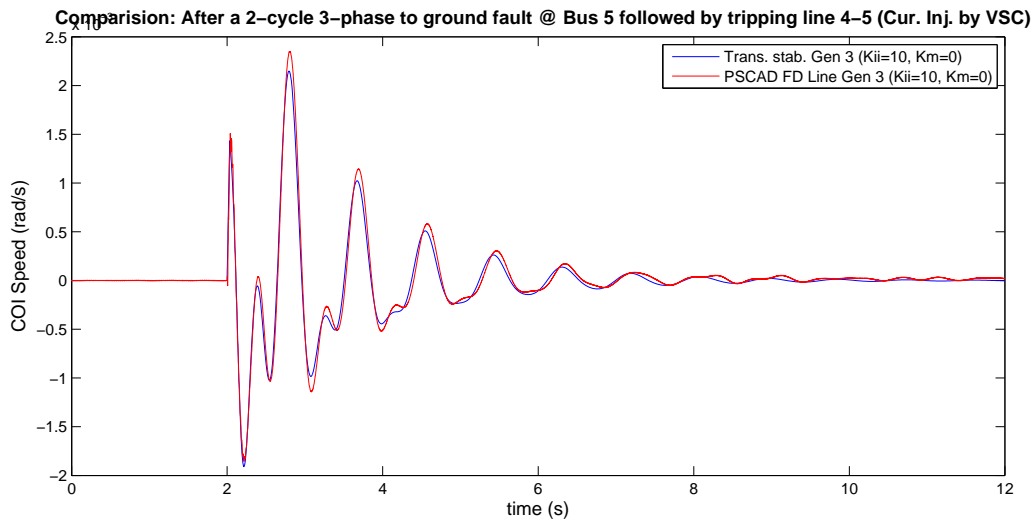


Figure 5.12: COI Speed for generator 3: Comparison between transient stability and the PSCAD the detailed VSC-HVDC model.

3. The behaviour of the current injection model VSC-HVDC and the detailed VSC-HVDC model agree closely. During the initial 4s duration (Fig. 5.8) the small variation is due to the high frequency transients that are not captured in TS simulation. Once these transients subside there is a complete match between TS and EMT simulation. The plots also highlight the inherent difference between the two environments, as the PSCAD software models the machine in full detail, it therefore captures the high



frequency modes as excited by the initiation of the fault and those related to HF switching. While the transient stability due to the simplified models is not able to capture them.

## 5.3 Performance evaluation of the proposed controller

### 5.3.1 Selective damping

The block diagram of the proposed damping controller is shown in Fig. 4.2. It was demonstrated in Chapter 4 in equation (4.32) that, change in the gains (i.e  $K_{ii}$  and  $K_m$ ) of the controller gain matrix  $[K]$  helps in damping the inter-area oscillations. Further, it was stated in Section-4.4.2, that the controller in addition to providing damping for the desired mode can be used to selectively damp out a particular mode by varying  $K_m$ .

It can be observed in Figs. 5.13 and 5.14, respectively, that as the value of  $K_m$  is

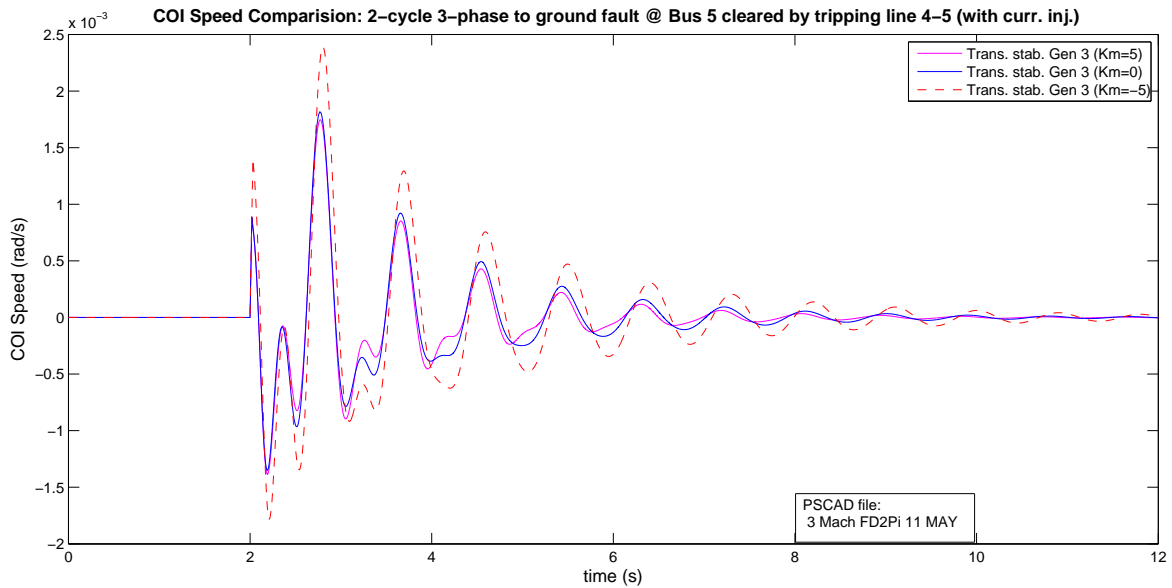


**Figure 5.13: COI Speed for generator 3: Effect of different gains on speed of machine in transient stability model.**

changed from +5 to -5 the damping of the swing mode improves/deteriorates. The effect of change in controller gain  $K_m$ , wherein the two swing modes are observable in the comparison of the COI speed for generator-3, is depicted. Table 4.4.2 provides a comparison of the eigenvalues computed by using the small-signal analysis program with

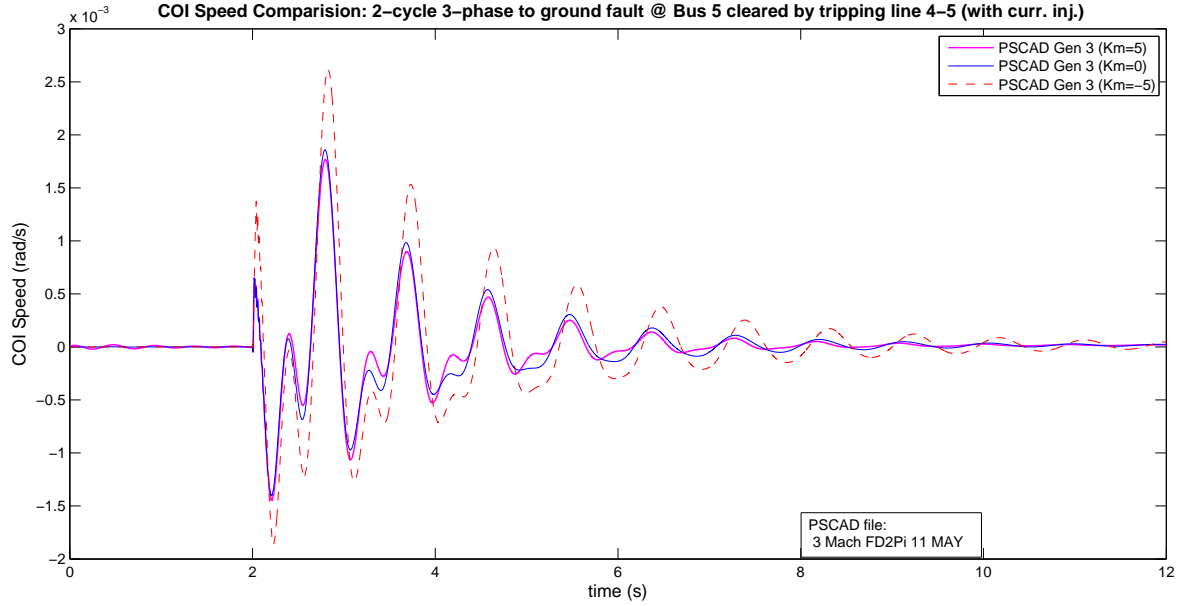


**Figure 5.14: COI Speed for generator 3: Effect of different gains on speed of machine in PSCAD model.**

those computed using the Prony analysis of the time-domain simulation of the COI speed waveform, for the change in controller gain  $K_m$  from +5 to -5.

The following can be observed from the traces in Figs. 5.13 and Table 5.1:

- As the gain  $K_m$  is changed from 0 to +5, there is improvement in the damping of the 7 rad/s and 14 rad/s modes. This improvement is demonstrated using both small-signal and Prony Analysis.
- However, on changing the value of  $K_m$  from 0 to -5, it can be observed that the

		<b>Km=5</b>	<b>Km=0</b>	<b>Km=-5</b>
<b>Mode-I</b>	Determined using Small-signal method	$-1.027 \pm j14.234$	$-0.8882 \pm j14.50$	$-1.375 \pm j14.553$
	Estimated using Prony analysis	$-1.038 \pm j14.110$	$-0.8989 \pm j14.202$	$-1.445 \pm j14.175$
<b>Mode-II</b>	Determined using Small-signal method	$-0.6879 \pm j6.994$	$-0.5467 \pm j7.046$	$-0.4298 \pm j6.889$
	Estimated using Prony analysis	$-0.7052 \pm j7.042$	$-0.5667 \pm j7.02$	$-0.4358 \pm j6.979$

**Table 5.1: Selective modal damping: Table compares the change in eigenvalues for with the values of  $K_m$  and the ability to selectively damp a particular mode.**

damping of the 14 rad/s mode is improved whereas the damping of the 7 rad/s mode deteriorates. (The damping of the 7 rad/s mode is, however, better than the case when there is No Control, where the eigenvalues are  $-0.8245 \pm j14.2465$  and  $-0.4113 \pm j6.9913$ ).

- This enforces the quality of the controller that in any circumstance the damping provided is always better than no control.

It has been shown that the plots between TS and EMT simulation agree closely, therefore, for clarity the transient stability and the PSCAD plots have not been superimposed on each other in one frame.

**Modulation power injection.** The effect of the controller can be better visualised when observing the amount of modulation power being injected by the controller through VSC-HVDC at the inverter bus. The effect of the controller on the modulation of injected powers at the respective inverter buses 4 and 9, as a result of controller action to damp the inter-area oscillations, has been validated as shown, in Figs. 5.15 and 5.16. The plots show complete agreement between the two simulation environments.

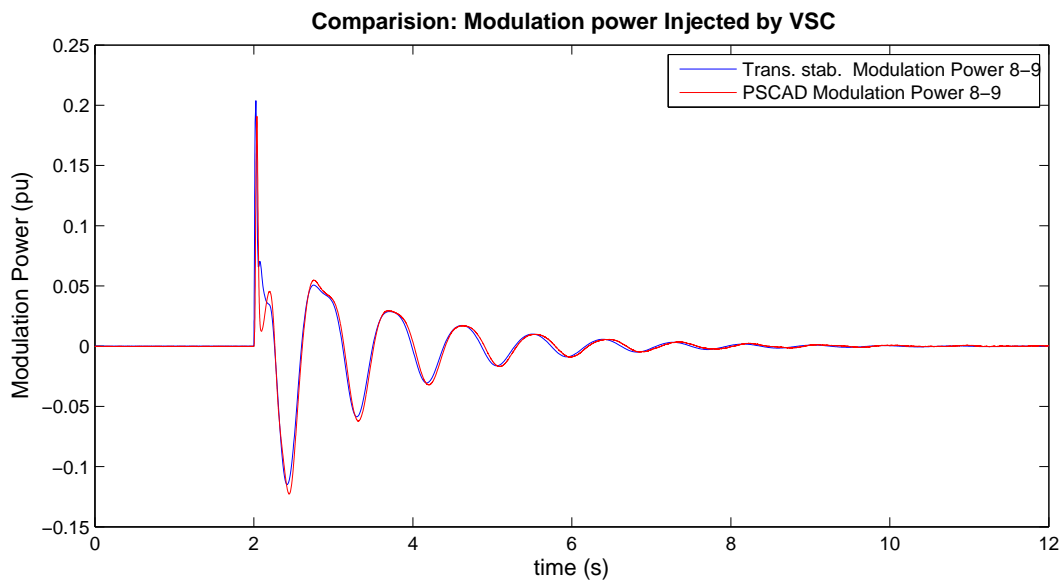


**Figure 5.15: Modulation power injection @ HVDC link 8-9: Comparison between transient stability and PSCAD simulation models.**

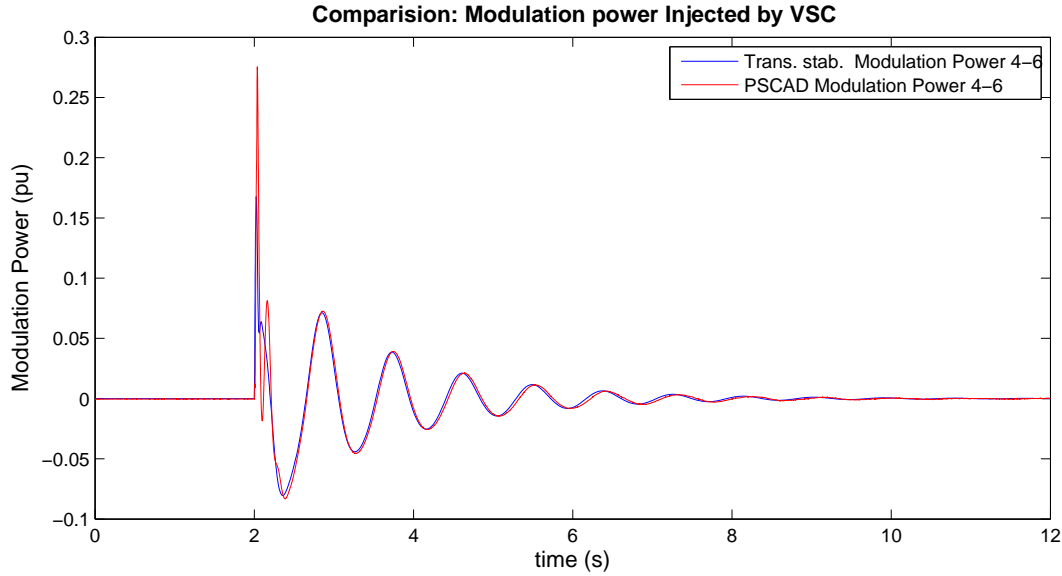


**Figure 5.16: Modulation power injection @ HVDC link 4-6: Comparison between transient stability and PSCAD simulation model.**

### 5.3.2 Effect of damping controller gains on system stability

In [36] it has been demonstrated that, using a controller based on bus voltage phase angular difference, *with an SPD gain matrix and for small gains*, the eigenvalues can be moved towards the left half plane, thereby providing better damping. In [82] and in Section 4.2.2 on the design of the proposed controller it is shown that, if the gain matrix in equation (4.32) is maintained as SPD, then with large increase in gains the open-loop poles move significantly towards the left hand side of the  $j\omega$  axis, resulting in increased damping. This in itself throws up a significant question, which is: “Can the controller gains be increased to a very large value so as to get a flat or very well damped system?” During the design of the damping controller [16, 55, 56], careful selection of various parameters are called for but no mention has been made on the limit of increase in the controller gains and its effect on system stability.

In the previous sections, I have shown that the small-signal model agrees very well with the TS model for small disturbances. As the TS model provides a time-domain plot, it is compared in this section, with EMT simulation to determine its accuracy, and thus, in turn, the accuracy of the small-signal model. This research has investigated through EMT simulation, the limit to which the controller gains can be increased beyond which

it would result in system instability. During this investigation the detailed model of the system (both machines and VSC-HVDC with controllers) has been used. The 3-machine,

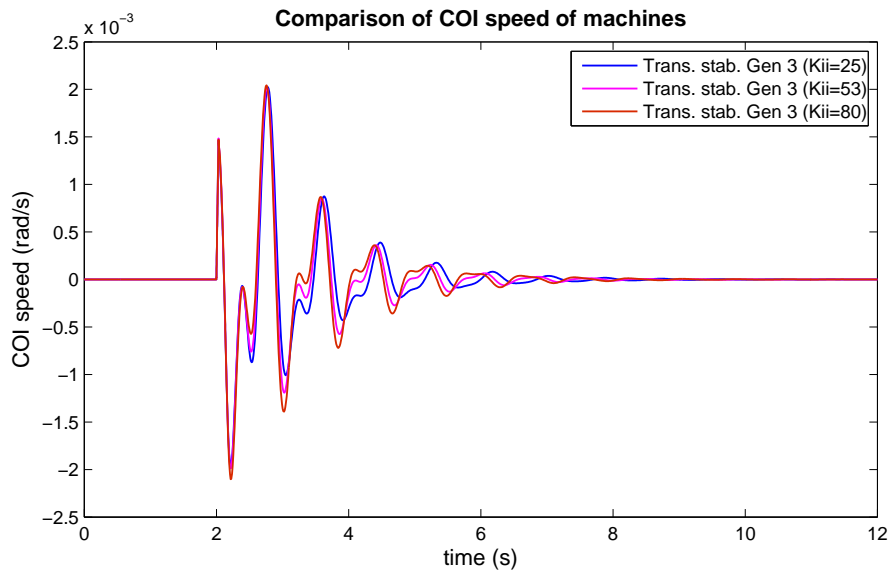


**Figure 5.17: Transient stability plot for varying  $K_{ii}$  depicting stable system**

9-bus test system was put through successive simulation in the TS program and in the PSCAD for different values of damping controller gain ( $K_{ii}$ ). It was observed that, with  $K_{ii} = 53$  in the PSCAD simulation, the system becomes unstable as seen from Figs. (5.18 - 5.19), as large power swings are introduced. In contrast the TS program in Fig. 5.17, shows that the system is stable even for  $K_{ii} = 80$ . The result obtained from EMT is compared with the TS analysis based current injection model of the HVDC system in the TS program. The traces above reflect that the TS simulation shows stable operation for the controller gain  $K_{ii} = 53$  whereas the EMT indicates instability. Now we definitely know that the instability it is not due to higher EMT details of T-lines or machines, but it is definitely due to the internal modes of the converters. The TS program is not able to capture these internal modes of the VSC-HVDC as the HVDC link is modelled as current injection in the TS program. A further investigation in the PSCAD/EMTDC simulation of the instability was carried out with the machines treated as voltage sources, thereby negating the effects caused by the dynamics of the machine. The simulation in Fig. 5.18 clearly shows that at  $K_{ii} = 53$ , a 9.1 Hz (57.2 rad/s) oscillations in the system starts to grow leading to instability. This further indicates that, the cause of instability in the system is not due to the behaviour of the machine but due to the interaction between

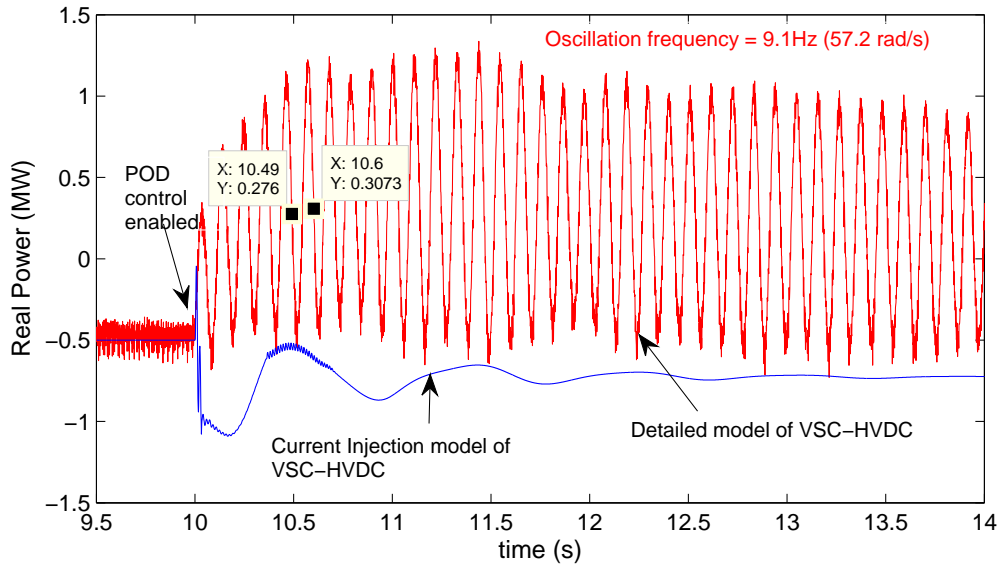


Figure 5.18: Comparison between detailed (PSCAD) VSC-HVDC model and TS current injection based HVDC model. At  $K_{ii} = 53$ , the PSCAD plot shows instability, whereas the TS plot indicates stable operation.

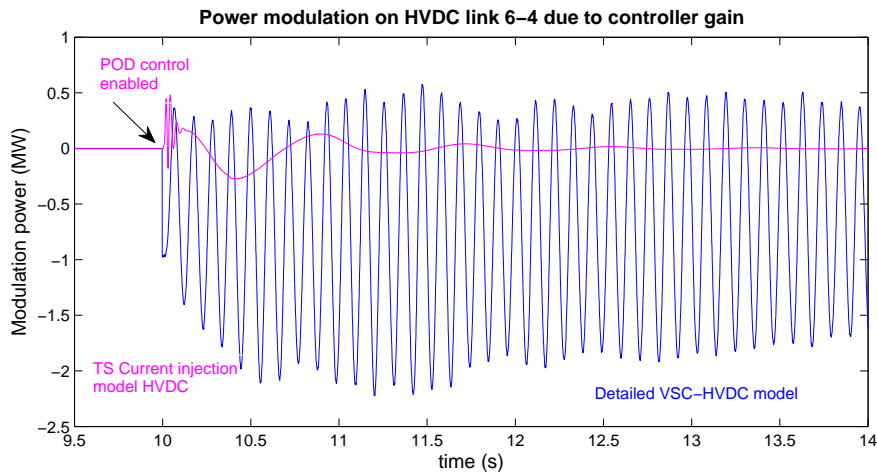


Figure 5.19: Comparison between the detailed VSC-HVDC model and TS current injection model for HVDC. At  $K_{ii} = 53$ , the PSCAD trace for modulation power injected signal depicts instability, whereas the TS trace depicts stable operation.

the damping controller and the controller of the VSC-HVDC.

It is difficult to analyse a complex system incorporating machines, transmission lines and multiple non-linear systems (VSC converter) analytically for system stability and quantify the response for a specific parameter (controller gain). To get over this hurdle of complex analytical solution, the analysis of frequency response of the system using

Nyquist stability criterion can be done to arrive at the stability limits. Frequency response analysis is dealt with in the next chapter.

## 5.4 Summary

This chapter described the effort involved in corroboration of TS and EMT simulations, its need in a system setting and the procedure adopted to evaluate the design of the proposed damping controller. The process has shown that the Transient Stability simulation agrees very closely with the EMT simulation. The EMT simulation (PSCAD/EMTDC) also captures the high frequency modes, which is expected as the machine and the AC transmission system are modeled in complete detail. The Transient Stability simulation software uses a simplified model of the machine and the fundamental frequency phasor model for the transmission lines; therefore it cannot capture the high frequency modes. The performance evaluation of the proposed damping controller by EMT simulation demonstrates the occurrence of system instability for a large controller gain value, which the Transient Stability simulation fails to show. This aspect of very large increase in controller gains of a POD controller that may lead to system instability has never been demonstrated.

# Chapter 6

## Frequency Scan and Nyquist Stability Criterion

The previous chapter demonstrated that, there is an upper limit to the increase in the gains of the damping controller. The small signal model predicted a value for this limit that was completely corroborated by the TS simulation model, and for a significant range of gains, this small signal model is perfectly adequate. However, the two simulation platforms (i.e. TS and EMT) indicate different value for the upper limit. Both the simulation methods do point out that there is an upper limit, with the TS simulation model indicating a very large value ( $K_{ii} = 115$ ) and the EMT simulation model indicates a relatively smaller value ( $K_{ii} = 53$ ). The previous chapter showed that this variation in the range was due to internal modes of the VSC, which were not modelled while developing the small-signal(SS) model, and also not included in the TS simulation model.

However, the EMT simulation model cannot be easily compared with a higher level SS model, as its complexity makes it difficult to obtain it. This chapter presents an alternative practical approach where using EMT simulation combined with a frequency scan we can develop a detailed SS model representation, that can be used to determine stability information using a Nyquist Stability Criterion. As pointed out in the previous chapter, the earlier simplified SS and TS simulation models are sufficient to analyse the majority of situations, and the higher order model is mainly recommended as a check to ascertain whether or not one is operating in the range of validity of the simplified SS model. The test system, due to its multi-input multi-output nature, is difficult to accurately anal-



yse and model. This chapter presents a brief description about the frequency scanning technique and how this technique can be employed to develop a transfer function for the complex system. The transfer function obtained through the use of frequency scanning is used to analyse the system response and comment on its stability. This chapter also describes the use of a Nyquist Stability Criterion, a frequency response method, based on a graphical procedure for determining stability information of a closed-loop system.

## 6.1 Introduction

The power network including the HVDC transmission system is composed of machines and power electronic (PE) devices such as converters and wide-band controllers. These power electronic devices generally are switched at high frequency, which causes harmonics in current and voltage waveforms. Such harmonics have the potential to adversely interact with the other elements of the network causing instability. Time-domain Electro-Magnetic Transient (EMT) simulation is the most accurate and reliable method to investigate such interactions. However, a large number of simulations with different parameter settings are needed for a comprehensive analysis. A better insight into the system behaviour due to change in parameters can be done by analysis of the linearised state-space model. Thus development of an accurate mathematical model for a given system is one way to do this analysis, but it may be difficult to obtain this for complex converter systems. Frequency scanning is a pragmatic alternative, which involves the use of a digital time-domain simulation program to numerically obtain the small-signal frequency response of a system [83]. The frequency scanning technique is used to obtain the transfer function and thus the state-space model for a system [84]. This technique is very useful as the model for any complex system can be obtained without compromising on the details or introducing simplifications. If a sinusoidal signal is applied as an input to a Linear Time-Invariant (LTI) system, then it produces the steady state output, which is also a sinusoidal signal, the ratio of the output to input in the frequency domain gives the transfer function (TF) at that frequency. The input and output sinusoidal signals have the same frequency, but different amplitudes and phase angles. The steady state frequency response of a system is the locus of the steady state transfer function, i.e. the

ratio of output over input, as a function of frequency.

## 6.2 The Frequency Scanning Technique

Frequency scanning is a simulation based method of extracting a small-signal frequency-domain model of a system from its time domain response to a small-amplitude wide-band signal injected at its input [83] as shown in Figs. 6.1a and 6.1b. There are no restrictions on the extent of detail in the system model in this approach. A user does not need to know the complete details of the study model as this is probed/observed only at available inputs/outputs. Frequency scanning and the subsequent use of the frequency response information is based on the model being Linear Time-Invariant (LTI) at least for small signal analysis.

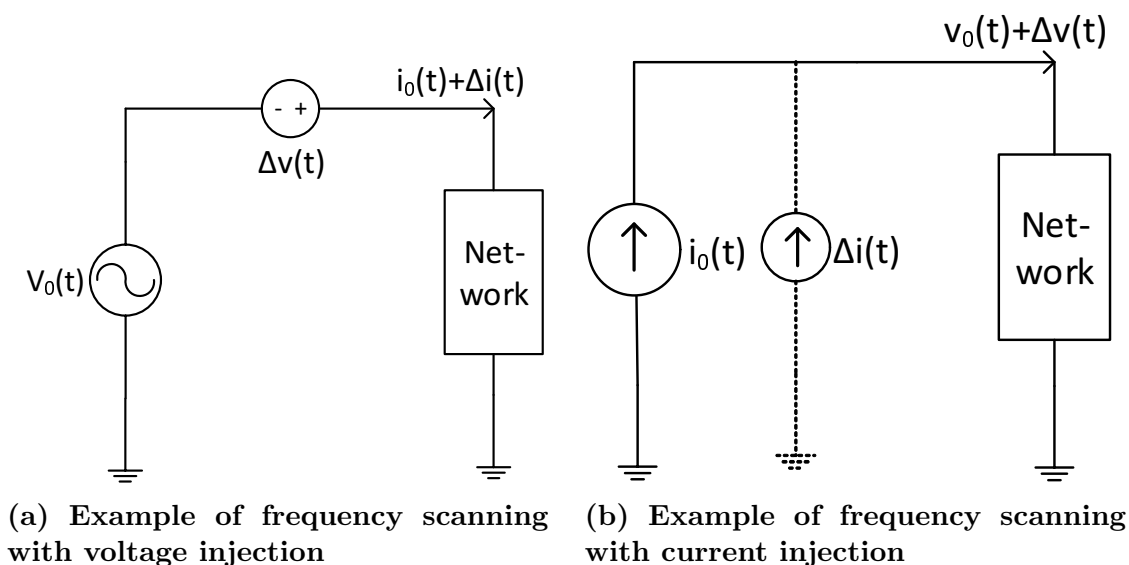


**Figure 6.1: Example of frequency scanning technique**

The system is injected with superimposed voltage/current signals starting from the equilibrium condition (operating point) around which the response to this injection is obtained. Each simulation is carried out for a sufficient duration so that the natural transients die out and we get the sinusoidal steady state response. Instead of obtaining the steady state response for each frequency separately (which is time consuming), a

multi-sine injection signal (see Fig. 6.2), of the following form is generally used [83].

$$u(t) = a \sum_{l=l_0}^N \sin(2\pi f_d l t + \delta_l) \quad (6.1)$$

All the frequency components of  $u(t)$  are multiples of  $f_d$ . Thus  $u(t)$ , is periodic with a

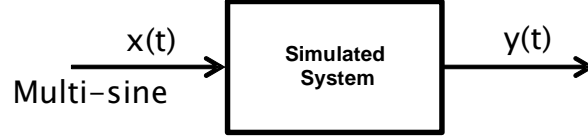


**Figure 6.2: Multi-sine signal for frequency scanning technique**

time period  $T_d = 1/f_d$ . As successive frequency components of  $u(t)$  are spaced-out over an interval  $f_d$ , it provides the resolution of the scan. Note that, if we selected  $\delta = 0$ , this would give an impulse train with a very large amplitude at the peaks. The amplitude  $u(t)$  is kept small as generally the PE systems and their controllers are non-linear systems, and we are interested in the small signal frequency response of the linearized system. The value of  $a$  and  $\delta_l$  are chosen such that the amplitude of  $u(t)$  remains small enough so that it does not excite the non-linearities of the model. For example, in the Schroeder multi-sine [85], for a given  $a$ , its possible to reduce the amplitude of  $u(t)$ , by choosing the  $\delta_l$  to have a quadratic dependence on  $l$ , as given below:

$$\delta_l = -\frac{(l - l_0)(l - l_0 + 1)}{N - l_0 + 1} \pi \quad (6.2)$$

Once the natural transients have died down, the response for a period  $T_d$  is stored, and a Fast Fourier Transform (FFT) of both the input and output signals is done to obtain the frequency response.

### 6.3 Nyquist Analysis

Nyquist analysis, is a graphical frequency response analysis method to determine absolute and relative stability of closed-loop systems. The stability information is directly available from the graph of the open-loop frequency response transfer function  $GH(\omega)$ . A Nyquist plot is a type of polar plot for finding the stability of the closed-loop system by varying the

frequency  $\omega$  from  $-\infty$  to  $\infty$ . Therefore, the Nyquist plots are used to draw the complete frequency response of the open loop transfer function.

### 6.3.1 Nyquist Stability Criteria

The study of interactions between the controller and the network can be done using stability analysis methods like the Nyquist Stability Criterion, provided the model is LTI. Small-signal instabilities can occur due to adverse interactions between connected systems or due to components of the system (e.g. controllers). The main use of frequency scanning is to analyse and study the occurrence of such adverse interactions in the system. As a preliminary step towards such a study, the complete system is represented as the combination of two independent systems as shown in Fig. 6.3a, whereas the closed loop frequency response of the system may be obtained as shown in Fig. 6.3b. In the following discussion, the POD controller has a transfer function  $G(s)$ , and the AC-DC networks transfer function is  $H(s)$ . Note that  $G(s)$  is chosen to have no poles in the RHP(Right Hand Plane)and it is assumed that the AC-DC network is stable and therefore it also has no poles in the RHP. Consequently  $GH$  has no poles in the RHP. As we know, the POD has 2-input, 2-output structure as shown in Fig. 4.2. So  $G$  and  $H$  must be multi-input, multi-output (MIMO) systems. However, to simplify the discussion, we consider a case with  $G$  and  $H$  as single-input, single-output(SISO) system, as shown in Figs. 6.3a,6.3b. This will be later extended to the MIMO system.

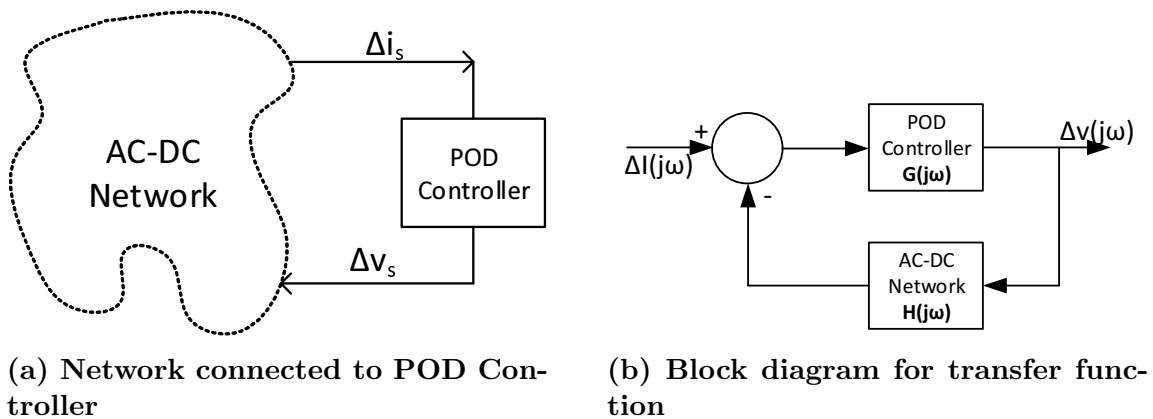


Figure 6.3: Example of frequency scanning of a network

A linear closed-loop system is absolutely stable if the roots of the characteristic equa-

tion have negative real part. Alternately, the poles of the closed-loop transfer function, or the *zeroes* of the denominator  $1 + GH(s)$  of the closed-loop transfer function must lie in the left-half plane (LHP). The Nyquist stability criterion works on the *Cauchy's Principle of Argument*. It states that, if there are  $P$  poles and  $Z$  zeroes, that are enclosed by the 's' plane closed path, then the corresponding  $1 + G(s)H(s)$  locus with  $s = j\omega$ , and  $\omega$  varying from  $-\infty$  to  $+\infty$  must encircle the origin  $P - Z$  times. Therefore, we can write the number of anti-clockwise encirclements  $N$  as,

$$N = P - Z \quad (6.3)$$

It is well known that the closed loop control system is stable if all the poles of the closed loop transfer function (i.e. roots of the characteristic equation) are in the LHP of the 's' plane. The system stability evaluation can be correlated by the following statements:

- The  $P$  poles of  $1 + G(s)H(s)$  are the same as the poles of the open-loop system.
- The  $Z$  zeros of  $1 + G(s)H(s)$  are same as the closed-loop poles of the system.

It is also well known that if an *open loop* system is stable, then  $1 + G(s)H(s)$  will have no pole in the the RHP of the 's' plane  $\implies P = 0$ . If the closed system is also stable, then  $1 + G(s)H(s)$  will have no right hand side zeroes as these are poles of the closed loop system. This condition is tantamount to, a closed-loop system is stable if  $N = 0$  (i.e. the locus of  $1 + G(s)H(s)$  has *no encirclement* around the origin). Hence, it can be summarized that, that if the open loop system  $G(s)H(s)$  is stable, then the closed-loop system is stable if and only if the locus of  $1 + G(s)H(s)$  has no encirclements of the origin. The above inferences are for a SISO system, for a MIMO system the closed-loop transfer function is a matrix, therefore, the Generalized Nyquist Criterion(GNC) [86] is used to check the stability of the closed-loop feedback system.

### 6.3.2 Generalized Nyquist Criteria

Extending the preceding discussion to the MIMO system case, the closed loop system is stable provided there is no encirclement of the contour of  $TF(j\omega) = \det(I + GH(j\omega))$  around the origin of the complex plane as  $\omega$  traverses from  $-\infty$  to  $\infty$ .  $H(j\omega)$  was obtained

using the method described in Section-6.2. The frequency response plots for each element (i.e.,  $H_{11}(j\omega)$ ,  $H_{12}(j\omega)$ ,  $H_{21}(j\omega)$  and  $H_{22}(j\omega)$ ) is shown in Fig. 6.4. The Frequency response of  $G(j\omega)$  was developed analytically from the structure in Fig. 4.2.

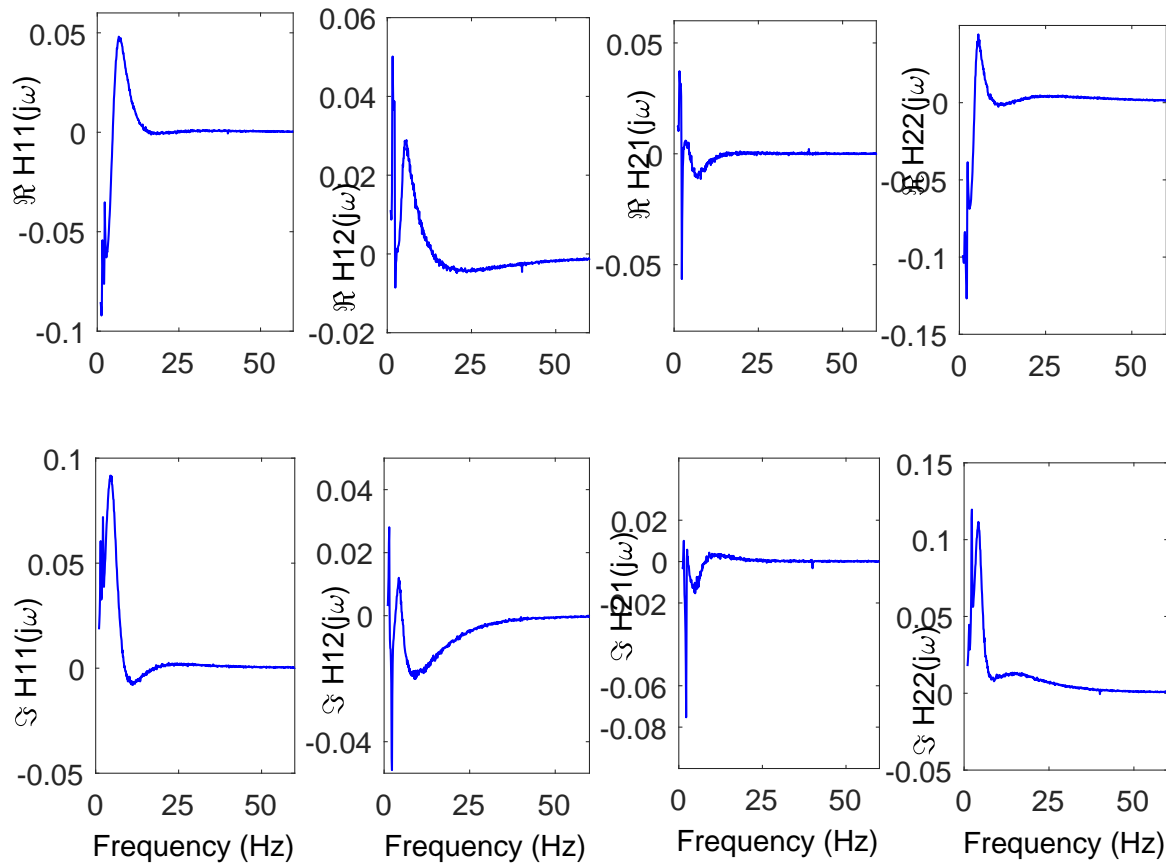


Figure 6.4: Frequency scan plot for the real and imaginary parts of transfer function  $H(j\omega)$  for the AC-DC system

## 6.4 Case Studies

In this section, I assess the ability of the frequency scan model obtained for the AC-DC system coupled with the POD controller model to analyse the overall system stability using the GNC.

### 6.4.1 POD controller - HVDC system interaction

Fig. 5.1 represents the AC-DC network with the proposed damping controller as shown in Fig. 4.2. The system operating point is obtained by the load-flow with quiescent power on the two HVDC links being zero. The system data is given in Appendix A. The frequency scan of the AC-DC system is obtained while the model of the proposed damping controller is known. The GNC is then used to evaluate the stability range for the controller with the change in controller gains  $K_{ii}$ .

A multi-sine input power signal of 0.1 MW with a frequency resolution of 0.1Hz was used for frequency scanning. The Nyquist contours (i.e., plot of  $\det(I+G(j\omega)H(j\omega))$ ) varying  $\omega$  from  $-\infty$  to  $+\infty$  is shown in Figs. 6.5 and 6.6 for gain  $K_{11} = K_{22} = 51$  and 53, respectively.

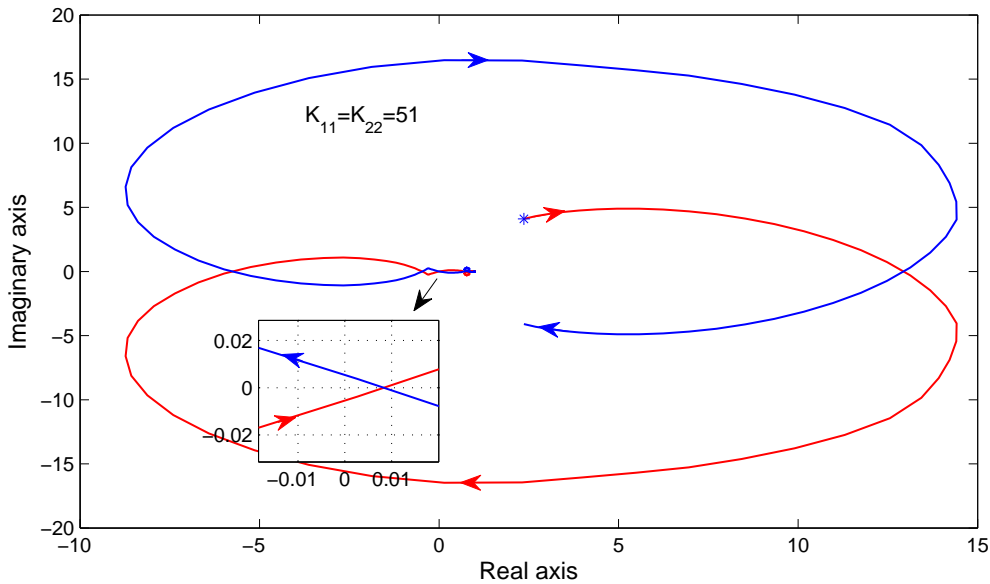


**Figure 6.5: Stable system condition: Nyquist contour for  $K_{ii} = 51$  showing no encirclements of origin.**

### Conclusion

The following inferences can be drawn from the traces Figs. 6.5 and 6.6 for varying  $K_{ii}$  values:

- The plot for  $K_{ii} = 51$  does not encircle the origin and therefore corresponds to a stable system.

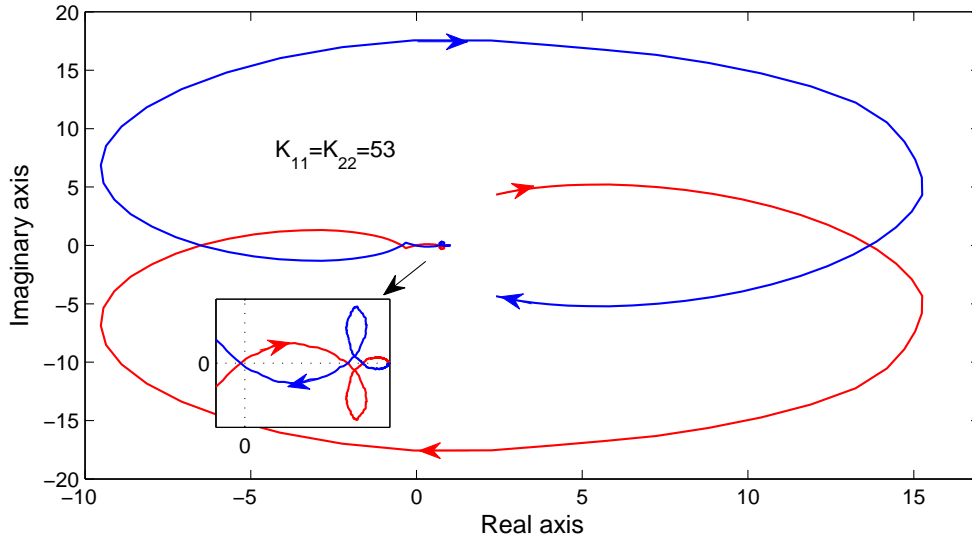


**Figure 6.6: Stable system condition: Nyquist contour for  $K_{ii} = 53$  showing Two encirclements of origin.**

- On the other hand, the contour plot for  $K_{ii} = 53$  encircles twice in the clockwise direction, indicating two poles of the closed loop system in the RHP, and hence an unstable system.
- Figs. 6.5 and 6.6 are consistent with the EMT simulation which shows instability for  $K_{ii} = 53$ .
- Note that the frequency response plots for  $G(j\omega)$  and  $H(j\omega)$  were obtained independently in this analysis. This confirms that the instability observed in the EMT simulation is not because of some numerical issues but are likely due to actual destabilization of the converter's internal dynamics which are ignored in the simplified small-signal model.

#### **6.4.2 Change in AC system operating point: POD controller - HVDC system interaction**

To further evaluate the performance of the proposed controller, the operating point of the AC system was changed such that, generation at machine-2 was reduced by 30% whereas the generation at machine-3 was increased by the same amount (refer to Table A.4 for



load-flow). This change provides us with a new operating point. The multi-sine signal as in Section 6.4.1, was used to scan the system. The proposed controllers' response to changes in the gain has been plotted using Nyquist contours to evaluate the system stability as a function of these gains.

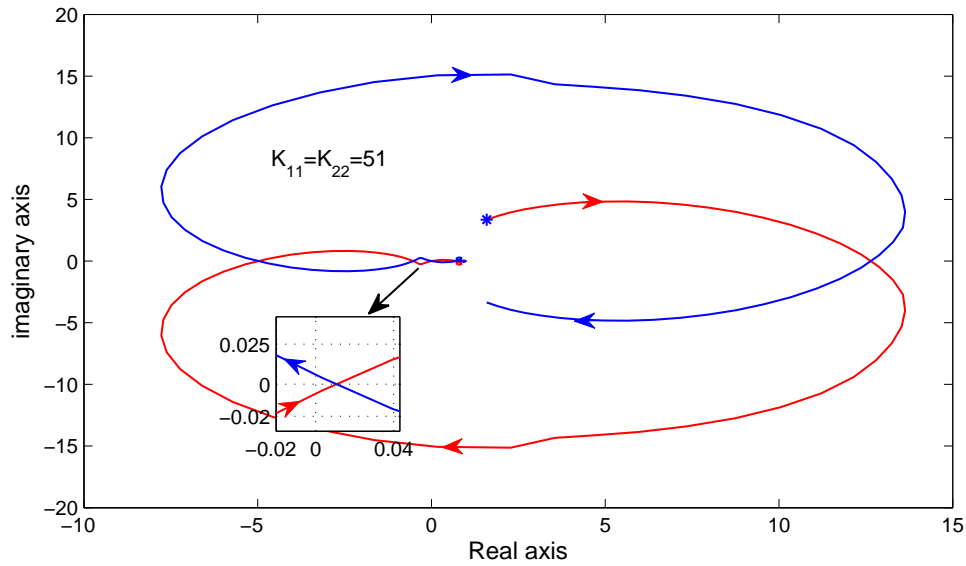


**Figure 6.7: Stable system condition: Nyquist contour for  $K_{ii} = 51$  showing one clockwise and one anti-clockwise or net zero encirclements of origin.**

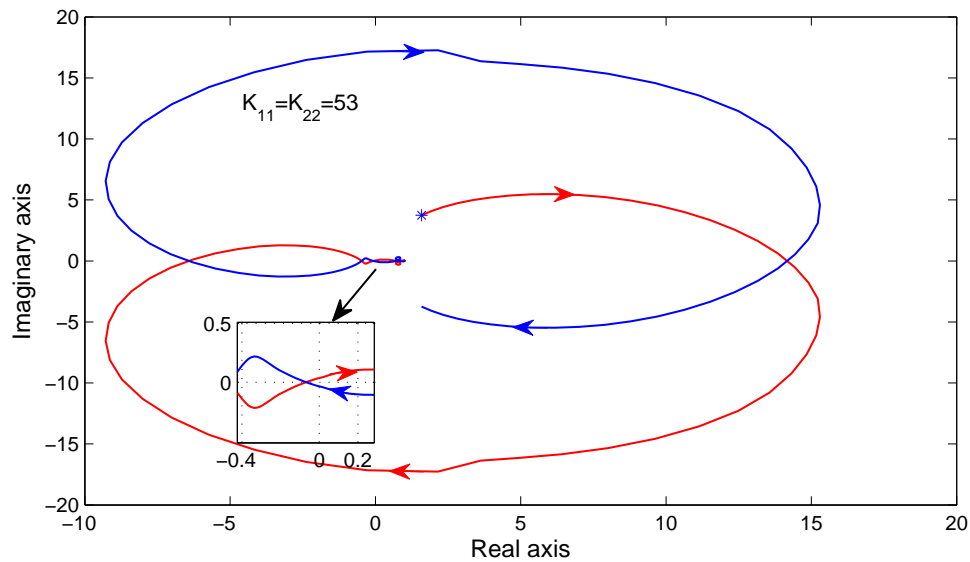


**Figure 6.8: Stable system condition: Nyquist contour for  $K_{ii} = 53$  showing Two encirclements of origin.**

Similarly, in Fig. 6.8 it can be noticed that as the gain  $K_{ii}$  is increased to 53, it

results in system instability. This is also depicted by the Nyquist contour which shows two clockwise encirclements of the origin.

## Conclusion

The traces above indicate that the instability onset gain is not significantly affected by the operating point of the converters. Although in this case the VSC-HVDC system in steady state was transmitting zero power.

### 6.4.3 Change in HVDC operating point: POD controller - HVDC system interaction

The HVDC links are carrying zero quiescent power in steady state. As has been shown in the previous case study, a significant change in the power output of the machines does not significantly alter the bus voltages at the converter bus. Therefore, a change in the operating point condition of the DC link can be obtained by changing the outer-loop controller parameters. Thus, the parameters of the power order controller shown in Fig. 2.3 were changed (proportional controller  $K_p$  changed from 0.1 to 0.4 and the time constant  $T_i$  changed from 0.01 to 0.05) to affect the operating point of the DC link. Again, the multi-sine signal described in Section 6.4.1, was used to obtain the frequency response of the system. The proposed controllers' response to changes in the gain is depicted using Nyquist contours to evaluate the system stability as a function of these gains. It can be observed from Fig. 6.9 that, when the gain  $K_{ii} = 42$ , there is one clockwise and one anti-clockwise encirclement of the origin. The net encirclements of the origin is zero, thus predicting a stable system. Similarly, from Fig. 6.10 it can be seen that as the gain  $K_{11} = K_{22}$  is increased to 45, system instability results. This can be corroborated by taking a look at the Nyquist contour which shows two clockwise encirclements of the origin.

## Conclusion

The Nyquist contour shows that the gain for onset of instability is significantly affected by the converter controller parameters.

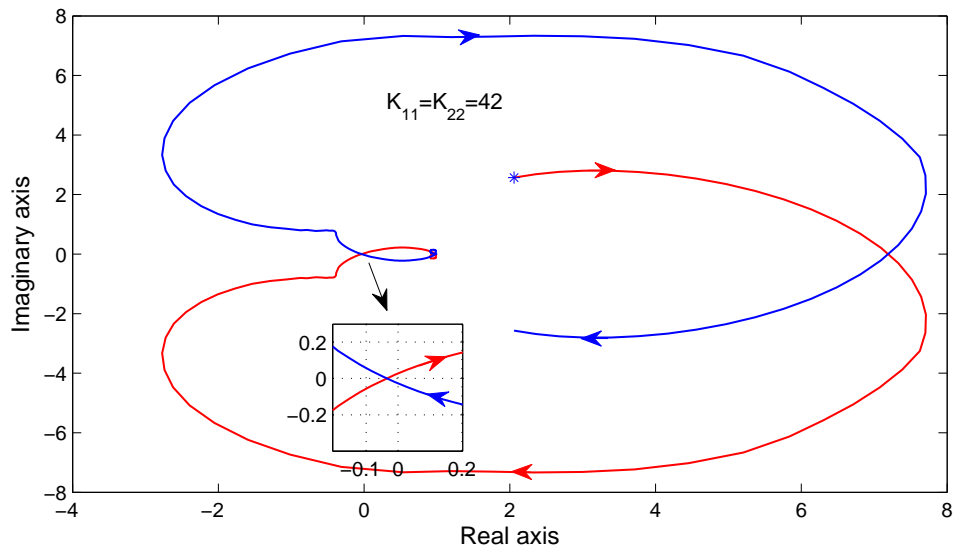


Figure 6.9: Stable system condition: Nyquist contour for  $K_{ii} = 42$  showing No encirclement of origin.

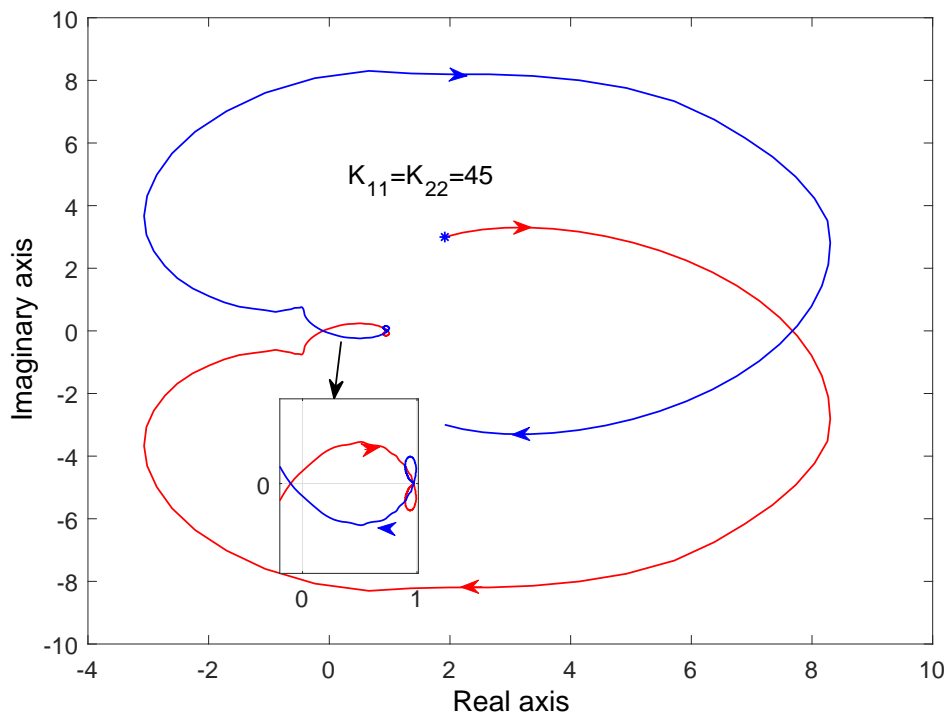
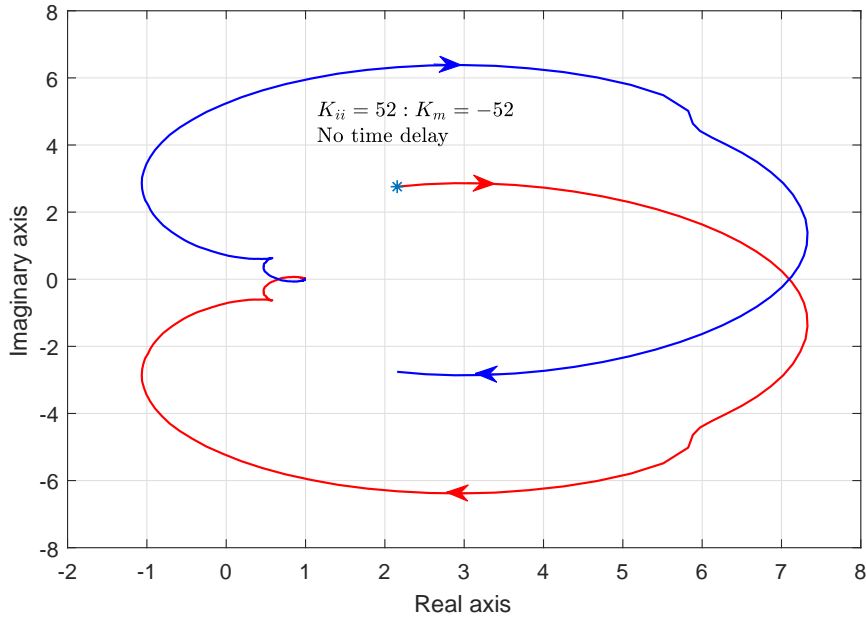


Figure 6.10: Stable system condition: Nyquist contour for  $K_{ii} = 45$  showing Two encirclements of origin.

#### 6.4.4 Communication delay: Effect on performance of controller

The performance of WAMS based POD controller as evaluated in section 6.4.1, showed the range of controller gains for a stable system. The performance evaluation of the controller assumed that the remote ( $K_m$ ) and local ( $K_{ii}$ ) signals are immediately available and there is no time delay associated with the remote signal  $K_m$ . The Nyquist plot with no communication delay contour for the case for ( $|K_m| = 52$ ) which is just below the critical value of 53 where the system becomes unstable, is shown in Fig. 6.11. This demonstrates that the system is stable as there is no encirclement of origin, although, because of its proximity to the stability limit, the plot comes very close to encircling it. In a practical application, the use of remote signals introduces a challenges into the



**Figure 6.11: Stable system condition: Nyquist contour for  $K_{ii} = 52$  and  $|K_m| = 52$ , with no communication delay shows no encirclements of origin.**

design of a wide area damping controller (WADC) due to the time delay caused by the communication technology. This delay may degrade the damping performance or may even cause instability of the closed-loop system [33]. The typical communication delay in a wide-area measurement system could range from tens to several hundred milliseconds [87, 33] depending upon communication medium, communication network length, network bandwidth, and several other factors. The delay associated with different communication

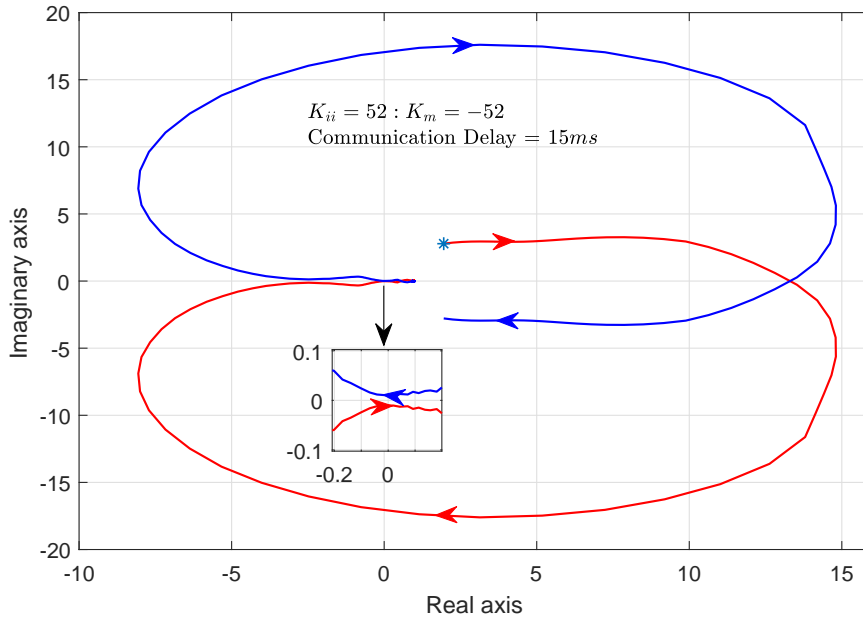


**Figure 6.12: Stable system condition: Nyquist contour for  $K_{ii} = 52$  and  $|K_m| = 52$ , with a communication delay of  $15ms$  shows no encirclements of origin.**

links is given in [88], which shows that the optical fiber communication link is the most suitable choice with lowest propagation delay. The study conducted by Bonneville Power Administration (BPA)[89] reported that the latency of fiber optic digital communication is approximately 38 ms, while that using modems via microwave is over 80 ms [89]. However, for dedicated links, the delays could be only a few ms larger than the travel time at the speed of light. In our case, the line length is  $115km$  which corresponds to a travel time of  $0.38ms$ . The delay in communicating the remote signal ( $K_m$ ) of the POD controller will manifest as phase delay at the swing mode frequency for this signal. The phase lag at a frequency either due to communication or transport delay is given by  $\omega T_d$ , where  $\omega$  is the frequency in radians/s. The delay may be variable, but this delay can be made constant by buffering the signals. The plot in Figs. 6.12 and 6.13 shows the effect communication delay has on the gain for the remote WAM signal ( $K_m$ ), and also on the system stability. As can be observed, at the peak value of local ( $K_{ii}$ ) and remote signal gains ( $K_m$ ) the critical time delay is  $15ms$  beyond which the system becomes unstable. These observations on the effect of time delays of  $15ms$  and  $16ms$  respectively, are also supported by the EMT simulations shown in Fig. 6.14a,6.14b.

A further investigation relating to the effect of communication delay on the gain ( $K_m$ )

of the remote signal was done and is shown in Fig. 6.15. In Fig. 6.15, the Y-axis relates to the maximum achievable gain ( $K_m$ ) for the remote signal, while the X-axis depicts time delay in  $ms$ . The plot shows that, for a delay of up to  $15ms$  both the local and the remote signal gain can be retained at the maximum value of 52. As the delay increases beyond  $16ms$  the maximum available value of the remote signal gain drops from 52 to 15, with the local gain at its maximum value. A  $10 - 15ms$  delay is entirely achievable with dedicated communication channels.

It can be observed in Fig. 6.15 that with a delay of  $16ms$  the gain  $K_m$  can only be increased to a value of 15 thereby compromising the ability to damp inter-area oscillations. However, as discussed in Section 4.2.2, the local signals along with the compromised gain for the remote signal provide improved damping as compared to “No Control” (when no damping controller is present). This ensures that, if the communication is lost, the damping is still better than without a damping controller. Hence, for excessive delay the

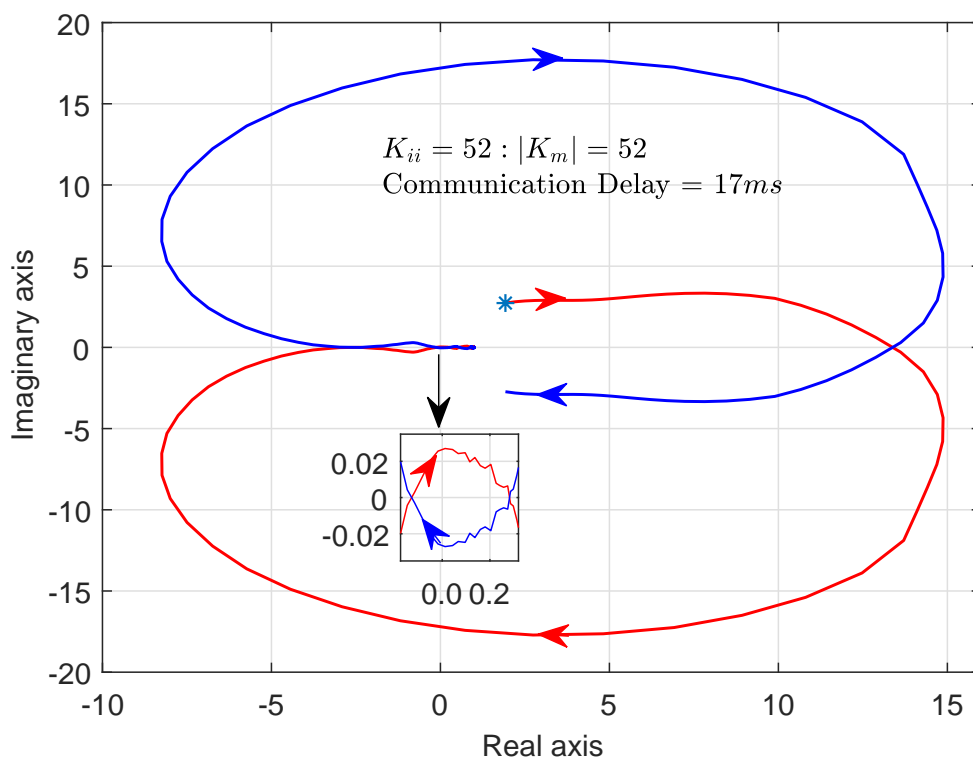
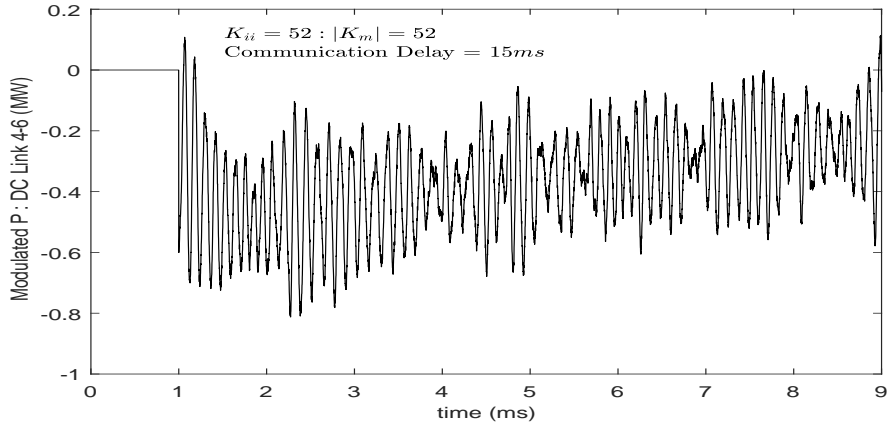
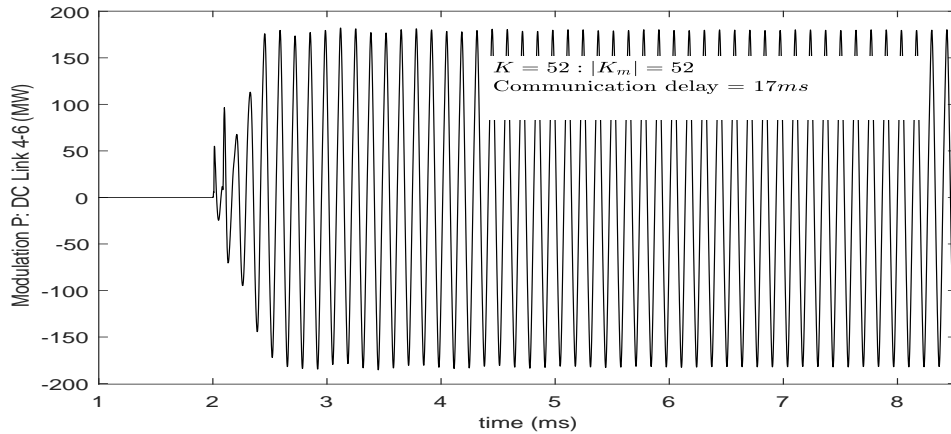


**Figure 6.13: Unstable system condition: Nyquist contour for  $K_{ii} = 52$  and  $|K_m| = 52$ , with a communication delay of  $16ms$  shows two encirclements of origin.**



(a)



(b)

**Figure 6.14: Effect of communication delay: (a) An EMT simulation with a delay of 15ms for local ( $K_{ii} = 52$ ) and remote ( $|K_m| = 52$ ) signal gains shows stable system. (b) As for a delay of 16ms with the same gains the system becomes unstable.**

remote gain  $K_m$  could be set to zero, i.e., the communication channel could be assumed to be lost. This is possible because the communicated signal would be in digital form with a GPS based time-stamp. Note that in order to have a minimal time delay, it is assumed that a dedicated communication link is available. Assuming that the signal travels at the speed of light ( $300kms/ms$ ), even a 10ms signal delay corresponds to a large geographical extent of  $3000kms$ . Additional time for coding etc. would be needed but could be relatively small in comparison to delay.

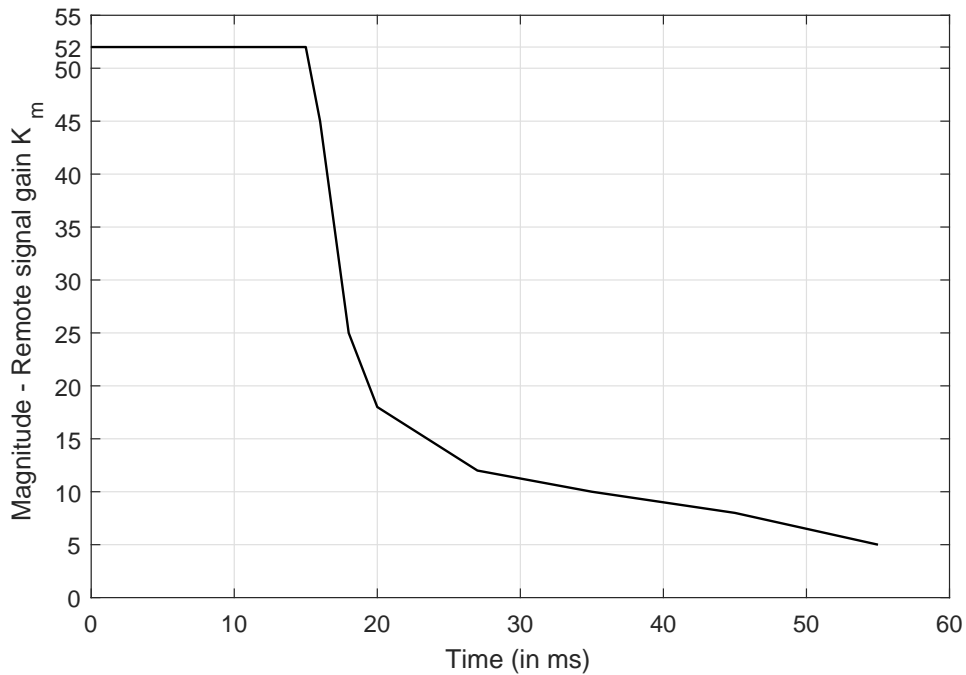


**Figure 6.15:** Effect of communication delay on maximum gain for remote signal  $K_m$ .

## Conclusion

It is observed that as the duration of communication delay increases beyond  $15ms$ , the allowable range of gains for the remote WAMS signal is considerably compromised. This finding is also corroborated by EMT simulation and Nyquist analysis. It is therefore suggested that, suitable phase lead compensation may have to be incorporated with the remote WAMS signal ( $K_m$ ) for a delay beyond  $15ms$  to compensate for the phase margin due to communication delay. However,  $15ms$  or smaller delay is entirely within the range of dedicated communication systems set up for control.

## 6.5 Summary

In the previous chapter it was observed through EMT simulation that a certain POD controller gain resulted in system instability. In this chapter, a transfer function model of the AC-DC system was obtained using the frequency scanning technique. This model, combined with the POD controller's transfer function which is already known, is analysed



based on the frequency response of the combined system to evaluate the performance of the POD controller. The frequency scanning technique is a practical approach to obtain the transfer function model of a complex PE system in the network as it provides an accurate model, which is free from approximations due to simplifications. The frequency response analysis using Nyquist stability criteria was used to provide qualitative assessment of the system behaviour. Through this approach, the performance of the proposed controller was evaluated to arrive at the critical gain value beyond which the POD adversely interacts with the AC-DC system resulting in instability. The results obtained from this analysis agree with the EMT simulation regarding the occurrence of system instability. The case studies show that the instability caused by the POD controller gains is due to its interaction with the high frequency modes of the converter, that were ignored in developing the simplified small-signal model. The allowable range of gain for the remote signal is significantly compromised by the duration of the delay, this has been supported both by Nyquist and EMT simulation.

# Chapter 7

## Conclusion and Future Work

Power systems are continuously evolving with many point-to-point HVDC links being added to transmit large amounts of power over large distances. The ever increasing share of renewable energy resources along with the aim of efficient utilisation of all types of generation resources, has spurred the development of HVDC grids to transmit power over pan-continent areas. All this will lead to increased complexity of the power systems. The existence of poorly damped low-frequency oscillations in an AC-DC system has the potential to cause catastrophic effects in the system due to angular instability. This can be in the form of phenomena such as loss of synchronism leading to loss of generation (black-outs).

The aim of the research presented herein was to investigate aspects related to methods to damp the low-frequency oscillations prevalent in an interconnected AC-DC system and to develop a controller design that is effective, robust and simple to implement. The proposed damping controller design makes use of system-wide network information and is implementable as an additional control module in existing point-to-point HVDC links.

The thesis presents a new design approach to determine the operational envelope for a synthesised modified feedback signal based POD controller utilising VSC-HVDC system. It extends a previous robust approach by allowing for more damping and, through the use of EMT simulation, shows new limitations not reported before. This research shows how EMT simulation can be usefully incorporated into the design approach to make it more comprehensive and applicable for field implementation.

## 7.1 Research Contributions

- A POD controller which is simple to design and implement based on modified feedback signal. The structure of the controller is simple to implement as the controller design has minimal blocks in comparison to traditional damping controllers that use cascaded lead-lag blocks in addition to other blocks for the same purpose.
- The design of a modified feedback signal based proposed damping controller Chapter 4 shows, analytically, that it is possible to have a wider range for controller gains as compared to the previous controller [36], to provide increased damping. This has been made possible due to the modified feedback signal that enables movement of open-loop zeroes significantly towards the left of the  $j\omega$  axis.
- The proposed controller retains the qualities of robustness to change in operating conditions and network topology, as described in [36]. It was shown in equation (4.17) during the analytical treatment that changes in either operating point or network topology will effect  $[B_\omega]$  or  $e_{\delta_i}$ , which being positive do not have an adverse effect on the response of the controller.
- The small-signal analysis based design of the proposed controller retains the major advantage of earlier, similar design procedures [36], in that, it will always ensure improved damping for all the swing modes if the gain matrix,  $K$ , is maintained as Positive Definite. The controller also retains the ability to selectively damp a targeted low-frequency mode by selectively tuning the parameter  $K_m$ . However, the controller design ensures that, then even with the selective mode damping, the damping of other low-frequency mode(s) is always better than when there is ‘no control’.
- This research suggests a simple approach for identifying the candidate locations of HVDC links with the aim to improve overall system stability of an AC-DC network through the use of residue criterion.
- The frequency domain design procedure ignores internal higher frequency modes. Although it appears to be validated when compared with the TS simulation. When

a detailed comparison with the EMT simulation is made, it reveals that the high value of POD gains can destabilize these internal modes. This aspect of instability due to large gains has only been conjectured and not previously reported.

- The critical gain value for the POD controller resulting in HF instability of the system can also be determined by conducting a frequency scan of the EMT simulation model without the proposed POD controller being active. The combined frequency response of the system and the POD controller can be qualitatively analysed using Nyquist stability criterion. The values obtained using this analysis agree with the EMT simulation of the whole system.
- The occurrence of instability due to increase in POD controller gains in the system has been further corroborated by an independent investigation carried out through frequency response analysis using Nyquist criteria. The result of this investigation agrees with conclusions arrived at by the EMT simulation.
- This research cautions the designer that though the small-signal analysis based approach is suitable for the design of a POD controller, there is a considerable gap in evaluation of the operational range of the controller obtained from TS simulation and EMT simulation. Thus, only following the results of TS simulation can lead to suggested operation in a non-viable region. Therefore, it is strongly recommended that a full EMT simulation be carried out to correctly predict the controller range.

## 7.2 Suggestions for Future Work

This work has looked at the design of a damping controller based on a modified feedback signal that was synthesized using system-wide information. The small-signal analysis based controller design corroborated using the TS simulation based time-domain analysis and the EMT simulation indicates that the small-signal model is sufficient for investigating low-frequency oscillations. The approach used a given input-output pair of signals to effect damping.

However, there exist other signal pairs e.g. shunt injected reactive current/voltage magnitude, series injected power/line current phase angle that can also be investigated

for a damping controller based on FACTS devices. The work can be extended to the use of such a controller on an HVDC grid, wherein the power modulation from different converters can be used to stabilise the AC network. The feasibility of extending this modal analysis approach to effectively damp sub-synchronous oscillations in an interconnected AC-DC system can also be explored.

# Appendix A

## 3-Machine 9-Bus System.

- All the values are in per unit.
- The base MVA = 100 MVA.

### Machine Data.

Gen No.	Xd	Xd'	Xd''	Td0'	Td0''	Xq	Xq'	Xq''	Tq0'	Tq0''	H	D	Xl
1	0.146	0.0608	0.0486	8.96	1.00	0.0969	0.3	0.02	0.31	0.03	23.64	0	0.01
2	0.8958	0.1198	0.1060	6.00	1.00	0.8645	0.1969	0.08	0.535	0.05	6.4	0	0.01196
3	1.3125	0.1813	0.152	5.89	1.00	1.2578	0.25	0.15	0.6	0.06	3.01	0	0.01811

**Table A.1: Machine data: 3 machine 9 bus system**

### Transmission Line Data.

Ser.no	From	To	r	x	B (total)
1	9	8	0.01005	0.1139	0.2001
2	9	6	0.01683	0.1922	0.3414
3	8	7	0.00720	0.0814	0.1427
4	7	5	0.01520	0.1733	0.3068
5	6	4	0.00837	0.0947	0.1661
6	5	4	0.00849	0.0961	0.1685
7	4	1	0.000	0.0576	1.000
8	3	9	0.000	0.0586	1.00
9	2	7	0.000	0.0625	1.00

**Table A.2: Line Data: 3 machine system**

Load Flow Data.

Ser. No	Voltage (pu)	Theta (deg)	Pg0	Qg0	PL0	QL0
1	1.0400	0.0000	0.7460	0.2272		
2	1.0250	9.5997	1.6300	0.1362		
3	1.0248	4.8269	0.8500	-0.0586		
4	1.0282	-2.3029	0.00	0.00		
5	0.9986	-4.2986	0.00	0.00	1.25	0.35
6	1.0181	-4.0698	0.00	0.00	0.9	0.3
7	1.0215	4.0163	0.00	0.00		
8	1.0107	0.5802	0.00	0.00	1.0	0.35
9	1.0293	2.1203	0.00	0.00		

**Table A.3: Load flow result: 3 machine system**

Load flow data for changed operating point.

Bus No.	V (pu)	Angle (deg)	Pg0 (pu)	Qg0 (pu)
<b>1</b>	1.040	0.000	0.98667	0.222993
<b>2</b>	1.025	3.856	1.1410	0.061724
<b>3</b>	1.0248	4.564	1.1050	-0.054326
<b>4</b>	1.029	-3.044	0.00	0.00
<b>5</b>	1.001	-6.216	0.00	0.00
<b>6</b>	1.019	-4.921	0.00	0.00
<b>7</b>	1.0236	-0.041	0.00	0.00
<b>8</b>	1.0122	-2.228	0.00	0.00
<b>9</b>	1.0298	1.046	0.00	0.00

**Table A.4: 3 machine system: Load flow data for 30% change in generation at machine-2 and 3**

# Bibliography

- [1] P. Kundur, *Power System Stability And Control*. EPRI power system engineering series, McGraw-Hill Education (India) Pvt Limited, 1994.
- [2] K. Padiyar, *Power System Dynamics : Stability & Control : 2Nd Ed.* BS Publications, 2002.
- [3] D. R. Davidson, D. N. Ewart, and L. K. Kirchmayer, “Long term dynamic response of power systems: An analysis of major disturbances,” *IEEE Transactions on Power Apparatus and Systems*, vol. 94, pp. 819–826, May 1975.
- [4] G. Rogers, *Power System Oscillations*. Kluwer Academic Publishers, Norwell, MA, 2000.
- [5] B. Chaudhuri and B. C. Pal, “Robust damping of multiple swing modes employing global stabilizing signals with a tcsc,” *IEEE Transactions on Power Systems*, vol. 19, pp. 499–506, Feb 2004.
- [6] J. Zhang, C. Y. Chung, S. Zhang, and Y. Han, “Practical wide area damping controller design based on ambient signal analysis,” *IEEE Transactions on Power Systems*, vol. 28, pp. 1687–1696, May 2013.
- [7] B. Chaudhuri, B. C. Pal, A. C. Zolotas, I. M. Jaimoukha, and T. C. Green, “Mixed-sensitivity approach to h infin; control of power system oscillations employing multiple facts devices,” *IEEE Transactions on Power Systems*, vol. 18, pp. 1149–1156, Aug 2003.
- [8] M. E. Aboul-Ela, A. A. Sallam, J. D. McCalley, and A. A. Fouad, “Damping controller design for power system oscillations using global signals,” *IEEE Transactions on Power Systems*, vol. 11, pp. 767–773, May 1996.
- [9] N. G. Hingorani and L. Gyugyi, *Understanding FACTS: Concepts and Technology of Flexible AC Transmission Systems*. Wiley-IEEE Press, 2000.
- [10] I. Kamwa, R. Grondin, D. Asber, J. P. Gingras, and G. Trudel, “Large-scale active-load modulation for angle stability improvement,” *IEEE Transactions on Power Systems*, vol. 14, pp. 582–590, May 1999.



- [11] J. J. Sanchez-Gasca, N. W. Miller, A. Kurita, and S. Horiuchi, "Multivariable control for damping interarea oscillations in power systems," *IEEE Control Systems Magazine*, vol. 9, pp. 28–32, Jan 1989.
- [12] I. Kamwa, R. Grondin, and Y. Hebert, "Wide-area measurement based stabilizing control of large power systems-a decentralized/hierarchical approach," *IEEE Transactions on Power Systems*, vol. 16, pp. 136–153, Feb 2001.
- [13] H. Nguyen-Duc, L. A. Dessaint, and A. F. Okou, "Power system robust stability analysis using structured singular value theory and model reduction method," in *2009 IEEE Power Energy Society General Meeting*, pp. 1–8, July 2009.
- [14] H. Wu, K. S. Tsakalis, and G. T. Heydt, "Evaluation of time delay effects to wide-area power system stabilizer design," *IEEE Transactions on Power Systems*, vol. 19, pp. 1935–1941, Nov 2004.
- [15] A. F. Snyder, N. Hadjsaid, D. Georges, L. Mili, A. G. Phadke, O. Faucon, and S. Vitet, "Inter-area oscillation damping with power system stabilizers and synchronized phasor measurements," in *Power System Technology, 1998. Proceedings. POWERCON '98. 1998 International Conference on*, vol. 2, pp. 790–794 vol.2, Aug 1998.
- [16] J. H. Chow, J. J. Sanchez-Gasca, H. Ren, and S. Wang, "Power system damping controller design-using multiple input signals," *IEEE Control Systems*, vol. 20, Aug 2000.
- [17] I. Kamwa, J. Beland, G. Trudel, R. Grondin, C. Lafond, and D. McNabb, "Wide-area monitoring and control at hydro-quebec: past, present and future," in *2006 IEEE Power Engineering Society General Meeting*, p. 12, 2006.
- [18] F. Okou, L. A. Dessaint, and O. Akhrif, "Power systems stability enhancement using a wide-area signals based hierarchical controller," *IEEE Transactions on Power Systems*, vol. 20, pp. 1465–1477, Aug 2005.
- [19] D. Dotta, A. S. e Silva, and I. C. Decker, "Wide-area measurements-based two-level control design considering signal transmission delay," *IEEE Transactions on Power Systems*, vol. 24, pp. 208–216, Feb 2009.
- [20] Y. Zhang and A. Bose, "Design of wide-area damping controllers for interarea oscillations," *IEEE Transactions on Power Systems*, vol. 23, pp. 1136–1143, Aug 2008.
- [21] Z. Hu and J. V. Milanovic, "Damping of inter-area oscillations by wam based supplementary controller," in *Power Engineering Society General Meeting, 2007. IEEE*, pp. 1–7, June 2007.

- [22] Z. Hu and J. V. Milanovic, "The effectiveness of wam based adaptive supervisory controller for global stabilization of power systems," in *Power Tech, 2007 IEEE Lausanne*, pp. 1652–1659, July 2007.
- [23] H. Ni, G. T. Heydt, and L. Mili, "Power system stability agents using robust wide area control," *IEEE Transactions on Power Systems*, vol. 17, pp. 1123–1131, Nov 2002.
- [24] A. C. Zolotas, B. Chaudhuri, I. M. Jaimoukha, and P. Korba, "A study on lqg/ltr control for damping inter-area oscillations in power systems," *IEEE Transactions on Control Systems Technology*, vol. 15, pp. 151–160, Jan 2007.
- [25] S. Skogestad and I. Postlethwaite, *Multivariable Feedback Control: Analysis and Design*. Wiley, 1996.
- [26] I. J. Perez-arriaga, G. C. Verghese, and F. C. Schweppe, "Selective modal analysis with applications to electric power systems, part i: Heuristic introduction," *IEEE Transactions on Power Apparatus and Systems*, vol. PAS-101, pp. 3117–3125, Sept 1982.
- [27] G. C. Verghese, I. J. Perez-arriaga, and F. C. Schweppe, "Selective modal analysis with applications to electric power systems, part ii: The dynamic stability problem," *IEEE Transactions on Power Apparatus and Systems*, vol. PAS-101, pp. 3126–3134, Sept 1982.
- [28] K. M. Son and J. K. Park, "On the robust lqg control of tcsc for damping power system oscillations," *IEEE Transactions on Power Systems*, vol. 15, pp. 1306–1312, Nov 2000.
- [29] J. Arrillaga, *High Voltage Direct Current Transmission*. Energy Engineering Series, Institution of Electrical Engineers, 1998.
- [30] A. Hammad, R. Minghetti, J. P. Hasler, P. A. Eicher, R. Bunch, and D. Goldsworthy, "Controls modelling and verification for the pacific intertie hvdc 4-terminal scheme," *IEEE Transactions on Power Delivery*, vol. 8, pp. 367–375, Jan 1993.
- [31] M. Xiao-ming, Z. Yao, G. Lin, and W. Xiaochen, "Researches on coordinated control strategy for inter-area oscillations in ac/dc hybrid grid with multi-infeed hvdc," in *2005 IEEE/PES Transmission Distribution Conference Exposition: Asia and Pacific*, pp. 1–6, 2005.
- [32] J. H. Chow, J. J. Sanchez-Gasca, H. Ren, and S. Wang, "Power system damping controller design-using multiple input signals," *IEEE Control Systems*, vol. 20, pp. 82–90, Aug 2000.

- [33] J. W. Stahlhut, T. J. Browne, G. T. Heydt, and V. Vittal, "Latency viewed as a stochastic process and its impact on wide area power system control signals," *IEEE Transactions on Power Systems*, vol. 23, pp. 84–91, Feb 2008.
- [34] X. Xie, Y. Xin, J. Xiao, J. Wu, and Y. Han, "Wams applications in chinese power systems," *IEEE Power and Energy Magazine*, vol. 4, pp. 54–63, Jan 2006.
- [35] B. Chaudhuri, R. Majumder, and B. C. Pal, "Wide-area measurement-based stabilizing control of power system considering signal transmission delay," *IEEE Transactions on Power Systems*, vol. 19, pp. 1971–1979, Nov 2004.
- [36] P. Agnihotri, *A Robust Wide Area Measurement Based Controller for Networks with Embedded HVDC Links*. PhD thesis, University of Manitoba, Winnipeg, 8 2016.
- [37] U. E., "Stabilization of an a.c. link by a parallel d.c. link," *Direct Current*, pp. 89–94, August 1964.
- [38] H. A. Peterson and P. C. Krause, "Damping of power swings in a parallel ac and dc system," *IEEE Transactions on Power Apparatus and Systems*, vol. PAS-85, pp. 1231–1239, Dec 1966.
- [39] I. C. Report, "Dynamic performance characteristics of north american hvdc systems for transient and dynamic stability evaluations," *IEEE Transactions on Power Apparatus and Systems*, vol. PAS-100, pp. 3356–3364, July 1981.
- [40] T. McNichol, *AC/DC: The Savage Tale of the First Standards War*. Wiley Press, 2006.
- [41] A. M. Gole, "Lecture notes on power systems transients simulation." <http://ece.eng.umanitoba.ca/graduate/ECE7310>, January 2015.
- [42] N. Flourentzou, V. G. Agelidis, and G. D. Demetriades, "Vsc-based hvdc power transmission systems: An overview," *IEEE Transactions on Power Electronics*, vol. 24, pp. 592–602, March 2009.
- [43] J. Z. Zhou and A. M. Gole, "Vsc transmission limitations imposed by ac system strength and ac impedance characteristics," in *10th IET International Conference on AC and DC Power Transmission (ACDC 2012)*, pp. 1–6, Dec 2012.
- [44] V. C. Billon, J. P. Taisne, V. Arcidiacono, and F. Mazzoldi, "The corsican tapping: from design to commissioning tests of the third terminal of the sardinia-corsica-italy hvdc," *IEEE Transactions on Power Delivery*, vol. 4, pp. 794–799, Jan 1989.
- [45] Wikipedia, "Hvdc italy–corsica–sardinia — wikipedia, the free encyclopedia," 2016. [Online; accessed 19-September-2016].

- [46] Wikipedia, “Quebec – new england transmission — wikipedia, the free encyclopedia,” 2016. [Online; accessed 14-November-2016].
- [47] X. Yang, C. Yuan, D. Yao, C. Yang, and C. Yue, “Dynamic performance of series multiterminal hvdc during ac faults at inverter stations,” in *2014 16th European Conference on Power Electronics and Applications*, pp. 1–9, Aug 2014.
- [48] N. Chaudhuri, B. Chaudhuri, R. Majumder, and A. Yazdani, *Multi-terminal Direct-Current Grids: Modeling, Analysis, and Control*. Wiley - IEEE, Wiley, 2014.
- [49] C. Schauder and H. Mehta, “Vector analysis and control of advanced static var compensators,” *IEE Proceedings C - Generation, Transmission and Distribution*, vol. 140, pp. 299–306, July 1993.
- [50] C. D. Barker and R. Whitehouse, “Autonomous converter control in a multi-terminal hvdc system,” in *9th IET International Conference on AC and DC Power Transmission (ACDC 2010)*, pp. 1–5, Oct 2010.
- [51] R. T. Pinto, S. Rodrigues, P. Bauer, and J. Pierik, “Description and comparison of dc voltage control strategies for offshore mt dc networks: Steady-state and fault analysis,” *EPE Journal*, vol. 22, no. 4, pp. 31–39, 2012.
- [52] N. Chaudhuri, B. Chaudhuri, R. Majumder, and A. Yazdani, *Multi-terminal Direct-Current Grids: Modeling, Analysis, and Control*. Wiley, 2014.
- [53] T. Nakajima and S. Irokawa, “A control system for hvdc transmission by voltage sourced converters,” in *1999 IEEE Power Engineering Society Summer Meeting. Conference Proceedings (Cat. No.99CH36364)*, vol. 2, pp. 1113–1119 vol.2, 1999.
- [54] J. Beerten, S. Cole, and R. Belmans, “Modeling of multi-terminal vsc hvdc systems with distributed dc voltage control,” *IEEE Transactions on Power Systems*, vol. 29, pp. 34–42, Jan 2014.
- [55] R. Preece, J. V. Milanović, A. M. Almutairi, and O. Marjanovic, “Damping of inter-area oscillations in mixed ac/dc networks using wams based supplementary controller,” *IEEE Transactions on Power Systems*, vol. 28, pp. 1160–1169, May 2013.
- [56] R. Preece, A. M. Almutairi, O. Marjanovic, and J. V. Milanović, “Damping of inter-area oscillations using wams based supplementary controller installed at vsc based hvdc line,” in *PowerTech, 2011 IEEE Trondheim*, pp. 1–8, June 2011.
- [57] Y. Pipelzadeh, B. Chaudhuri, and T. C. Green, “Coordinated damping control through multiple hvdc systems: A decentralized approach,” in *2011 IEEE Power and Energy Society General Meeting*, pp. 1–8, July 2011.

- [58] Y. G. Rebours, D. S. Kirschen, M. Trotignon, and S. Rossignol, “A survey of frequency and voltage control ancillary services mdash;part i: Technical features,” *IEEE Transactions on Power Systems*, vol. 22, Feb 2007.
- [59] Eltra, “Wind turbines connected to grids with voltages below 100 kv, technical regulations for the properties and the control of wind turbines,” tech. rep., Hydro-Quebec, May 2004.
- [60] “Requirements for the connection of generation facilities to the hydro-quebec transmission system,supplementary requirements for wind generation,” tech. rep., Hydro-Quebec, May 2003.
- [61] I. Erlich and M. Wilch, “Primary frequency control by wind turbines,” in *IEEE PES General Meeting*, pp. 1–8, July 2010.
- [62] U. P. Mhaskar and A. M. Kulkarni, “Power oscillation damping using facts devices: modal controllability, observability in local signals, and location of transfer function zeros,” *IEEE Transactions on Power Systems*, vol. 21, pp. 285–294, Feb 2006.
- [63] CIGRE, *CIGRE TF 38.01.07 Broch. 111, Analysis and control of power system oscillations*. CIGRE, Dec 1996.
- [64] N. Martins and L. T. G. Lima, “Determination of suitable locations for power system stabilizers and static var compensators for damping electromechanical oscillations in large scale power systems,” *IEEE Transactions on Power Systems*, vol. 5, pp. 1455–1469, Nov 1990.
- [65] CIGRE, *CIGRE JointWG 33.02, Guidelines for Representation of Networks Elements when Calculating Transients*. CIGRE Brochure, 1990.
- [66] “IEEE Recommended Practice for Emergency and Standby Power Systems for Industrial and Commerical Applications,” *ANSI/IEEE Std 446-1987*, Feb 1987.
- [67] IEC, *IEC 60071-1, ed. 8;IEC 60071-2, 3rd ed.,Insulation Coordination, Definitions, Principles, and Rules;Application Guide*. International Electrotechnical Commission, Mar. 1996.
- [68] H. Dommel, *Electromagnetic Transients Program: Reference Manual : (EMTP Theory Book)*. Bonneville Power Administration, 1986.
- [69] H. W. Dommel, “Digital computer solution of electromagnetic transients in single- and multiphase networks,” *IEEE Transactions on Power Apparatus and Systems*, vol. PAS-88, pp. 388–399, April 1969.
- [70] A. M. Gole, R. W. Menzies, H. M. Turanli, and D. A. Woodford, “Improved interfacing of electrical machine models to electromagnetic transients programs,” *IEEE*

- Transactions on Power Apparatus and Systems*, vol. PAS-103, pp. 2446–2451, Sept 1984.
- [71] J. He, C. Lu, X. Wu, P. Li, and J. Wu, “Design and experiment of wide area hvdc supplementary damping controller considering time delay in china southern power grid,” *IET Generation, Transmission Distribution*, vol. 3, January 2009.
- [72] E. Johansson, K. Uhlen, A. B. Leirbukt, P. Korba, J. O. Gjerde, and L. K. Vormedal, “Coordinating power oscillation damping control using wide area measurements,” in *Power Systems Conference and Exposition, 2009. PSCE '09. IEEE/PES*, March 2009.
- [73] K. Uhlen, L. Vanfretti, M. M. de Oliveira, A. B. Leirbukt, V. H. Aarstrand, and J. O. Gjerde, “Wide-area power oscillation damper implementation and testing in the norwegian transmission network,” in *2012 IEEE Power and Energy Society General Meeting*, July 2012.
- [74] E. V. Larsen, J. J. Sanchez-Gasca, and J. H. Chow, “Concepts for design of facts controllers to damp power swings,” *IEEE Transactions on Power Systems*, vol. 10, pp. 948–956, May 1995.
- [75] O. Samuelsson and B. Eliasson, “Damping of electro-mechanical oscillations in a multimachine system by direct load control,” *IEEE Transactions on Power Systems*, vol. 12, pp. 1604–1609, Nov 1997.
- [76] B. Pal and B. Chaudhuri, *Robust Control in Power Systems*. Power Electronics and Power Systems, Springer, 2005.
- [77] O. Samuelsson, “Load modulation for damping of electro-mechanical oscillations,” in *Power Engineering Society Winter Meeting, 2001. IEEE*, vol. 1, pp. 241–246 vol.1, Jan 2001.
- [78] Y. Liang, X. Lin, A. M. Gole, and M. Yu, “Improved coherency-based wide-band equivalents for real-time digital simulators,” *IEEE Transactions on Power Systems*, vol. 26, pp. 1410–1417, Aug 2011.
- [79] X. Lin, A. M. Gole, and M. Yu, “A wide-band multi-port system equivalent for real-time digital power system simulators,” *IEEE Transactions on Power Systems*, vol. 24, pp. 237–249, Feb 2009.
- [80] P. Anderson, A. Fouad, I. of Electrical, and E. Engineers, *Power system control and stability*. IEEE Press power engineering series, IEEE Press, 2003.
- [81] M. H. R. Centre, *PSCAD/EMTDC User’s guide*. Winnipeg, Canada, 2010.

- [82] R. Vaid, P. Agnihotri, A. M. Gole, A. M. Kulkarni, and X. Chen, “Wide-area control of multi-infeed hvdc links for targeted swing mode damping using special feedback signals,” in *13th IET International Conference on AC and DC Power Transmission (ACDC 2017)*, pp. 1–6, Feb 2017.
- [83] X. Jiang and A. M. Gole, “A frequency scanning method for the identification of harmonic instabilities in hvdc systems,” *IEEE Transactions on Power Delivery*, vol. 10, pp. 1875–1881, Oct 1995.
- [84] M. K. Das, A. M. Kulkarni, and P. B. Darji, “Comparison of dq and dynamic phasor based frequency scanning analysis of grid-connected power electronic systems,” in *2016 Power Systems Computation Conference (PSCC)*, pp. 1–7, June 2016.
- [85] R. Pintelon and J. Schoukens, *System Identification: A Frequency Domain Approach*. Wiley, 2012.
- [86] N. M. Wereley, *Analysis and control of linear periodically time varying systems*. PhD thesis, Massachusetts Institute of Technology, Dept. of Aeronautics and Astronautics, 1991.
- [87] H. Wu, K. S. Tsakalis, and G. T. Heydt, “Evaluation of time delay effects to wide-area power system stabilizer design,” *IEEE Transactions on Power Systems*, vol. 19, pp. 1935–1941, Nov 2004.
- [88] B. Naduvathuparambil, M. C. Valenti, and A. Feliachi, “Communication delays in wide area measurement systems,” in *Proceedings of the Thirty-Fourth Southeastern Symposium on System Theory (Cat. No.02EX540)*, pp. 118–122, 2002.
- [89] C. W. Taylor, D. C. Erickson, K. E. Martin, R. E. Wilson, and V. Venkatasubramanian, “Wacs-wide-area stability and voltage control system: R d and online demonstration,” *Proceedings of the IEEE*, vol. 93, pp. 892–906, May 2005.